



PREVENTIVE EFFECT OF UNRIPE *CARICA PAPAYA* JUICE EXTRACT ON HYDROGEN  
PEROXIDE INDUCED OXIDATIVE STRESS IN HUMAN ENDOTHELIAL CELLS



WATTANASED JARISARAPURIN

ฤทธิ์ของน้ำมะละกอดิบสกัดในการป้องกันเซลล์เยื่อหุ้มหลอดเลือดจากภาวะเครียดออกซิเดชัน เมื่อ  
ถูกกระตุ้นด้วยไฮโดรเจนเปอร์ออกไซด์



ปริญญานิพนธ์นี้เป็นส่วนหนึ่งของการศึกษาตามหลักสูตร  
ปรัชญาดุษฎีบัณฑิต สาขาวิชาอณูชีววิทยา  
คณะแพทยศาสตร์ มหาวิทยาลัยศรีนครินทรวิโรฒ  
ปีการศึกษา 2563  
ลิขสิทธิ์ของมหาวิทยาลัยศรีนครินทรวิโรฒ

PREVENTIVE EFFECT OF UNRIPE *CARICA PAPAYA* JUICE EXTRACT ON HYDROGEN  
PEROXIDE INDUCED OXIDATIVE STRESS IN HUMAN ENDOTHELIAL CELLS



A Dissertation Submitted in Partial Fulfillment of the Requirements  
for the Degree of DOCTOR OF PHILOSOPHY  
(Molecular Biology)

Faculty of Medicine, Srinakharinwirot University

2020

Copyright of Srinakharinwirot University

THE DISSERTATION TITLED  
PREVENTIVE EFFECT OF UNRIPE *CARICA PAPAYA* JUICE EXTRACT ON HYDROGEN  
PEROXIDE INDUCED OXIDATIVE STRESS IN HUMAN ENDOTHELIAL CELLS

BY  
WATTANASED JARISARAPURIN

HAS BEEN APPROVED BY THE GRADUATE SCHOOL IN PARTIAL FULFILLMENT  
OF THE REQUIREMENTS FOR THE DOCTOR OF PHILOSOPHY  
IN MOLECULAR BIOLOGY AT SRINAKHARINWIROT UNIVERSITY

-----  
(Assoc. Prof. Dr. Chatchai Ekpanyaskul, MD.)  
Dean of Graduate School  
-----

ORAL DEFENSE COMMITTEE

..... Major-advisor	..... Chair
(Assoc. Prof.Suvara Wattanapitayakul)	(Assoc. Prof.Nuntiya Sompam)
..... Co-advisor	..... Committee
(Assoc. Prof.Linda Chularojmontri)	(Assoc. Prof.Teeraporn Bureerug)
	..... Committee
	(Assoc. Prof.Punnee Nusuetrong)

Title	PREVENTIVE EFFECT OF UNRIPE <i>CARICA PAPAYA</i> JUICE EXTRACT ON HYDROGEN PEROXIDE INDUCED OXIDATIVE STRESS IN HUMAN ENDOTHELIAL CELLS
Author	WATTANASED JARISARAPURIN
Degree	DOCTOR OF PHILOSOPHY
Academic Year	2020
Thesis Advisor	Associate Professor Suvara Wattanapitayakul
Co Advisor	Associate Professor Linda Chularojmontri

Cardiovascular disease (CVD) is the main cause of death worldwide. Reactive oxygen species (ROS) play an important role in CVD via damaged endothelial cells. An excess of ROS can induce endothelial cell death and dysfunction, leading to atherosclerosis and CVD. Antioxidants play a crucial role in controlling ROS levels via direct elimination of ROS, maintaining cell homeostasis, and reducing cell death and inflammation. Unripe *Carica papaya* (UCP) is a naturally high antioxidant fruit that can prevent ROS-induced endothelial cell oxidative stress. This study investigated antioxidant properties and their preventive effects on H<sub>2</sub>O<sub>2</sub>-induced EA hy926 cell oxidative stress. The antioxidant activity of UCP was determined by antioxidant capacities and scavenging assays. The HPLC was prepared for screening antioxidant compounds of UCP. The toxicity of UCP and its preventive effect on H<sub>2</sub>O<sub>2</sub>-induced EA hy926 cell death was evaluated by MTT. The treated cells determined the intracellular ROS levels and percent cell apoptosis using a fluorescence microscope and flow cytometer, respectively, and found enzymatic antioxidant activity and signaling pathways. There was also an investigation of UCP due to the high antioxidant potential to decrease excessive ROS in H<sub>2</sub>O<sub>2</sub>-induced endothelial cell oxidative stress leading to cytoprotection against cell death and apoptosis. UCP also reduced cell inflammation via NF- $\kappa$ B pathways and maintained cell homeostasis, leading to the stabilization of Nrf2 levels on damaged cells. The pretreatment of UCP increased SOD activity and restored the CAT activity used to eliminate H<sub>2</sub>O<sub>2</sub> and increase SOD activity. Furthermore, UCP might be used in alternative medicine as health supplements for reducing risks of CVDs and oxidative stress-related diseases.

Keyword : unripe *Carica papaya*, Oxidative stress, Endothelial cell, Endothelial dysfunction, Cardiovascular diseases, Antioxidant, Reactive oxygen species

## ACKNOWLEDGEMENTS

I am thankful to my advisor Assoc.Prof.Suvara Wattanapitayakul for giving me an opportunity to study in the Ph.D. program. My advisor and co-advisor Assoc.Prof. Linda Chularojanamontri provide the best advices and warm taking care of me throughout my Ph.D. study. I would like to say thank you to my lab partner Khwandow Kunchana for their help and support. I appreciate The Royal Golden Jubilee Ph.D. program (PHD57K0036) that provides funding. Thank you for the superb experience and support from Srinakharinwirot University.

WATTANASED JARISARAPURIN



## TABLE OF CONTENTS

	Page
ABSTRACT .....	D
ACKNOWLEDGEMENTS.....	E
TABLE OF CONTENTS.....	F
TABLE OF TABLES.....	L
TABLE OF FIGURES.....	M
LIST OF ABBREVIATIONS.....	P
CHAPTER 1 INTRODUCTION .....	1
1.1 Background.....	1
1.2 Objective of the study .....	5
1.3 Hypothesis .....	5
1.4 Conceptual framework.....	5
CHAPTER 2 LITERATURE REVIEW.....	6
2.1 Reactive oxygen species (ROS).....	6
2.1.1 Classification of ROS.....	6
2.1.1.1 Radicals .....	6
2.1.1.1.1 OH <sup>•</sup> .....	6
2.1.1.1.2 O <sub>2</sub> <sup>•-</sup> .....	7
2.1.1.1.3 RO <sup>•</sup> and ROO <sup>•</sup> .....	7
2.1.1.2 Non-radicals.....	7
2.1.1.2.1 H <sub>2</sub> O <sub>2</sub> .....	7
2.1.1.2.2 HOCl .....	8

2.1.2 Sources of ROS .....	9
2.1.2.1 Endogenous sources of ROS .....	9
2.1.2.1.1 Mitochondria .....	10
2.1.2.1.2 Peroxisomes .....	10
2.1.2.1.3 Endoplasmic reticulum (ER) .....	11
2.1.2.2 Exogenous sources of ROS.....	13
2.1.2.2.1 Radiation .....	13
2.1.2.2.2 Smoking .....	14
2.1.3 ROS elimination .....	15
2.1.3.1 Enzymatic antioxidants .....	15
2.1.3.1.1 SOD.....	15
2.1.3.1.2 CAT .....	15
2.1.3.1.3 GPX.....	16
2.1.3.1.4 TrxP .....	16
2.1.3.1 Non-enzymatic antioxidants .....	17
2.1.3.1.1 Endogenous antioxidants .....	17
2.1.3.1.2 Exogenous antioxidants .....	17
2.1.4 ROS, Oxidative stress, and cells damage .....	19
2.1.4.1 ROS damaging biomolecules .....	19
2.1.4.1.1 Lipid peroxidation .....	20
2.1.4.1.2 Protein oxidation and peroxidation.....	21
2.1.4.1.3 DNA oxidation.....	23
2.1.4.2 ROS and cell signaling pathways.....	24



2.1.4.2.1 ROS effect on MAPKs signaling pathway .....	24
2.1.4.2.2 ROS effect on NF- $\kappa$ B signaling pathway .....	26
2.1.4.2.3 ROS effect NRF2 signaling pathway .....	27
2.1.4.2.4 ROS effect PI3K/Akt signaling pathway .....	28
2.1.4.2.5 ROS and protein kinase signaling pathway .....	29
2.1.4.2.6 ROS regulate ubiquitination and proteasome system .....	29
2.1.4.2.7 ROS mediate program cell death.....	29
2.2 Endothelial cells .....	31
2.2.1 Endothelial function .....	31
2.2.1.1 Barrier function.....	31
2.2.1.2 Vasculogenesis and Angiogenesis .....	32
2.2.1.3 Vascular tone .....	32
2.2.1.4 Anticoagulation .....	34
2.2.1.5 Immune system.....	34
2.2.2 Oxidative stress induces endothelial dysfunction and cardiovascular disease .....	34
2.2.2.1 Uncoupled eNOS .....	35
2.2.2.2. Vascular wall permeability .....	36
2.2.2.3. Excessive of angiogenesis .....	37
2.2.2.4. Endothelial cells death and inflammation.....	37
2.2.2.5 Endothelial dysfunction associated with cardiovascular disease (CVD).....	39
2.2.3 Prevention of endothelial dysfunction and antioxidant .....	39
2.3 <i>Carica papaya</i> .....	41

2.3.1 Background.....	41
2.3.2 Medical research.....	42
2.3.2.1 Leaf extract .....	43
2.3.2.2 Seed extract.....	43
2.3.2.3 Latex extract.....	43
2.3.2.4 Unripe fruit extract .....	43
CHAPTER 3 RESEARCH METHODOLOGY .....	45
3.1 Chemicals and Equipment.....	45
3.1.1 Chemicals.....	45
3.1.2 Equipment .....	47
3.2 Preparation of unripe <i>Carica papaya</i> fruit juice extraction .....	49
3.3 The chemical components analysis of UCP using High-performance liquid chromatography (HPLC).....	49
3.3.1 Analysis of ascorbic acid .....	50
3.3.2 Analysis of ellagic acid.....	50
3.3.3 Analysis of gallic acid.....	50
3.3.4 Analysis of chlorogenic acid and quercetin .....	51
3.4 Antioxidant scavenging capacity of <i>Carica papaya</i> fruit juice extraction .....	51
3.4.1 Evaluation of hydroxyl radical scavenging activity.....	51
3.4.2 Evaluation of hypochlorous acid scavenging activity assay .....	53
3.4.3 Evaluation of superoxide anion scavenging activity.....	54
3.4.4 Evaluation of hydrogen peroxide scavenging activity.....	56
3.5 Ferric reducing antioxidant power (FRAP) .....	57

3.6 Oxygen radical absorbance capacity (ORAC) .....	58
3.7 Ferric thiocyanate (FTC) assay .....	60
3.8 Cell culture and treatment.....	61
3.9 Cell viability assay .....	62
3.10 Measurement of intracellular ROS by flow cytometry assay .....	63
3.11 Measurement of apoptotic cells .....	64
3.12 Measurement of superoxide dismutase activity .....	66
3.13 Measurement of catalase activity .....	67
3.14 Measurement of glutathione peroxidase activity.....	68
3.15 Measurement of intracellular total glutathione levels .....	70
3.16 Measurement of an Nrf2 transcription factor.....	71
3.17. Western blot analysis .....	73
3.18. Statistical analysis .....	74
CHAPTER 4 RESULT .....	75
4.1 Phytochemical constituent of UCP .....	75
4.2 Evaluation of the antioxidant potential of UCP .....	85
4.2.1 Determination of antioxidant scavenging activity .....	85
4.2.1.1 Hydroxyl radical scavenging activity.....	85
4.2.1.2 Hypochlorous acid scavenging .....	87
4.2.1.3 Superoxide anion scavenging activity.....	89
4.2.1.4 Hydrogen peroxide scavenging activity.....	91
4.2.2 Determination of UCP capacity.....	93
4.2.2.1 Ferric Reducing Antioxidant Power .....	93

4.2.2.2 Oxygen radical absorbance capacity .....	95
4.2.2.3 Ferric Thiocyanate .....	98
4.3 Preventive effect of UCP against H <sub>2</sub> O <sub>2</sub> -induced cell death.....	100
4.4 Effect of UCP on H <sub>2</sub> O <sub>2</sub> -induced EA hy926 cell apoptosis .....	101
4.5 Effect of UCP on intracellular ROS .....	103
4.6 Effect of UCP on endogenous enzymatic antioxidant activity and glutathione levels .....	106
4.6.1 Effect of UCP on SOD activity .....	106
4.6.2 Effect of UCP on CAT activity.....	107
4.6.3 Effect of UCP on GPX activity .....	109
4.6.4 Effect of UCP on total GSH levels .....	111
4.7 Effect of UCP on the cell signaling pathways.....	112
4.7.1 Effect of UCP on Akt phosphorylation.....	112
4.7.2 Effect of UCP on p38 phosphorylation.....	113
4.7.3 Effect of UCP on JNK phosphorylation .....	115
4.7.4 Effect of UCP on NF- $\kappa$ B phosphorylation.....	117
4.7.5 Effect of UCP on Nrf2 phosphorylation and transcription factor .....	118
CHAPTER 5 SUMMARY DISCUSSION AND SUGGESTION .....	122
REFERENCES.....	125
VITA .....	141

## TABLE OF TABLES

	Page
Table 1 Classification of ROS .....	9
Table 2 Production of ROS and RNS by peroxisomal enzymes.....	11
Table 3 Appearance of papaya fruit in different ripening stages.....	42
Table 4 Antioxidant capacity of papaya fruit in different ripening stages.....	42
Table 5 The gradient elution of quercetin and chlorogenic acid in HPLC detection .....	51
Table 6 Linear regression and IC50 values of Trolox and UCP on OH <sup>•</sup> scavenging activity.....	85
Table 7 Linear regression and IC50 values of ascorbic acid and UCP on HOCl scavenging activity.....	87
Table 8 Linear regression and IC50 values of ascorbic acid and UCP on O <sub>2</sub> <sup>-•</sup> scavenging activity.....	89
Table 9 Linear regression and IC50 values of Trolox and UCP on H <sub>2</sub> O <sub>2</sub> scavenging activity.....	91

## TABLE OF FIGURES

	Page
Figure 1 Enzymatic sources of ROS production.....	13
Figure 2 Exogenous sources of ROS.....	14
Figure 3 Types of antioxidant enzymes and their reaction.....	16
Figure 4 The interrelationship of vitamins and GPX thiol cycle.....	19
Figure 5 Lipid peroxidation of PUFA.....	21
Figure 6 Protein oxidation and their effects.....	22
Figure 7 Effect of ROS on DNA damage and mutagenesis.....	24
Figure 8 MAPK pathway activation by ROS.....	26
Figure 9 ROS effect on NF- $\kappa$ B pathway.....	27
Figure 10 Response of Keap1-NRF2-ARE signaling pathway to ROS.....	28
Figure 11 ROS induce cell death.....	31
Figure 12 Vascular tone regulation by NO and ET1.....	33
Figure 13 Causes of endothelial dysfunction and eNOS uncoupled.....	36
Figure 14 ROS induce endothelial cell inflammation via MAPK/c-Jun and NF $\kappa$ B pathways.....	38
Figure 15 The reaction of hydroxyl radical scavenging activity.....	52
Figure 16 The reaction of hypochlorous acid scavenging activity.....	53
Figure 17 The reaction of superoxide anion scavenging activity.....	55
Figure 18 The reaction of hydrogen peroxide scavenging activity.....	56
Figure 19 The reaction of FRAP assay.....	57
Figure 20 The reaction of ORAC assay.....	59
Figure 21 The reaction of FTC assay.....	60

Figure 22 The reaction of MTT assay.....	62
Figure 23 The reaction of DCFH-DA staining .....	63
Figure 24 The reaction of Hoechst and PI staining .....	65
Figure 25 The reaction of SOD ELISA kit .....	66
Figure 26 The reaction of CAT activity assay .....	67
Figure 27 The reaction of GPX activity assay .....	69
Figure 28 The reaction of tGSH levels assay.....	70
Figure 29 The reaction of Nrf2 transcription factor ELISA kit .....	72
Figure 30 The HPLC analytical chromatography graph of ascorbic acid.....	76
Figure 31 The HPLC analytical chromatography graph of ellagic acid. ....	78
Figure 32 The HPLC analytical chromatography graph of gallic acid. ....	80
Figure 33 The HPLC analytical chromatography graph of quercetin.....	82
Figure 34 The HPLC analytical chromatography graph of chlorogenic acid.....	84
Figure 35 The OH <sup>•</sup> scavenging activity graph of standard Trolox and UCP.....	86
Figure 36 The HOCl scavenging activity graph of standard ascorbic acid and UCP. ....	88
Figure 37 The O <sub>2</sub> <sup>•-</sup> scavenging activity graph of standard ascorbic acid and UCP. ....	90
Figure 38 The H <sub>2</sub> O <sub>2</sub> scavenging activity graph of standard Trolox and UCP. ....	92
Figure 39 The linear regression curve data of FRAP assay. ....	94
Figure 40 The ORAC assay graph data of standard Trolox. ....	96
Figure 41 The ORAC assay curve of UCP. ....	97
Figure 42 The linear regression curve of the Trolox equivalent of UCP. Data are shown as mean ± SEM (n ≥ 3) .....	98
Figure 43 The linear regression curves of Trolox standard and UCP in FTC assay. ....	99

Figure 44 The histogram chart data of H <sub>2</sub> O <sub>2</sub> toxicity on EA hy926 cells. ....	100
Figure 45 The histogram data of UCP preventive effect on H <sub>2</sub> O <sub>2</sub> -induced cell death... ..	101
Figure 46 The apoptotic EA hy926 cells stained with Hoechst and PI under the fluorescence microscope.....	102
Figure 47 The histogram of percent apoptotic cells of EA hy926 cells after treatment. ....	103
Figure 48 The UCP antioxidant effect on intracellular ROS of H <sub>2</sub> O <sub>2</sub> -induced cells oxidative stress.....	105
Figure 49 The effect of UCP pretreated on SOD activity.....	107
Figure 50 Effect of UCP on CAT activity. ....	108
Figure 51 The UCP effect on GPX activity of H <sub>2</sub> O <sub>2</sub> -induced EA hy926 cell oxidative stress. ....	110
Figure 52 UCP effect on GSH level of H <sub>2</sub> O <sub>2</sub> -induced cell oxidative stress. ....	111
Figure 53 The Akt protein response to UCP pretreated on H <sub>2</sub> O <sub>2</sub> -induced EA hy926 cell oxidative stress.....	113
Figure 54 The p38 phosphorylation response of UCP pretreated on H <sub>2</sub> O <sub>2</sub> -induced cell oxidative stress.....	114
Figure 55 The JNK phosphorylation response to UCP pretreated on H <sub>2</sub> O <sub>2</sub> -induced cell oxidative stress.....	116
Figure 56 The NF- $\kappa$ B protein response of UCP pretreated on H <sub>2</sub> O <sub>2</sub> -induced EA hy926 cell oxidative stress. ....	118
Figure 57 Effect of UCP preincubation to Nrf2 activation on H <sub>2</sub> O <sub>2</sub> -induced EA hy926 cell oxidative stress.....	119
Figure 58 UCP pretreatment effect on the Nrf2 transcription factor on H <sub>2</sub> O <sub>2</sub> -induced EA hy926 cell oxidative stress. ....	121



## LIST OF ABBREVIATIONS

$^1\text{O}_2$	Singlet oxygen
8-OHdG	8 hydroxyl-2'-deoxyguanosine
AA	Arachidonic acid
AAPH	2,2'-azobis(2-amidino-propane) dihydrochloride
ADMA	Asymmetric dimethylarginine
AIF	Apoptosis inducing factor
Akt	Protein kinase B
Ang2	Angiopoetin-2
AMPK	AMP-activated protein kinase
ANOVA	One-way analysis of variance
APC	Activated protein C
APCs	Antigen presenting cells
AP-1	Activator protein 1
ARE	Antioxidant response element
ASK1	Apoptosis signal-regulating kinase 1
AT	Anti-thrombin
ATP	Adenosine triphosphate
AUC	Area under the curve
$\text{BH}_4$	Tetrahydrobiopterin
$\text{BH}_2$	Dihydrobiopterin
BAD	Bcl-2-associated death promoter
BBB	Blood brain barrier
bFGF	basic fibroblast growth factor
BMK1	Big-MAPK-1
BSA	Bovine serum albumin

CaMKII	Ca/calmodulin independent protein kinase II
CAT	Catalase enzyme
cGMP	Cyclic guanosine monophosphate
CH <sub>3</sub>	Methyl group
CoQ	Coenzyme Q
COPD	Chronic obstructive pulmonary disease
COX	Cyclooxygenase
Cu	Copper
Cul3	Culin E3-ubiquitin ligase
CVD	Cardiovascular disease
Cyt c	Cytochrome C
CYP	Cytochrome p450
DCs	Dendritic cells
DCFH-DA	2',7'-Dichlorofluorescein diacetate
DMEM	Dulbecco's modified Eagle medium
DMSO	Dimethylsulfoxide
DNA	Deoxyribonucleic acid
dsDNA	Double strand DNA
DTNB	5,5'-dithiobis(2-nitrobenzoic acid)
DUBs	Deubiquitinases
DUSP	Dual-specificity phosphatase
EA hy926	Human endothelial cell line
ECs	Endothelial cells
ECL	Enhanced chemiluminescence
ECM	Extracellular matrix
EDTA	Ethylenediaminetetraacetic acid
EGF	Epidermal growth factor

eNOS	Endothelial nitric oxide synthase
ERK	Extracellular signal-regulated protein kinase
ERO1	ER oxidoreductin 1
ET1	Endothelin-1
FAK	Focal adhesion kinase
FBS	Fetal bovine serum
Fe	Ferrous
FeCl <sub>3</sub>	Ferrous (III) chlorite
FeSO <sub>4</sub>	Ferrous (II) sulfate
FGF2	Fibroblast growth factor
FOXO	Forkhead box O
FRAP	Ferric reducing antioxidant powder
FTC	Ferric thiocyanate
GDP	Guanosine diphosphate
GPX	Glutathione peroxidase
GR	Glutathione reductase
GRB2	Growth Factor Receptor Bound Protein 2
GSH	Glutathione reduced form
GSSG	Glutathione oxidized form
GTP	Guanosine triphosphate
GTPCH	GTP cyclohydrolase
H <sup>+</sup>	Proton
H <sub>2</sub>	Hydrogen
HCl	Hydrochloric acid
HIF-1	Hypoxia-inducible factor 1
HNE	4-hydroxynonenal
HOBr	Hypobromide acid

HOCl	Hypochlorous acid
H <sub>2</sub> O <sub>2</sub>	Hydrogen peroxide
HPLC	High-performance liquid chromatography
HRP	Horseradish peroxidase
HS	Heparansulfate
H <sub>2</sub> SO <sub>4</sub>	Sulfuric acid
HUVEC	Human umbilical vein endothelial cells
HVA	Homovalinic acid
IAPs	Inhibitor of apoptosis proteins
ICAM1	Intracellular adhesion molecule 1
IgG	Immunoglobulin G
IgM	Immunoglobulin M
IKK	IκB kinase complex
iNOS	Inducible nitric oxide synthase
IQGAP1	IQ Motif Containing GTPase Activating Protein 1
JAM	Junctional adhesion molecule
JNK	C-Jun N-terminal kinase
Keap1	Kelch-like ECH-associate protein 1
KH <sub>2</sub> PO <sub>4</sub>	Potassium phosphate buffer
KIO <sub>4</sub>	Potassium periodate
KOH	Potassium hydroxide
L <sup>•</sup>	Lipid radical
LDL	low-density lipoprotein
LOO <sup>•</sup>	Lipid peroxy radical
LOX	Lipoxygenases
LOX-1	lectin-like oxidized LDL receptor 1
MAPK	Mitogen-activated protein kinase

MAPKK	Mitogen-activated protein kinase kinase
MAPKKK	Mitogen-activated protein kinase kinase kinase
MCP-1	Monocyte chemoattractant protein-1
MDA	Malondialdehyde
MeOH	Methanol
MHC I	Major histocompatibility class I
MHC II	Major histocompatibility class II
MLCK	Myosin light chain kinase
MLKL	Mixed lineage kinase domain-like
MMP	Matrix metallo-protease
MPK	MAP kinase phosphatase
MPO	Myeloperoxidase
mTOR	Mammalian target of rapamycin
MTT	4,5-dimethylthiazol-2-yl)-2,5-diphenyltetrazolium bromide
NaBH <sub>4</sub>	Sodium borohydride
NaCl	Sodium chloride
NADH	Nicotinamide adenine dinucleotide
NaF	Sodium fluoride
NaHCO <sub>3</sub>	Sodium bicarbonate
Na <sub>2</sub> HPO <sub>4</sub>	Sodium phosphate dibasic
NaOCl	Sodium hypochlorite
NAC	N-acetylcysteine
NADPH/NADP <sup>+</sup>	Nicotinamide adenine dinucleotide phosphate
NBT	Nitro blue tetrazolium
NF- <del>κ</del> B	Kappa-light-chain-enhancer of activated B cells
NIK	NF-kappa-B-inducing kinase
nNOS	Neuronal nitric oxide synthase

NO/NO <sup>•</sup>	Nitric oxide
NOS	Nitric oxide synthase
NOX	NADPH oxidase
NOX4	NADPH oxidase 4
Nrf2	Nuclear factor (erythroid-derived 2)-like-2
O <sub>2</sub>	Oxygen
O <sub>2</sub> <sup>•-</sup>	Superoxide anion
OH <sup>•</sup>	Hydroxyl radical
OONO <sup>-</sup>	Peroxynitrite
ORA1/CRAC	Calcium release-activated calcium channel protein 1
ORAC	Oxygen radical absorbance capacity
Ox-LDL	Oxidized LDL
PAGE	poly acrylamide gel electrophoresis
PAMPs	Pathogen-associated molecular pattern
PAR-1	Protease-activated receptor 1
PARs	Pattern-recognition receptor
PB	Phosphate buffer
PBS	Phosphate buffer saline
PC	Protein C
PDGF	Platelet-derived growth factor
PGE <sub>2</sub>	Prostaglandin E <sub>2</sub>
PGG <sub>2</sub>	Prostaglandin G <sub>2</sub>
PGH <sub>2</sub>	Prostaglandin H <sub>2</sub>
PI	Propidium iodide
PI3K	Phosphoinositide-3-kinase
PIP2	Phosphatidylinositol 4,5-di phosphate
PIP3	Phosphatidylinositol 3,4,5-di phosphate

PKA	Protein kinase C
PKC	Protein kinase C
PKC- $\alpha$	Protein kinase C alpha
PKD	Protein kinase D
PKE	Protein kinase E
PMS	Phenazine methosulfate
PMSs	Polymorphonuclear leukocytes
PPAR $\alpha$	Proliferator-activated receptor alpha
PPRs	Pattern-recognition receptor
PUFA	Polyunsaturated fatty acid
PTEN	Phosphatase and tensin homolog (PTEN)
PVDF	Polyvinylidene difluoride
Q	Ubiquinone
Q $^{\cdot-}$	Semiquenone
R $^{\cdot}$	Radical
Rbx1	Cul3/Ring-Box
RIP1	Interacting protein kinase 1
RIP3	Interacting protein kinase 3
RFU	Reactive fluorescent unit
RNS	Reactive nitrogen species
RO $^{\cdot}$	Alkoxy radical
ROH	Organic alkoxide
ROO $^{\cdot}$	Peroxy radical
ROOH	Organic peroxide
ROS	Reactive oxygen species
SCN	Thiocyanate
SD	Standard deviation

SDS-PAGE	SDS-poly acrylamide gel electrophoresis
SEM	standard error of the mean
sGC	Soluble guanylatecyclase
Smac	Second mitochondria-derived activator of caspases
SMCs	Smooth muscle cells
SOD	Superoxide dismutase
SOS	Son of sevenless protein
TBA	2-Thiobarbituric acid
TBST	Tris buffer saline containing 0.1% tween
TCA	Trichloroacetic acid
TEMED	Tetramethylethylenediamine
TLRs	Toll-like receptors
TNB	5-thio-2-nitrobenzoic acid
TNF- $\alpha$	Tumor necrosis factor-alpha
TNFR	Tumor necrosis factor receptor
t-PA	Tissue-type plasminogen activator
TPTZ	2,4,6-Tri(2-pyridyl)-s-triazine
TRAIL-R	TNF-related apoptosis-inducing ligand
Trolox	6-Hydroxy-2,5,7,8-tetramethylchroman-2-carboxylic acid
TRP	transient receptor potential
Trx	Thioredoxin
TrxP	Thioredoxin peroxidase
TrxR	Thioredoxin reductase
Ub	Ubiquitin
UCP	Unripe <i>Carica papaya</i>
UPS	Ubiquitination/Proteosome system
VCAM-1	Vascular cell adhesion protein 1



VE-cadherin	Vascular endothelial cadherin
VEGF	Vascular endothelial growth factor
VEGFR	Vascular endothelial growth factor receptor
WHO	World Health Organization
WST-1	(2-(4-Iodophenyl)- 3-(4-nitrophenyl)-5-(2,4-disulfophenyl)-2H-tetrazolium, monosodium salt
XO	Xanthine oxidase
Zn	Zinc



# CHAPTER 1

## INTRODUCTION

### 1.1 Background

Reactive oxygen species (ROS) are highly reactive molecules composed of the oxygen atom, including hydroxyl radical ( $\text{OH}^\bullet$ ), hypochlorite acid ( $\text{HOCl}$ ), hydrogen peroxide ( $\text{H}_2\text{O}_2$ ), and superoxide anion ( $\text{O}_2^{\bullet-}$ ). ROS are formed by sequential reduction of oxygen via electron addition. ROS are derived from endogenous and exogenous sources. The endogenous sources are intracellular ROS that are generated from cellular metabolism and signaling cascades consisting of mitochondrial respiratory chains, peroxisomal metabolism, endoplasmic reticulum redox reactions, NADPH oxidase (NOX), xanthine oxidase (XO), nitric oxide synthase (NOS), Cytochrome P450 (CYP), cyclooxygenases (COXs), Myeloperoxidases (MPOs) and others (1). The redox-sensitive organelles including mitochondria, peroxisome, and endoplasmic reticulum are the main sources of ROS, in which oxygen obtains electron generating  $\text{O}_2^{\bullet-}$  and catalyzed into  $\text{H}_2\text{O}_2$  by enzymatic antioxidants (2, 3). The exogenous sources, of ROS are derived from environments such as tabaco smoking, radiation, ionization, and chemicals (4). ROS participates in the physiological activity of cells via cell signaling pathways involving cell proliferation, differentiation, migration, inflammation, aging, and death (5, 6). In the body defense mechanisms, ROS are released from phagocytes leading to the destruction of pathogenic microbes through an activation of the immune system and the direct elimination of the microorganisms (7). In normal conditions, endogenous ROS act as a key role in driving normal cell functions while high ROS levels induce oxidative stress. This event can activate the immune system by elevating the pro-inflammatory cytokine secretion and immune cell proliferation causing autoimmunity, stem cell exhaustion, and premature aging (8). Moreover, oxidative stress can cause cell dysfunction, damage, and death via cell signaling and death pathway (9). To balance ROS, antioxidant mechanisms are activated to eliminate the excessive ROS by the activation of enzymatic antioxidants including superoxide dismutase (SOD), glutathione peroxidase (GPX), and

catalase (CAT). SOD is a catalytic enzyme that converting  $O_2^{\cdot-}$  into  $O_2$  and  $H_2O_2$ . GPX cycle catalyzes  $H_2O_2$  into  $H_2O$  which has the same function as CAT (10, 11). In addition, non-enzymatic antioxidants such as ascorbic acid (vitamin C), alpha-tocopherol (vitamin E), and others can protect oxidative damage and eliminate ROS via redox reaction (4). The lack of balance between ROS and antioxidants is the cause of many human diseases such as cardiovascular diseases (CVDs), which arise from endothelial dysfunction and vascular injury (12). ROS-sensitive signaling pathway activation is consistently increased in cancer via the function of normal cellular mechanisms such as cell growth/ proliferation (13). Moreover, ROS directly stimulate immune pathways inducing exacerbation of autoimmune response in autoimmune disease (14). Endothelial cells (ECs) are a thin layer of simple squamous cells lining the surface of the blood vessel. The vascular walls formed by ECs are selective permeable membrane barriers that protect the invasion of microorganisms and selectively allow biochemical molecules passing through the lumen and surrounding tissues (15). For example, the blood-brain barrier (BBB) is a highly specialized transporter, which regulates the access of molecules being transported into the brain. BBB disruption can cause edema and neuropathological disorders (16). ECs also involve in angiogenesis and vasculogenesis by the stimulation of angiogenic factors and vascular endothelial growth factor (VEGF) to induce filopodia production, cell proliferation, and, migration leading to blood vessel formation and stabilization by pericytes (17). The main function of ECs is regulating by the action of vascular tone. In which, endothelial nitric oxide synthase (eNOS) to produce nitric oxide (NO) that induce smooth muscle relaxation causing vasodilation via soluble guanylyl cyclase (sGC) activation. Which, the relaxation of blood vessel, blood flow is rised leading to the reduction of vascular resistance, which increases the transportation of  $O_2$  into  $O_2$ -needed tissues. This function facilitates the elasticity of the blood vessel responding to shear stress and preventing an increase of blood pressure (18). EC functions also include anticoagulation and thrombosis formation via anticoagulant protein C (PC) and heparan sulfate pathways. These processes induce binding of thrombin and PC to produce activated PC (APC) (19) and activation of anti-

thrombin (AT) via binding of heparan sulfate and AT to inhibit thrombin formation (20). Moreover, ECs have an important role in the immune system, in which pro-inflammatory cytokines released from ECs induce attachment and invasion of immune cells due to immune response (21). Taking all together, ECs demonstrate an important role to prevent risks of CVDs and other diseases.

Endothelial dysfunction is the loss of endothelial homeostasis causing endothelial systematic disorder. Oxidative stress is the main cause of endothelial dysfunction and cell death via an imbalance of NO production and inflammatory cytokine release. ROS are the main cause of uncoupled eNOS under oxidative stress condition, in which tetrahydrobiopterin ( $BH_4$ ), an eNOS cofactor is oxidized to dihydrobiopterin ( $BH_2$ ) producing  $O_2^{\cdot-}$ . The reaction between produced- $O_2^{\cdot-}$  and NO generates peroxy nitrite ( $OONO^{\cdot}$ ). Uncoupled eNOS reduces NO production and induces an imbalance of vasodilation and vasoconstriction, leading to endothelial dysfunction. This incidence reduces blood pressure and shear stress resistance on vascular walls leading to endothelial damage and inflammation, inducing atherosclerotic plaque formation, and CVDs in the end (22). ROS cause ECs inflammation and injury, which increase inflammatory cytokines (IL-6) and their signaling molecules such as nuclear factor kappa- B (NF- $\kappa$ B) (23). ROS involve in ECs death and survival via mitogen-activated protein kinases (MAPK) and phosphatidylinositol-3-kinase (PI3K)/protein kinase B (Akt) signaling pathways (6). ROS also induce low-density lipoprotein (LDL) oxidation under endothelial walls, which can be converted to oxidized LDLs (oxLDLs), induction of foam cell formation, and inflammation, leading to atherosclerotic plaque formation. Plaque formation is the main cause of CVDs (24), which is reported as the main cause of death worldwide (WHO fact sheet). Therefore, reducing ROS formation in ECs is interesting in the aspect of cardiovascular research to reduce the risks of CVDs.

The  $H_2O_2$ -induced oxidative stress is the current model for studying cellular oxidative damage of ECs in vitro research, in which  $H_2O_2$  can induce ECs survival, apoptosis, cell death, inflammation, and antioxidant via signaling pathways composing

of MAPK, VEGF, Akt, NF- $\kappa$ B, cyclooxygenase-2 (COX2) and nuclear factor erythroid 2-related factor 2 (Nrf2) (25-28). Previous studies report that curcumin attenuates oxidative damage and cell death in a human endothelial cell line (EA hy926) via the Akt/mTOR pathway (29) and *Phyllanthus emblica* protected against H<sub>2</sub>O<sub>2</sub>-induced cell death (30). Moreover, the primary ingredient of garlic named allicin (31) and grape named resveratrol attenuate H<sub>2</sub>O<sub>2</sub>-induced apoptosis in HUVECs via oxidative stress pathway (32). Isoquercitrin inhibits H<sub>2</sub>O<sub>2</sub>-induced apoptosis in EA hy926 cells via the PI3K/ Akt/ GSK3 $\beta$  signaling pathway (33). Ginsenoside Rb1 stimulated the sirtuin-1 pathway, which protected the senescence of HUVECs induced by H<sub>2</sub>O<sub>2</sub> (34). The preventive effect of natural compounds is interest for in alternative treatment for ROS-induced human diseases.

*Carica papaya* is a tropical fruit that belongs to the family of Caricaceae. The plant grows in tropical areas worldwide such as South-East Asia, South American, and Mexico. Papaya serves as a component of meals in many cuisines. In Thailand, Papaya is called Malakor, in which unripe fruit is an important ingredient of Thai food, known as papaya salad, the most popular Thai dish. Papaya fruits are nutritional containing vitamins A, B, and C, terpenoids, alkaloids, flavonoids, steroids, papain, and others (35). Previous studies have shown the preventive effects of many parts of papaya (36). For example, the papaya seed water extract had an antioxidant effect and decreased human skin fibroblast cell death in H<sub>2</sub>O<sub>2</sub>-induced oxidative stress (37). Papaya also increases the skin wound healing rate in a rat model (38). Unripe papaya fruit extract administration ameliorated oxidative stress in acrylamide-exposed rats by increasing antioxidant enzymes (SOD, GPX, and CAT), immune (IgG and IgM) mechanism, and decreasing lipid peroxidation (39). Different parts of the papaya plant showed significant anti-inflammatory and immunomodulatory activity (40). Moreover, it also showed significant anti-cancer activity (41) and reduced risks of other human diseases, including CVDs, neurodegenerative, and infectious diseases (42-44). However, unripe papaya fruit activity in cardiovascular research had not been reported. Therefore, this study is aimed to investigate the antioxidant activity of unripe *Carica papaya* fruit and its

mechanism of action against  $H_2O_2$ -induced cell death in human endothelial cells. In the experiment, unripe *Carica papaya* fruits were crushed to unripe *Carica papaya* fruit juice (UCP) using a juice extractor. The UCP was filtered and lyophilized to dry powders and stored at  $-40\text{ }^\circ\text{C}$  until used. The dry UCP powders were used for experimental studies of their antioxidant by using antioxidant scavenging and capacity assay. The preventive effect of dry UCP powder on ECs oxidative stress were evaluated using the  $H_2O_2$ -induced EA hy926 cell oxidative stress model.

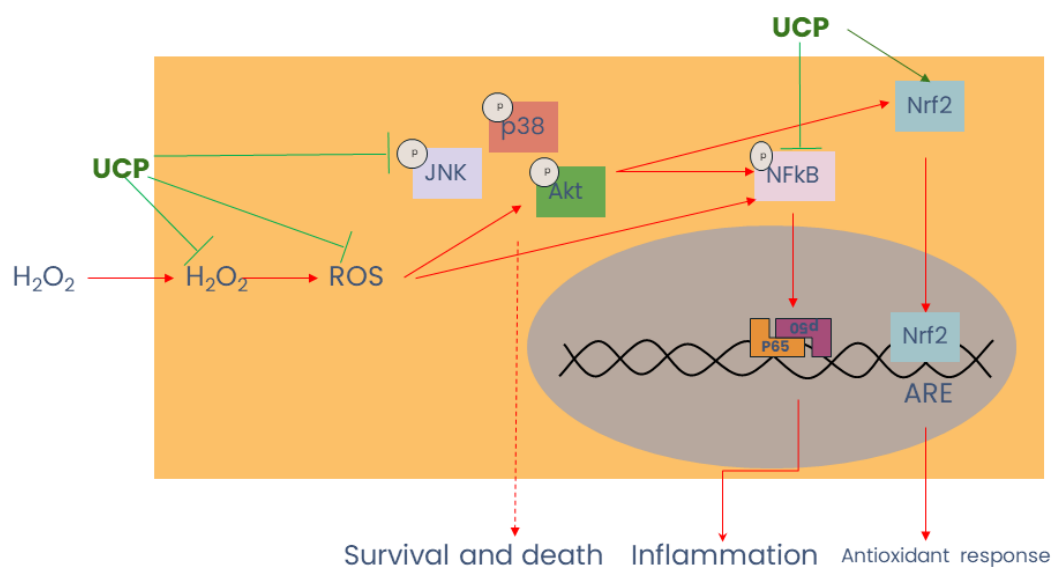
## 1.2 Objective of the study

To evaluate the preventive effect and mechanisms of unripe *Carica papaya* fruit juice extract on  $H_2O_2$ -induced EA hy926 cell oxidative stress and death.

## 1.3 Hypothesis

Unripe *Carica papaya* juice extract prevents  $H_2O_2$ -induced EA hy926 cell death by a decrease of intracellular ROS, modification of signaling pathways, and antioxidant mechanisms.

## 1.4 Conceptual framework



## CHAPTER 2

### LITERATURE REVIEW

#### 2.1 Reactive oxygen species (ROS)

ROS are highly reactive chemical species containing oxygen atoms. It can contain one or more unpaired electrons in the outer orbits of the electron shell, which makes them highly reactive and unstable. The instability of ROS facilitates them to attract electrons from other molecules to attain stability. The loss of electrons causes a chain reaction cascade and damages nearby cells. The chain reactions involved in cell signaling pathways play both benefits and toxicity roles in the living cells. Imbalance of ROS is toxic to living cells by damaging biomolecules, including lipid, protein, DNA, and carbohydrate. These biomolecules damage lead to various disease conditions (45).

##### 2.1.1 Classification of ROS

ROS are classified into two groups composed of radicals and non-radicals. They are derived from endogenous (a cellular mechanism) and exogenous sources, which are the cause of various diseases.

##### 2.1.1.1 Radicals

The radical group contains unpaired electrons, which makes them unstable and can lead to other highly reactive molecules. The radical species can obtain or donate electrons from other molecules to attain their stability that instantly damage other compounds and severe damage to the cells (45). The members of this group are  $\text{OH}^\cdot$ ,  $\text{O}_2^\cdot$ , alkoxy radical ( $\text{RO}^\cdot$ ), and peroxy radical ( $\text{ROO}^\cdot$ ).

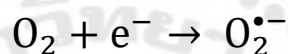
##### 2.1.1.1.1 $\text{OH}^\cdot$

$\text{OH}^\cdot$  is formed by intracellular Fenton reaction, in which  $\text{Fe}^{2+}$  is oxidized by  $\text{H}_2\text{O}_2$  into  $\text{Fe}^{3+}$  producing  $\text{OH}^\cdot$  and  $\text{OH}^-$ . This ROS is an extremely reactive free radical that can severely damage cellular biological molecules, including protein, DNA, lipid, and carbohydrate, consequential damage, and disturb cellular mechanisms (46).



#### 2.1.1.1.2 $O_2^{\bullet-}$

$O_2^{\bullet-}$  is normally generated in cellular mechanisms, mostly mitochondrial respiratory chain and enzymatic reactions, including XO, LOX, COX, and NOX. This radical generates from the reduction reaction of  $O_2$  via these mechanisms, which obtained electrons made them highly reactive. This reactive molecule can convert to other ROS and RNS such as  $H_2O_2$  via catalytic enzyme SOD and peroxynitrite (ONOO $^-$ ) when reacting with nitric oxide (NO) leading to cellular molecule damaged and changed in the signaling pathways causing various diseases (47, 48).



#### 2.1.1.1.3 $RO\cdot$ and $ROO\cdot$

The decomposition of alkyl peroxides (ROOH) can generate  $RO\cdot$  and  $ROO\cdot$ . The reaction of the alkyl radical ( $R\cdot$ ) and  $O_2$  also produces  $ROO\cdot$ . These radicals are frequently found in lipid peroxidation processes producing lipid peroxidation end-products including 4-hydroxy-2-nonenal (4-HNE) and malondialdehyde (MDA), which induce cell damage and death (49).

#### 2.1.1.2 Non-radicals

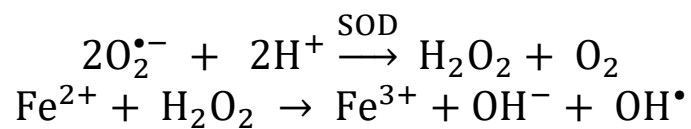
Non-radical contain oxygen molecules likely radical group but they are absent unpaired electrons. Although, this group is not a highly reactive molecule it is easy to decompose into free radicals and attacks biomolecules of living cells. Members include  $H_2O_2$ , HOCl, hypobromous acid (HOBr), ozone ( $O_3$ ), and singlet oxygen ( $^1O_2$ ). The mainly effective intracellular ROS in this group is  $H_2O_2$  and HOCl (43).

##### 2.1.1.2.1 $H_2O_2$

$H_2O_2$  is generated by the catalyzation of SOD, which converts  $O_2^{\bullet-}$  into  $H_2O_2$  and  $O_2$  (50). Although it is not free radical, it can induce oxidative stress and damage biological molecules by producing  $OH\cdot$ , which is strongly reactive via Fenton reaction (46, 51). Besides,  $H_2O_2$  plays an important role in redox signaling pathways on



cell homeostasis and pathology, which can regulate cell proliferation, inflammation, and death (52, 53).



#### 2.1.1.2.2 HOCl

HOCl is produced via the catalyzation of  $\text{H}_2\text{O}_2$  and chloride (Cl) by MPO (54). It is the major ROS to protect against microorganisms by direct attacking and inducing oxidative stress. However, excess ROS can induce oxidative damage in mammalian cells causing cell damage and death. Its toxicity is lower than  $\text{H}_2\text{O}_2$  (55) but has a high potential for antimicrobial effect than  $\text{H}_2\text{O}_2$  (56).

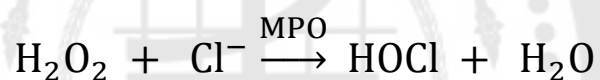


Table 1 Classification of ROS .

Reactive oxygen species (ROS)	Symbol
<b>Radical group</b>	
Superoxide anion radical	$O_2^{\cdot-}$
Hydroxyl radical	$OH^{\cdot}$
Alkoxy radical	$RO^{\cdot}$
Peroxy radical	$ROO^{\cdot}$
<b>Non-radical group</b>	
Hydrogen peroxide	$H_2O_2$
Singlet oxygen	$^1O_2$
Ozone	$O_3$
Organic peroxide	$ROOH$
Hypochlorous acid	$HOCl$
Hypobromous acid	$HOBR$

Source: Phaniendra A, Jestadi DB, and Periyasamy L. (2015) Free radicals: properties, sources, targets, and their implication in various diseases: Indian journal of clinical biochemistry p.11-26.

### 2.1.2 Sources of ROS

ROS can be produced in endogenous and exogenous sources, which living cell mechanisms are major production sites to generate intracellular ROS, and exposure of some risks from the environment also affect intracellular ROS production levels.

#### 2.1.2.1 Endogenous sources of ROS

These sources are from intracellular compartments including mitochondria, peroxisome, endoplasmic reticulum, and others. Moreover, they can be

produced by catalytic enzymes such as NOX, XO, NOS, CYP, COX, LOX, and MPO (57).

#### 2.1.2.1.1 Mitochondria

Mitochondria is the main source of  $O_2^{\bullet-}$  that are produced via a mitochondrial respiratory chain reaction. In normal conditions, NADH and  $FADH_2$  donate electrons to complex I and complex II, respectively. Then electrons flow through coenzyme Q (CoQ) and complex III. In complex III, electrons proceed to cytochrome c (Cyt c) and move to complex IV. Electrons are transferred from complex I and II to complex III to form an unstable intermediate semiquinone anion ( $Q^{\bullet-}$ ) and then the unstable semiquinone anion immediately donated an electron to  $O_2$ , resulting in  $O_2^{\bullet-}$  generation, which is the cause of cell damage (58). Excessive of  $O_2^{\bullet-}$  powerful damage on cellular biomolecules and effect on cell signaling pathways inducing cell inflammation and death. SOD is  $O_2^{\bullet-}$  eliminator to balance these ROS levels.

#### 2.1.2.1.2 Peroxisomes

The peroxisome is a metabolically active organelle, containing various enzymes, involved in lipid metabolism, including fatty acid  $\alpha$  and  $\beta$ -oxidation and ether-phospholipid biosynthesis (59).  $H_2O_2$  is the major ROS production in peroxisomal metabolism (60). ROS are degraded by the activation of nuclear receptors of the peroxisome, named peroxisome proliferator-activated receptor alpha ( $PPAR\alpha$ ), which has an important role to activate catalase in living cells (61). The ROS/RNS production in different peroxisomal enzymes is shown in table 2. Produced-ROS from peroxisome can affect the living cell on biomolecules and their signaling pathways inducing cell inflammation, aging, and death, causing various human diseases such as CVDs, neurodegenerative diseases, diabetes mellitus, and aging (61, 62).

Table 2 Production of ROS and RNS by peroxisomal enzymes

Enzyme	Substrate	ROS
Acyl CoA-oxidases (enzymes of $\beta$ -oxidase)	Fatty acids	$H_2O_2$
D-aminoacid oxidase	D-proline	$H_2O_2$
L- $\alpha$ -hydroxyl oxidase	Glycolate	$H_2O_2$
Urate oxidase	Uric acid	$H_2O_2$
Pipecolic acid oxidase	L-pipecolic acid	$H_2O_2$
Polyamine oxidase	N-Acetyl spermine/spermidine	$H_2O_2$
Nitric oxide synthase	L-arginine	NO
Sarcosine oxidase	Sarcosine, pipecolate	$H_2O_2$
D-aspartate oxidase	D-aspartate	$H_2O_2$
Xanthine oxidase	Xanthine	$O_2^{\cdot-}, H_2O_2$

Sources: Phaniendra A, Jestadi DB, and Periyasamy L. (2015) Free radicals: properties, sources, targets, and their implication in various diseases: Indian journal of clinical biochemistry p.11-26. Schrader M and Fahimi HD. (2006). Peroxisomes and oxidative stress: Biochimica et Biophysica Acta (BBA) - Molecular Cell Research p. 1755-66.

#### 2.1.2.1.3 Endoplasmic reticulum (ER)

ER is an intracellular organelle for secretory pathways that involves biosynthesis, protein folding, maturation, and assembly. ROS are produced via their enzymes, such as NADPH oxidase 4 (NOX4), CYP, and ER oxidoreductin 1 (ERO1), which  $H_2O_2$  is a major product in this source (63). The production of ROS in ER induces self-stress leads to cell death by inducing oxidative stress and damaging mitochondria,

activating apoptotic pathways. Oxidative stress and ER stress are causes of various human diseases consisting of metabolic diseases, neurodegenerative diseases, neoplastic diseases, and immune diseases (64).

The intracellular ROS sources are generated by several enzymes that can be found in the cytosol, organelles, cellular components, and metabolism (65). They are composed of NOX, XO, LOXs, MPO, NOS, COXs, and others.

The membrane-bound enzyme complex on the plasma membrane, NOX is the main phagocytic enzyme of phagocytes that produced and released  $O_2^{\cdot-}$  to phagosomes and extracellular matrix inducing oxidative stress and inflammation. XO expresses in the GI tract such as liver and small intestinal mucosa, which can be found on the plasma membrane surface and cytoplasm. XO cooperated with the NADPH cofactor catalyzes hypoxanthine into xanthine and then uric acid, in which this reaction can generate short half-life  $O_2^{\cdot-}$  and transform into  $H_2O_2$  leading to GI injury. LOXs are deoxygenated catalyzing enzymes of polyenoic fatty acid, which their reaction cycles can produce  $O_2^{\cdot-}$  via activation of NOX. MPO is a heme-enzyme that can be found in the lysosome of phagocytes. This enzyme chlorinates  $H_2O_2$  and generates HOCl, which reacts with  $H_2O_2$  to generate  $^1O_2$ . NOS generates nitric oxide using substrates L-arginine and  $O_2$  cooperating with their cofactor. Low L-arginine and cofactor ( $BH_4$ ) concentrations induce uncoupled NOS and generate  $O_2^{\cdot-}$ , which combines with NO to produce  $OONO^-$ . Production of  $OONO^-$  and NO can generate other nitrite molecules, which further interact with biological molecules by the reaction of nitration and nitrosation. COXs are bi-functional enzymes, including COX and peroxidase. Arachidonic acid (AA) is catalyzed into prostaglandin  $G_2$  ( $PGG_2$ ) then converted to prostaglandin  $H_2$  ( $PGH_2$ ) by the peroxidase enzyme and stable prostanoids. This reaction can generate  $O_2^{\cdot-}$  and prostaglandin  $E_2$  ( $PGE_2$ ), which induce oxidative damage and inflammation (Figure 1) (57).

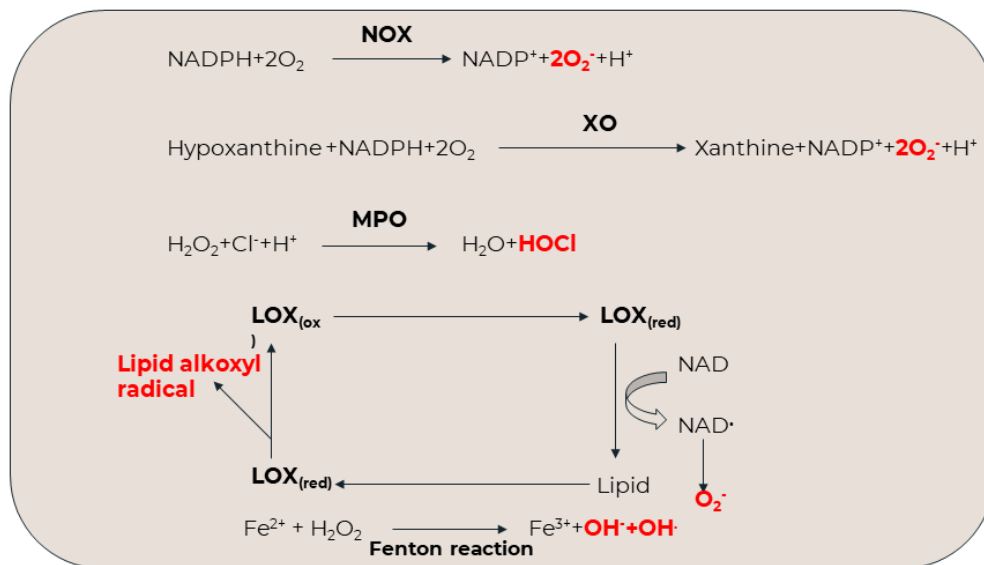


Figure 1 Enzymatic sources of ROS production

Source: Bhattacharyya A, Chattopadhyay R, Mitra S, and Crowe SE. (2014). Oxidative stress: an essential factor in the pathogenesis of gastrointestinal mucosal diseases: Physiological reviews. p. 329-54.

### 2.1.2.2 Exogenous sources of ROS

Exogenous sources include radiation, ionization, tobacco smoke, drugs, pollution, chemicals, and others. These sources can be directly or indirectly induced ROS production in the cells (Figure 2).

#### 2.1.2.2.1 Radiation

Radiation can cause direct or indirect damage to the cells. The direct action of radiation can damage DNA molecules causing cell injury and death. The surviving cell after being damaged by radiation might be transformed into cancer or other abnormal cells. The indirect action of radiation can hit molecules in the cells, such as highly reactive  $\text{OH}^\cdot$  produced by catalyzation of  $\text{H}_2\text{O}_2$  directly damage cellular biomolecules, especially DNA causing various diseases (66).

### 2.1.2.2.2 Smoking

Smoking is the most important environmental cause of human mortality. The particle phase of tobacco called tar can produce  $O_2^{\bullet-}$  which can be converted to  $H_2O_2$  and then to  $OH^{\bullet}$  leading to oxidative stress and molecular damage (67).

Other exogenous sources including heavy metals, pollution, and exercise also can generate intracellular ROS via their toxicity pathways.

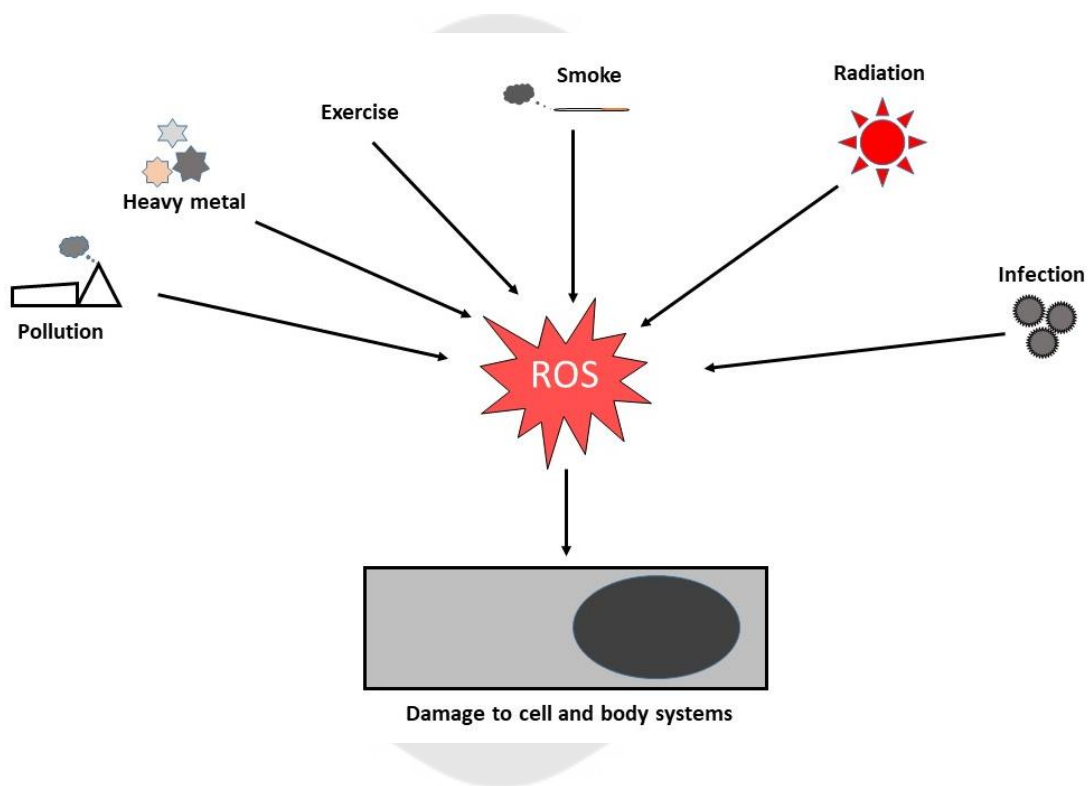


Figure 2 Exogenous sources of ROS

Source: Aseervatham GS, Sivasudha T, Jeyadevi R, and Arul Ananth D. (2013). Environmental factors and unhealthy lifestyle influence oxidative stress in humans--an overview: Environmental science and pollution research international p. 4356-69.

### 2.1.3 ROS elimination

The imbalance of ROS causes cellular disorder whereas Lowing decreases signaling of ROS-dependent signaling pathways leading to a reduction of cell proliferation, growth inability, and homeostasis. In contrast, the excess of ROS, called oxidative stress, induces cellular damage and many diseases (68). ROS can be eliminated by antioxidants, which convert reactive into stable molecular form via electron donation or electron acceptance. Some antioxidants are cofactors and substrates of enzymatic antioxidants involved in ROS elimination. Antioxidants are classified into two groups including enzymatic and non-enzymatic antioxidants.

#### 2.1.3.1 Enzymatic antioxidants

Enzymatic antioxidants are catalyzing enzymes in cell mechanisms to eliminate excessive ROS. The majority of these antioxidant enzymes include SOD, GPX, and CAT as well as thioredoxin peroxidase (TrxP).

##### 2.1.3.1.1 SOD

SOD is a catalytic enzyme that dismutates  $O_2^{\cdot-}$  into  $O_2$  and  $H_2O_2$  to protect cellular oxidative damage induced by  $O_2^{\cdot-}$ . SOD is composed of three major subtypes includes Fe/Mn-SOD, Cu/Zn-SOD, and EC-SOD. The Fe/Mn-SOD is localized in mitochondria, which has an important role in the eliminating of  $O_2^{\cdot-}$  production in mitochondria, as much as 90% . The Cu/Zn-SOD is localized in the cytoplasm and intermembrane space of mitochondria involving in scavenging mechanisms of copper reduction and reoxidation. Whereas the extracellular matrix, fluid, and cell surface are composed of EC-SOD in which acts similar to CuZn-SOD (Figure 3) (69).

##### 2.1.3.1.2 CAT

CAT is a catalytic enzyme that catalyzes  $H_2O_2$  into  $H_2O$  and  $O_2$  via the conversion of two conformations composing ferricatalase and compound I. Inactive forms of catalase including compound II and III arise after catalase exposed to  $H_2O_2$  and  $O_2^{\cdot-}$ , which can be reversed into active form at a low concentration of ROS. The reducing equivalent NADPH prevents oxidative inactivation of this enzyme by binding with CAT and reducing  $H_2O_2$  into  $H_2O$  (Figure 3) (70).



### 2.1.3.1.3 GPX

GPX is a tetrameric enzyme, which their redox cycles cooperating glutathione reduced form (GSH) convert  $\text{H}_2\text{O}_2$  into  $\text{H}_2\text{O}$ . GSH is oxidized into glutathione oxidized form (GSSG) can be reversed into GSH through NADPH and glutathione reductase (GR) and then return the glutathione redox cycle (Figure 3) (4).

### 2.1.3.1.4 TrxP

TrxP is a catalytic enzyme that converts  $\text{H}_2\text{O}_2$  into  $\text{H}_2\text{O}$  by cooperating with thioredoxin (Trx) reduced form. Trx is converted into oxidized form and can be reversed into reduced form by thioredoxin reductase (TrxR) cooperating NADPH, and return the TrxP cycle (Figure 3) (71).

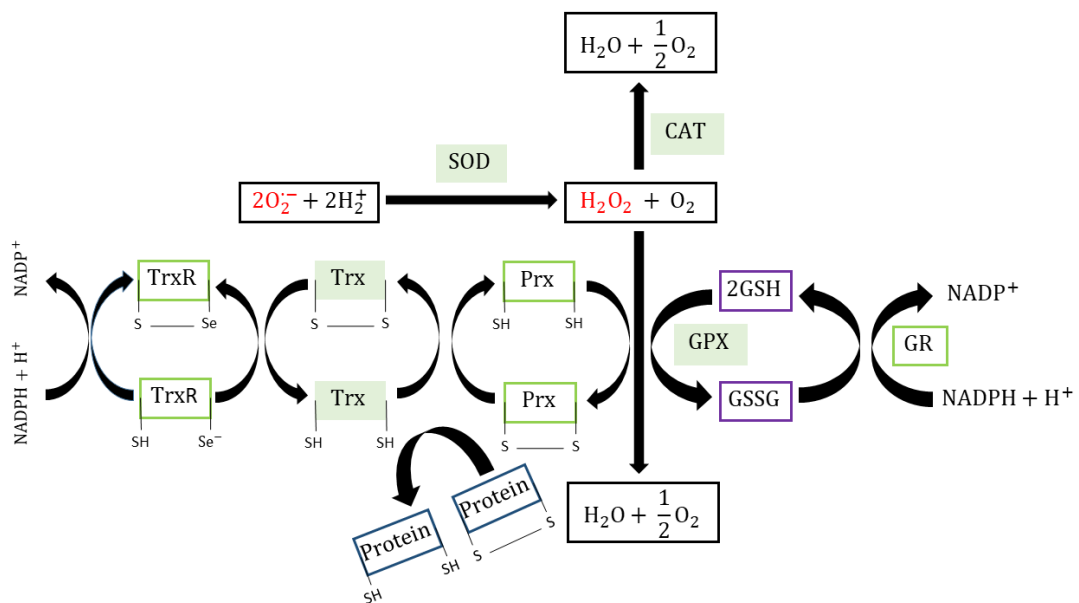


Figure 3 Types of antioxidant enzymes and their reaction

Source: Lu J, and Holmgren A. (2014). The thioredoxin antioxidant system. Free radical biology & medicine. p.75-87.

### 2.1.3.1 Non-enzymatic antioxidants

These groups are several antioxidants that can be found in endogenous and exogenous sources. The endogenous antioxidants are the intracellular components found in cellular mechanisms, including GSH, Trx, and melatonin. Exogenous antioxidants are naturally found in receiving food such as vegetables and fruit, in which these antioxidants include vitamins, carotenoids, minerals, polyphenols, flavonoids, and others.

#### 2.1.3.1.1 Endogenous antioxidants

Endogenous antioxidants are substrates of antioxidant enzymes or direct antioxidants. GSH is an antioxidant substrate in the GPX thiol cycle, which degrades  $H_2O_2$  into  $H_2O$ . The GSH and stimulated GSH-dependent enzymes are received by the intake of fruit and vegetables (57). Trx is an antioxidant substrate in the thioredoxin antioxidant thiol cycle. Cooperation of Trx peroxidase and Trx reduced form can convert  $H_2O_2$  into  $H_2O$ . Then Trx is reversed into reduced form by Trx reductase and NADPH. This antioxidant cycle can scavenge ROS with a fast reaction rate (71). Both substrates are important in thiol cycles to eliminate intracellular ROS. Melatonin is a hormone produced from the pineal gland, which can cross the blood-brain barrier. This hormone can be found in lymphocytes, retina, bone marrow, and dietary sources such as vegetables. Melatonin is a free radical scavenger by direct free radical scavenging and stimulates antioxidant enzymes. Moreover, melatonin is irreversibly oxidized, which is referred to as terminal or suicidal antioxidants (57). Thus this antioxidant group has an important role to scavenge intracellular ROS via direct antioxidant and stimulated antioxidant enzyme.

#### 2.1.3.1.2 Exogenous antioxidants

Exogenous antioxidants are compounds from natural fruits, vegetables, or other consumption sources. Examples of antioxidants are vitamins, carotenoids, alkaloids, and polyphenols (phenolic compounds, phenol compounds, and flavonoids). Vitamin C or ascorbic acid can be received from fruit and vegetables. It directly reduces ROS by electron donation and improving the thiol cycle (GPX and Trx). Moreover, heavy metal ions including Fe and Cu can induce ROS production via the

Fenton reaction, in which vitamin C can inhibit this chain reaction. Ascorbic acid is proved that the main antioxidant to protect against oxidative stress improving ROS-induced cell damage and various diseases (72). Vitamin E is one of the antioxidants that have a crucial role to protect the cell membrane from lipid peroxidation by scavenging lipid peroxy radicals ( $\text{LOO}^\bullet$ ). In which alpha-tocopherol is the most biologically active form of vitamin E. The interrelationship of glutathione-vitamin C-vitamin E is the high potential cycle on ROS detoxification by vitamins directly eliminate ROS and support the GPX thiol cycle (Figure 4) (73). Carotenoids, tetraterpenoids are substrates of vitamin A, which can be obtained from dietary sources such as fruit and vegetables, as well as some bacterial and fungi. Tetraterpenoids directly scavenge  $\text{ROO}^\bullet$ ,  $\text{OH}^\bullet$ , and  $\text{O}_2^{\bullet-}$ . Heavy metal (Cu, Mn, and Zn) are key components of the enzymatic antioxidant system, which maintain redox homeostasis. Polyphenols include flavonoids, phenol, phenolic acid, lignin, and tannin. Flavonoids inhibit endogenous sources of ROS such as XO, COX, LOX, and NOX to reduce ROS production. Moreover, they also chelate heavy metals that are the core of antioxidant enzymes to reduce ROS (4, 57, 74). Quercetin is a bioactive flavonoid in pharmacological benefits involving antioxidant and anti-inflammation to prevent CVDs and other human diseases (75). Gallic acid and chlorogenic acid are phenolic compounds, have pharmacological effects on antioxidants, anti-inflammation, and antibacterial, which reduce risks of various human diseases (76, 77). A natural phenolic antioxidant, named ellagic acid also shows a high antioxidant effect to improve and scavenge ROS (78).

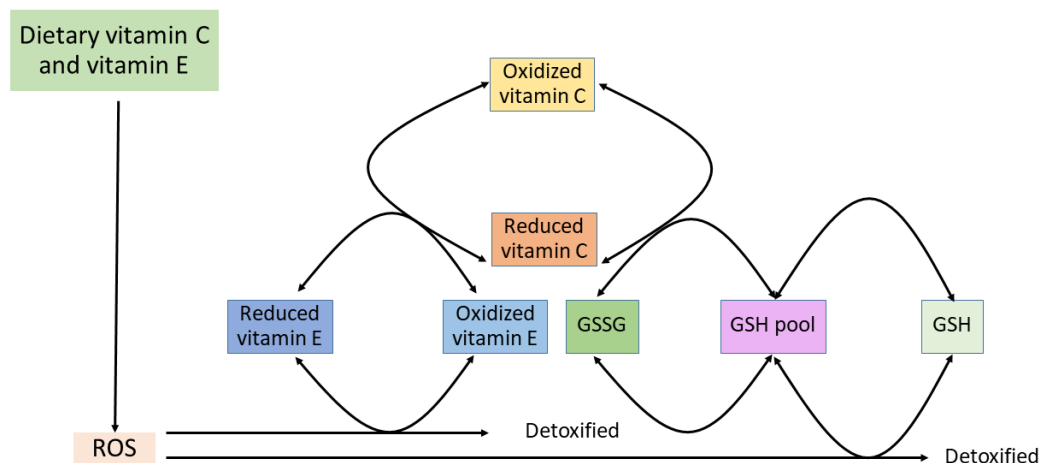


Figure 4 The interrelationship of vitamins and GPX thiol cycle

Source: Zhou S-S. (2015). Vitamin paradox in obesity: Deficiency or excess?: World Journal of Diabetes p.1158.

Non-enzymatic antioxidants show high potential effects to scavenge ROS and decrease oxidative stress leading to the reduction of cell death and inflammatory pathways. The beneficial effect of antioxidants protects against risks of human diseases for example chronic obstructive pulmonary disease (COPD), cardiovascular, autoimmune, and other diseases (79)

#### 2.1.4 ROS, Oxidative stress, and cells damage

The imbalance between ROS and antioxidants induces oxidative stress. Under oxidative stress conditions, ROS attack living cells by stealing electrons from biomolecules, and causing DNA, protein, and lipid oxidation and peroxidation. ROS also affects cell signaling pathways, resulting in the changing of cell mechanisms and leading to cell dysfunction and death. Thus damaged biomolecules and changed cell signaling pathways are mainly caused by ROS.

##### 2.1.4.1 ROS damaging biomolecules

ROS damage macromolecules consisting of DNA, carbohydrates, proteins and, lipids via oxidation and peroxidation, resulting in cellular damage and dysfunction.

#### 2.1.4.1.1 Lipid peroxidation

Lipid peroxidation is the oxidative damage of lipids by free radicals via receiving electrons of lipid membranes and other lipid components, resulting in cell damage and inflammation. The most effective in this process are polyunsaturated fatty acids (PUFA) because they contain multiple double bonds between the methyl groups ( $\text{CH}_3$ ). Double bonds cause weakness of methylene  $-\text{C}-\text{H}_2-$  bond and easier for hydrogen atom abstraction. The unpaired electron on carbon atom induces carbon-centered radical formation, which can stabilize by a molecule rearrangement of double bonds, forming conjugated diene, and  $\text{ROO}^\bullet$  after reacted with  $\text{O}_2$ . These ROS abstracts a hydrogen atom from another PUFAs and starting the chain reaction. Thus, this chain reaction initiates hydrogen abstraction by free radical ( $\text{OH}^\bullet$ ,  $\text{RO}^\bullet$ , and  $\text{R}^\bullet$ ), resulting in  $\text{ROO}^\bullet$  generation. Lipid peroxidation is a cause of lipid membrane modification, resulting in membrane disruption and further peroxidation, effects on cell physiology leading to cell dysfunction, damage, and death (80). PUFA and their metabolites have important roles in cell physiology including membrane structure, flexibility, selective permeability of the cellular membrane, cell signaling pathways, and gene expression. The peroxidative decomposition of PUFA can produce aldehydes such as MDA and HNE, which are highly stable and can damage biomolecules such as DNA (81). MDA and HNE are major oxidative products used as biomarkers of lipid peroxidation and oxidative stress (Figure 5). Lipid peroxidation affects cells and organelles composed of lipid bilayer inducing membrane permeability and finally cell death (82). Besides, in Alzheimer's disease, amyloid  $\beta$ -peptide ( $\text{A}\beta$ ) attacks on lipid membrane leading to acrolein, HNE, and MDA production and nerve cell damage (83).

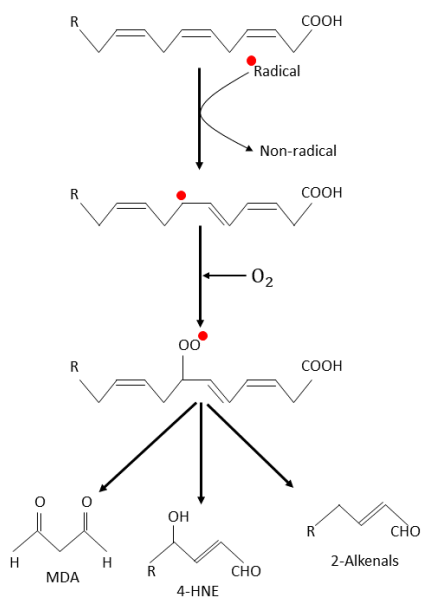


Figure 5 Lipid peroxidation of PUFA

Source: Shah D, Mahajan N, Sah S, Nath SK, and Paudyal B. (2014). Oxidative stress and its biomarkers in systemic lupus erythematosus: Journal of biomedical science p. 21-23.

#### 2.1.4.1.2 Protein oxidation and peroxidation

Protein oxidation and peroxidation are defined as the oxidative modification of proteins induced by ROS and by-products of oxidative stress that cause cell damage and death. ROS can receive hydrogen and electron on protein side chains and amino acids causing hydrogen atom abstraction from C-H bonds. The hydrogen abstraction of amino acids induces carbon radical production ( $R^{\bullet}$ ,  $RO^{\bullet}$ , and  $ROO^{\bullet}$ ) and other chemical group addition such as tyrosine nitration and carbonylation. These processes induce protein cross-link, amino acid side chain modification, and protein fragmentation that directly change cellular mechanisms, which can induce cell dysfunction and death (84, 85). The protein oxidative modification can be classified into two groups. First, irreversible protein oxidative modifications include carbonylation and tyrosine nitration that damage the protein target. The protein carbonyls are formed by

carbonylation of several amino acids including arginine, histidine, lysine, proline, threonine, and cysteine, which are used as biomarkers of protein oxidation and oxidative stress in various diseases. Protein nitrotyrosine is formed by the reaction of reactive nitrogen species (RNS) and a protein tyrosine residue, which nitrate target proteins. Nitrotyrosine is used as a biomarker of protein oxidation. Second, reversible protein oxidation modifications or protein cysteine modifications are the oxidation of cysteine that induces cysteine oxidation and by-product generation. These products include disulfide formation, S-glutathionylation, S-nitrosylation, and sulfenic acid formation, which are involved in redox regulation of protein function (86). Therefore, protein oxidation is one of the causes of protein modifications and cell damage (Figure 6).

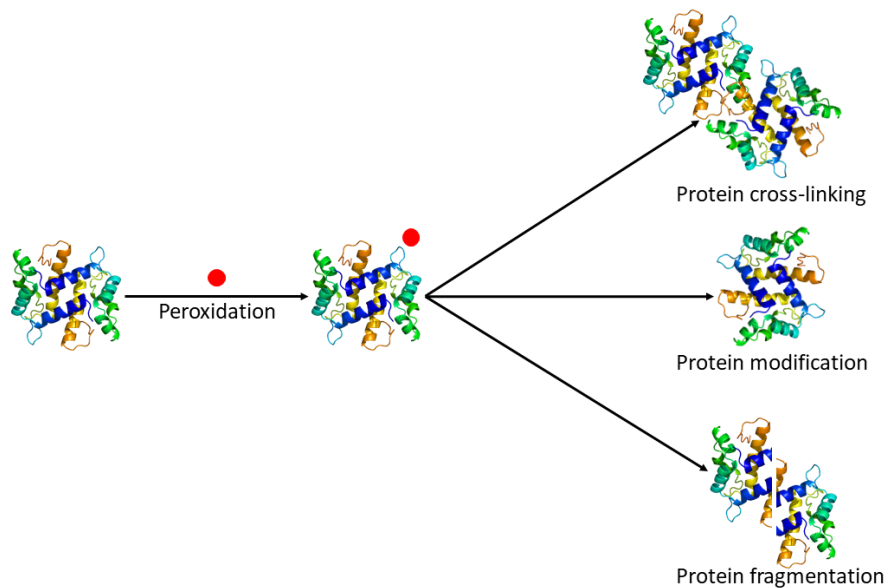


Figure 6 Protein oxidation and their effects

Source: Lund MN, Heinonen M, Baron CP, and Estevez M. (2011). Protein oxidation in muscle foods: a review: *Mol Nutr Food Res* p. 83-95.

#### 2.1.4.1.3 DNA oxidation

DNA oxidation is the oxidative damage to DNA by free radicals, which induces DNA base deletion, pyrimidine dimer formation, DNA crosslink, DNA double-strand breaks, and DNA modification (87). The  $\text{OH}^\bullet$  is the most reactive ROS, which is the main ROS in the process of DNA damage. The reaction of  $\text{OH}^\bullet$  damages all of four bases of DNA via hydrogen abstraction, addition, and electron transfer. The hydrogen abstraction of DNA forms the carbon-centered radical, which reacts with other molecules induced  $\text{ROO}^\bullet$  and non-radical ROS production resulting in strand break and DNA damage. The addition reaction of  $\text{OH}^\bullet$  reacts with a heterocyclic base inducing base radical formation.  $\text{ONOO}^-$  specifically reacts with guanine inducing 8-oxo-7,8-dihydroguanine (8-oxo-dG), 8-nitroguanidine, and other oxidative guanine productions (Figure 7). The 8-oxo-dG is the major product of DNA oxidative damage by  $\text{OH}^\bullet$  and  $\text{ONOO}^-$ . They are used as biomarkers of oxidative stress-induced damage (88). 8-oxo-dG (paring with cytosine) and apurinic site (AP site) on DNA strand induce adding of adenine on reverse DNA strand while replication leading to thymine adding when DNA repair. This incident leads to C-to-A or T-to-G mutation on DNA (Figure 7) (89). ROS-induced DNA damage effects on cellular physiology such as protein synthesis, cell growth, and development (87).



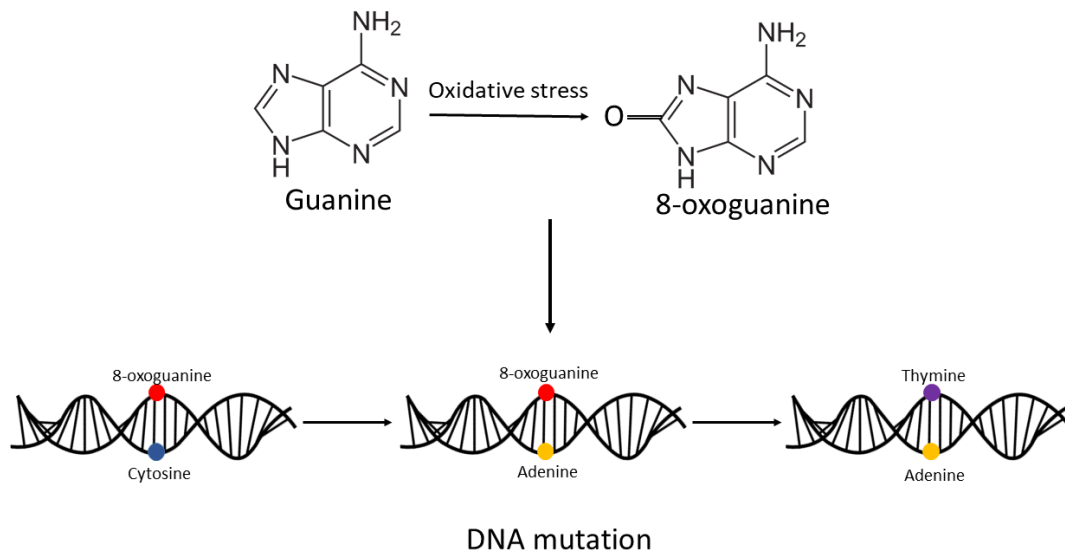


Figure 7 Effect of ROS on DNA damage and mutagenesis

Poetsch AR. (2020). The genomics of oxidative DNA damage, repair, and resulting mutagenesis: *Computational and Structural Biotechnology Journal* p. 207-19.

#### 2.1.4.2 ROS and cell signaling pathways

##### 2.1.4.2.1 ROS effect on MAPKs signaling pathway

The MAPK signaling pathways includes the four major pathways consisting of the extracellular signal-regulated protein kinase (ERK), the c-Jun N-terminal kinase (JNK), the p38 kinase, and the big MAPK1 (BNK1/ERK5) pathways. These pathways play important roles in cell growth, cell differentiation, cell survival, and cell death. The activation of four pathways is stimulated by extracellular or intracellular stimuli. The core of these pathways is phosphorylated MAPKKK cascades. Then MAPKK is activated by MAPKKK phosphorylation and then MAPK is phosphorylation. The activated MAPK phosphorylates substrate proteins to initiate cellular activity (Fig 2.9) (90).

The ERK1/2 pathway is stimulated by growth factors (EGF, PDGF, and mitogenic stimuli) binding to the tyrosine kinase receptor, and activating protein

subunits such as GRB2 and SOS. The inactive Ras-GDP is activated by binding to receptor complex exchanging GDP to GTP. The activated Ras binds and activates Raf (MAPKKK) inducing MEK1/2 (MAPKK) and ERK1/2 (MAPK) phosphorylation. MAPK activates transcription factors that translocate to the nucleus and activate target gene to produce specific proteins (91). ROS can auto-phosphorylate tyrosine kinase without the binding of receptor and ligand. It activates Ras and ERK pathways, resulting in cell survival and proliferation (6). On the other hand, ROS inhibits ERK-specific phosphatase (DUSP) and decreases ERK activation, causing apoptosis, senescence, and autophagy (92).

Environmental stress, cytokines, and growth factors affect to JNK signaling pathway activating MAPKKK include MEKK1-4, MLK, and ASK1, and then MAPKK consists of MKK3, 4, 6, and 7 promoting cell growth, differentiation, inflammation, and apoptosis. Whereas ROS activate JNK by activating ASK1 and inhibit MAP kinase phosphatase (MPK) the regulation of MAPK pathways induces apoptosis and cell death (6, 93).

Extracellular oxidative stress, growth factor, and inflammatory cytokine are key factors of the p38 pathway stimulation. The activation of Cdc42 initiates this pathway via Ras and Rac, which activate ASK1, MLK3, MKK3, MKK6, and finally p38. The ASK1 can be activated by the JNK pathway, which can crosstalk to activate the p38 pathway (6). ROS activates the p38 pathway via their MAPKK.

The BMK1 is activated by ROS through direct activation of MEKK2 and MEKK3 stimulation. The downstream target Mef2C, c-Mys, and NRF2 are activated, which are involved in cellular mechanisms such as cell survival, angiogenesis, and proliferation (6).

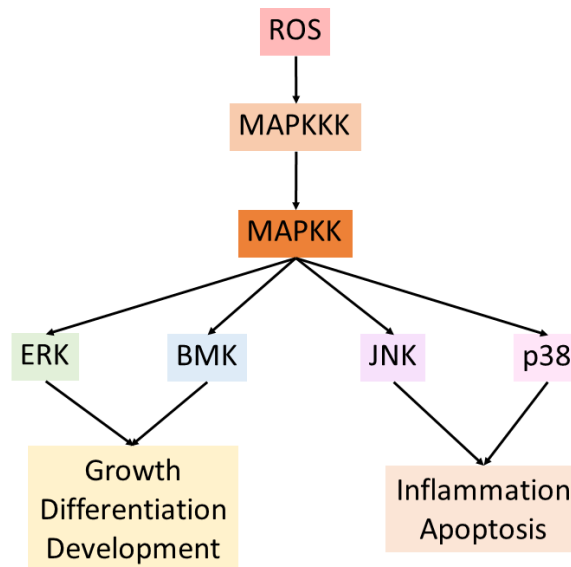


Figure 8 MAPK pathway activation by ROS

Source: Valko M, Leibfritz D, and et al. (2007). Free radicals and antioxidants in normal physiological functions and human disease: The international journal of biochemistry & cell biology p. 44-84.

#### 2.1.4.2.2 ROS effect on NF- $\kappa$ B signaling pathway

The cell inflammation, death, injury, and others are regulated by the transcription factor NF- $\kappa$ B. In which, this pathway has two distinct activation mechanisms, including canonical and non-canonical pathways. Non-canonical, binding receptor activates IKK $\alpha$  complex, which phosphorylates NF- $\kappa$ B/RelB complex inducing proteolytic process NF- $\kappa$ B2/p100 precursor. To activate the canonical pathway, the I $\kappa$ B kinase (IKK) complex is activated and phosphorylated I $\kappa$ B complex, which is degraded by the proteasome. After the degradation of the I $\kappa$ B complex, NF- $\kappa$ B is translocated into the nucleus and activated a lot of genes involved in inflammatory protein production (94). ROS inhibits phosphorylation of I $\kappa$ B $\alpha$  induced degradation of I $\kappa$ B $\alpha$  and then activate the NF- $\kappa$ B pathway. ROS-activated MEKK induces phosphorylation of IKK complex and activation of the NF- $\kappa$ B pathway. ROS also activates NF- $\kappa$ B inducing

kinase ( NIK) that phosphorylates  $IKK\alpha$  inducing non-canonical pathway activation ( Figure 9) (6, 95). Thus ROS are the cause of NF- $\kappa$ B activation that is involved in inflammatory pathways.

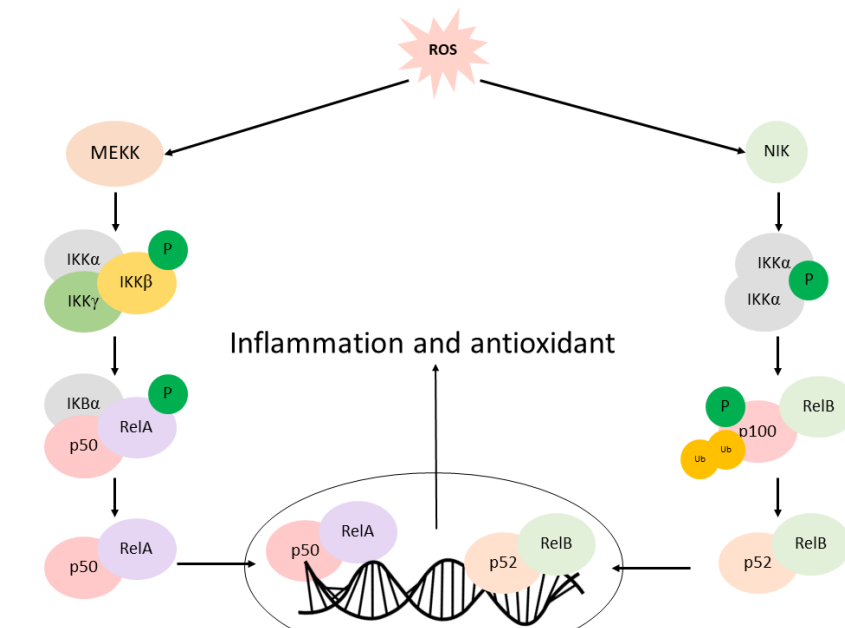


Figure 9 ROS effect on NF- $\kappa$ B pathway

Source: Zhang J, Wang X, and et al. (2016). ROS, and ROS-Mediated Cellular Signaling: Oxidative Medicine and Cellular Longevity p. 2016-18.

#### 2.1.4.2.3 ROS effect NRF2 signaling pathway

The Nrf2 is a transcription factor that regulates the expression of antioxidant proteins to protect against intracellular ROS and oxidative damage. This pathway also involves the balance of antioxidants and ROS. In normal conditions, Nrf2 is bound by Kelch-like ECH-associate protein 1 ( Keap1) and culin E3-ubiquitin ligase (Cul3), which induces Nrf2 ubiquitination and degradation by the proteasome. Under the oxidizing condition, Nrf2 and Keap1 are dissociated causing Nrf2 transferred to the

nucleus and dimerized to the antioxidant response element ( ARE) and transcribes antioxidant enzymes to protect against ROS (Figure 10) (6, 95).

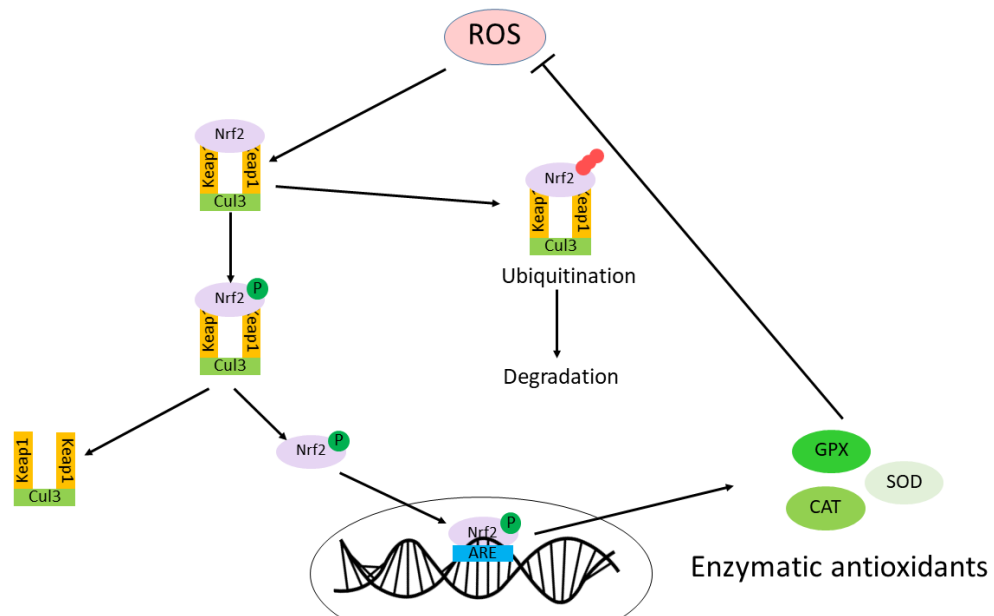


Figure 10 Response of Keap1-NRF2-ARE signaling pathway to ROS

Source: Zhang J, Wang X, and et al. (2016). ROS, and ROS-Mediated Cellular Signaling: Oxidative Medicine and Cellular Longevity p. 16-18.

#### 2.1.4.2.4 ROS effect PI3K/Akt signaling pathway

This pathway is activated by phosphoinositide-3-kinase ( PI3K) tyrosine kinase. The activated PI3K is bound with phosphatidylinositol 4,5-diphosphate (PIP2) and phosphorylated, and then PIP2 is converted into phosphatidylinositol 3,4,5-diphosphate (PIP3). The PIP3 activates Akt, which activates and transcript target protein including Bcl-2-associated death promoter ( BAD) , p53, mTOR, and Forkhead box O (FOXO). ROS activates PI3K via PIP2 phosphorylation that PIP2 is converted into PIP3 leading to induce Akt activation. ROS inhibit phosphatase and tensin homolog (PTEN) causing cleave phosphoric acid on PIP3, which inhibits the conversion of PIP3 into PIP2. Moreover, ROS also activate casein kinase II for PTEN degradation, resulting in Akt

activation. Therefore, ROS activate the Akt pathway via direct PIP3 phosphorylation, restrain inhibition factor, and activate cell survival mechanism (6, 95).

#### 2.1.4.2.5 ROS and protein kinase signaling pathway

ROS play crucial roles in the protein kinase signaling pathway by the activation of protein kinase C (PKC), A (PKA), and D (PKD). The activation of PKC affects membrane channels including  $\text{Ca}^{2+}$  channel,  $\text{Na}^+$  channel, sodium-calcium exchanger, target proteins sensing to different cellular mechanisms such as cell proliferation, survival, death, and differentiation. The PKA activation affects the  $\text{Ca}^{2+}$  channel,  $\text{Na}^+/\text{K}^+$ -ATPase, and target proteins to activate the MAPK pathway involving in cell survival and death. PKD and PKC activation regulate the action of growth factor, neurotransmitters, and growth hormone, as well as PKD-NF- $\kappa$ B to repress for excessive ROS. ROS also activates  $\text{Ca}/\text{calmodulin}^{2+}$  independent protein kinase II (CaMKII) involved in the regulation of cardiomyocytes (96).

#### 2.1.4.2.6 ROS regulate ubiquitination and proteasome system

Ubiquitination/Proteasome system (UPS) composed of proteasomes, ubiquitins, deubiquitinases (DUBs), and the ubiquitination machinery, plays an important role to regulate cellular mechanism involved in inflammation, survival, homeostasis, and cell cycle. The ubiquitination initiates by activation of ubiquitin-activating enzymes (E1), which transfers the ubiquitin to the ubiquitin-conjugating enzyme (E2). The ubiquitin ligase (E3) transfer ubiquitins and elongate polyubiquitin chain to the target protein. Polyubiquitinated proteins are degraded via specific proteolytic activities of the proteasome. Then deubiquitination is performed by DUBs. ROS interact UPS and inactive Ubc12 enzyme reducing Cul3/Ring-Box (Rbx1) dependent complex activity. Ubiquitination and phosphorylation on Nrf2 and  $\text{I}\kappa\text{B}\alpha$  induce degradation of these proteins, respectively (96).

#### 2.1.4.2.7 ROS mediate program cell death

ROS regulate three major types of program cell death including apoptosis, necrosis, and autophagy. The lower levels of ROS in the normal cell can induce cell growth and survival to promote cancer progression. Opposite, elevate of

ROS levels can induce normal and cancer cell death via activation of cell death pathways (97).

In apoptosis pathways, ROS are generated in both intrinsic and extrinsic apoptotic pathways. ROS damage mitochondria and increase mitochondrial ROS levels leading to pro-apoptotic protein activation. The releasing of Cyt c activate caspase 9 and then cleaved caspase 3 inducing cell apoptosis via the intrinsic pathway. The extrinsic pathway occurring from TNF- $\alpha$  induce ROS production and cell apoptosis through the JNK signaling pathway (98).

In necroptosis, ROS induce mitochondrial oxidative stress and The receptor-interacting protein kinase 1 (RIP1)/ receptor-interacting protein kinase 3 (RIP3) activation. The activation of regulated Receptor-interacting serine/ threonine-protein (RIP1/RIP3) activates mixed lineage kinase domain-like (MLKL) oligomerization leading to plasma membrane permeabilization and necrosis, whereas The inhibition of caspase 8 also induces necroptosis (99).

In autophagy, ROS activate MAPK (p38, JNK, and ERK) pathway inducing autophagy. The AMP-activated protein kinase (AMPK) pathway is activated to inhibit the mammalian target of rapamycin complex 1 (mTORC1) whereas the Akt pathway is inhibited. The decrease in mTORC1 leads to a reduction of autophagy. Therefore, ROS effect in both autophagy induction and inhibition (100).

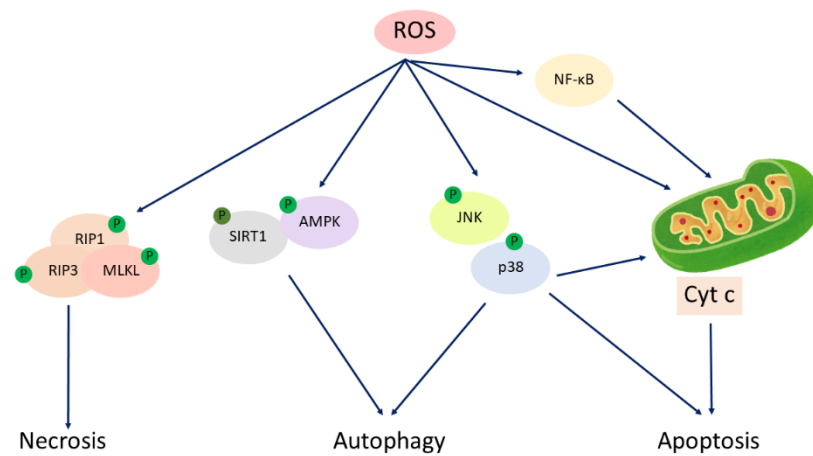


Figure 11 ROS induce cell death

Source: Fang C, Gu L, Smerin D, Mao S, and Xiong X. (2017) The Interrelation between Reactive Oxygen Species and Autophagy in Neurological Disorders: Oxidative Medicine and Cellular Longevity.

## 2.2 Endothelial cells

Endothelial cells are simple squamous cells lining in blood vessels called the endothelium. The thin monolayer of Ecs involves many processes of blood vessel function such as vascular tone and vascular barrier, which are important blood circulating processes in the human body.

### 2.2.1 Endothelial function

#### 2.2.1.1 Barrier function

The endothelial cell adhesion by the cell to cell junction including integrins, actin, tight junction ( claudin, junctional adhesion molecule ( JAM) and occluding) , gap junction, adhesion junction ( vascular endothelial cadherin or VE-cadherin) , and surface receptors to form the vascular selective walls. The endothelial wall restricts the movement of biomolecules in the lumen that permeated into the surrounding tissues. Moreover, this barrier is involved in the Immune system. The immune cells can cross the vascular walls under inflammatory conditions. The weakness



of endothelial walls can be induced by ROS, cytokine, and protease (15). The BBB is a highly specialized endothelial structure of vascular walls, which is specific and selective to biomolecule transport and protects against microorganisms that are dangerous to the brain (16).

### 2.2.1.2 Vasculogenesis and Angiogenesis

In vasculogenesis, mesodermal cells are differentiated into hemangioblasts then migrated to form a blood island. Blood island forming cells on the outside of the blood island are differentiated into angioblasts, which are differentiated into Ecs and build the blood vessel walls. The inside hemangioblast will create blood cells. The fibroblast growth factor (FGF2) involves in mesomal and angioblasts induction. If Ecs are forming vascular walls, tight junctions are formed between endothelial cells to generate vascular walls. Lumen is generated inside vascular walls and the basement membrane is deposited along the basolateral endothelial cell surface. VEGF is involved in the vasculogenesis formation process (101). In angiogenesis, vascular endothelial cells are activated by angiogenic stimuli (VEGF, hypoxia, NO, or Ang2) causing destabilization of vascular walls, where endothelium and pericyte contraction are disrupted. Ecs form filopodia and sprouting. This process involves in Notch and Delta4. Then extracellular matrix (ECM) is degraded by protease, which is released from Ecs consist of matrix metalloprotease (MMP) and others. Then Ecs are migrated by the induction of VEGF, angiopoietin (Ang), FGF, and others. The spouting is converted and the lumen is formed by ECM-associated proteins. After that, vessels are stabilized by ECM production and pericyte attachment. This process is regulated by platelet-derived growth factor (PDGF), Ang, and others (102).

VEGF and VEGF receptors play important roles in vasculogenesis and angiogenesis by activating many signaling pathways involving in EC motility via FAK and IQGAP1 pathways, EC migration and proliferation via PKC, MAPK and Src, vascular permeability via Src and eNOS, and EC survival via Akt (101).

### 2.2.1.3 Vascular tone

The contractile activity of vascular smooth muscle cells induces vasoconstriction and vasodilation. The relationship of them makes elasticity on vascular

walls leading to blood pressure resistance. Ecs play important role in the regulation of vascular tone by released the endothelium-derived-vasodilator including NO, prostacyclin, and bradykinin, endothelium-derived-vasoconstrictor consisting of endothelin-I (ET1) and angiotensin II (Ang 2). The ET1 and NO are major factors of vascular tone regulation. In vasodilation, NO is produced by NOS, which has three major isoforms including neuronal nitric oxide synthase (nNOS), inducible nitric oxide synthase (iNOS), and endothelial nitric oxide synthase (eNOS). In vascular tone regulation, NO is produced by oxidation of L-arginine and oxygen via eNOS and their cofactor (BH<sub>4</sub> and NADPH). Soluble guanylate cyclase (sGC) in smooth muscle cells is activated by NO to induce cGMP activation and vasodilation. NO inhibits ET1 synthesis at transcription levels, which represses the vasoconstriction process. In vasoconstriction, ET1 is produced by Ecs and then activates ET<sub>A</sub> and ET<sub>B</sub> receptors in smooth muscle cells to induce vasoconstriction. However, activation of ET<sub>B</sub> can activate endothelium-derived-vasodilator including NO and prostacyclin production (Figure 12) (103).

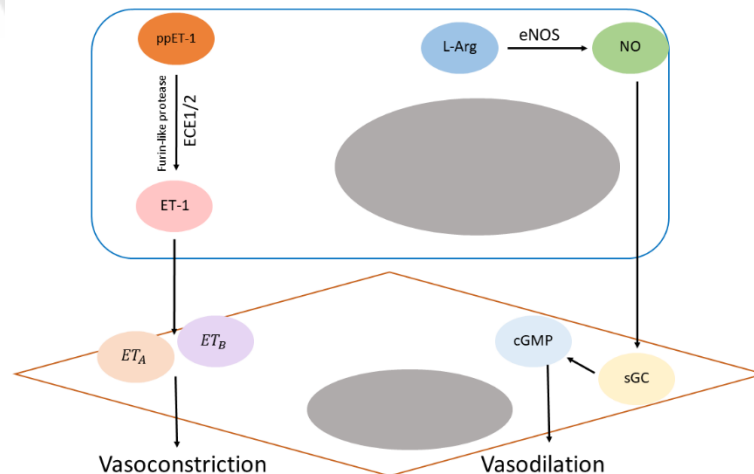


Figure 12 Vascular tone regulation by NO and ET1

Source: Alonso D and Radomski MW. (2003). The nitric oxide-endothelin-1 connection: Heart failure reviews p. 107-115.

#### 2.2.1.4 Anticoagulation

The vascular damage can induce an accumulation of platelet on the damaged area leading to coagulant cascade activation. Then thrombin and fibrin are generated, resulting in platelet coagulation and blood clot. The protein C and heparan sulfate (HS) on the EC surface has an important role in the anticoagulation of blood vessel. The binding of HS and anti-thrombin (AT) generate the activated form of AT, which inhibits blood coagulation factor Xa and thrombin (IIa), and inhibit thrombin formation (Fig 2. 18B) (104). The PC is activated into APC after thrombin binding to thrombomodulin. The APC inhibits coagulation factor Va and VIIIa to shut down thrombin formation. Moreover, thrombin and APC activate protease-activated receptor 1 (PAR-1) leading to NO production and reduces platelet activation. PAR-1 also induces tissue-type plasminogen activator (t-PA) release that binding with fibrin cause fibrinolysis (105).

#### 2.2.1.5 Immune system

ECs are the first interaction with the microbial component, where Toll-like receptors (TLRs) and NOD-like receptors are expressed on ECs like dendritic cells (DCs). ECs also secrete pro-inflammatory cytokines that respond to microbial stimulation. ECs are involved in antigen-presenting cells (APCs) by expression of the major histocompatibility class I (MHC I), II (MHC II), and pattern-recognition receptor (PPRs) on EC surface, which is detected by pathogen-associated molecular pattern (PAMPs). Then endothelial antigens are presented to immune cells. PPRs also detect the inflammation stimulus and the risk factor for immune response. Moreover, surface adhesion molecules expressed on the EC surface can induce the immune cell adhesion, which invades the endothelium and underlying tissues for the response to stimuli. Therefore, ECs have an important role in immune response and inflammation (21).

#### 2.2.2 Oxidative stress induces endothelial dysfunction and cardiovascular disease

Loss of normal function of ECs including vasoconstriction and vasodilation, anti-coagulant, barrier function, is called endothelial dysfunction. ROS are the main cause of endothelial dysfunction leading to cell inflammation and death. Endothelial

dysfunction leads to various human diseases such as cardiovascular disease, diabetic mellitus, kidney failure, cancer, and autoimmune diseases (106).

#### 2.2.2.1 Uncoupled eNOS

eNOS has an important role in NO production of ECs. In normal conditions, eNOS is coupled, which  $BH_4$  and NADPH cofactor to convert L-arginine into L-citrulline and NO in this reaction.  $BH_4$  deficiency by the oxidation of  $BH_4$  into  $BH_2$  is the cause of uncoupled eNOS, in which the NO production is reduced but the ROS consisting  $O_2^{\cdot-}$  and  $ONOO^-$  are increased (107). The  $ONOO^-$  generated by uncoupled eNOS can oxidize the  $BH_4$  cofactor to form an endogenous eNOS inhibitor asymmetric dimethylarginine (ADMA), which is a competitor of the eNOS substrate L-arginine. Another cause of uncoupled eNOS is the arginase enzyme that catalyzing the L-arginine substrate into urea and ornithine, which plays a competitive role in eNOS (Figure 13). Shear stress, inflammation (TNF- $\alpha$ , Ang, NF- $\kappa$ B), and other pathways also induce uncoupled eNOS via gene expression and cell signaling control (108). Loss of NO reduces sGC activation and ET1 inhibition in smooth muscle, resulting in endothelial dysfunction leads to vascular inflammation and injury (109).

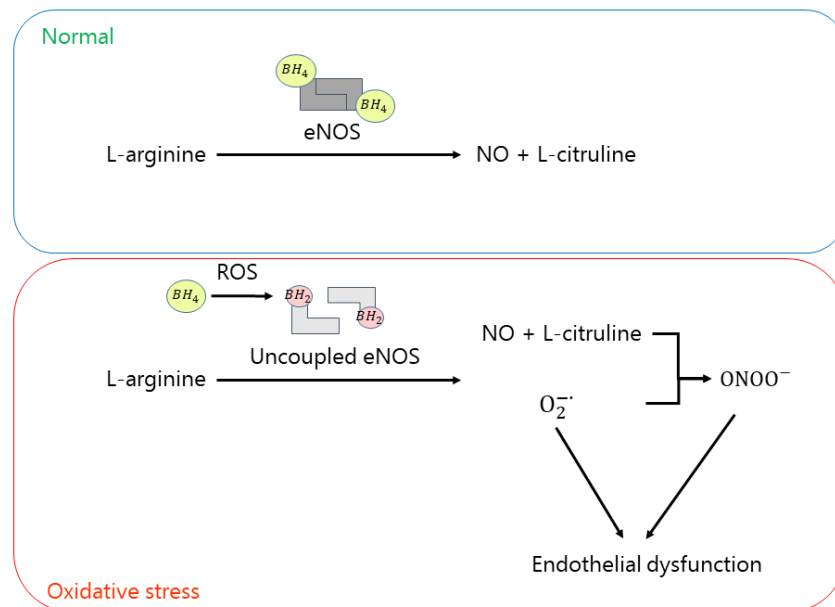


Figure 13 Causes of endothelial dysfunction and eNOS uncoupled

Source: Yang Z and Ming XF. (2006). Recent advances in understanding endothelial dysfunction in atherosclerosis: Clinical medicine & research p. 53-65. Cai H and Harrison DG. (2000). Endothelial dysfunction in cardiovascular diseases: the role of oxidant stress: Circulation research p. 840-4.

#### 2.2.2.2. Vascular wall permeability

The vascular wall formed by ECs is selective walls. It has an important role in immune response and molecular transport between the vascular lumen and surrounding tissue. ROS released from polymorphonuclear leukocytes (PMNs) and other sources can induce endothelial barrier permeability by activation of calcium signaling mechanism. The oxidant-sensitive transient receptor potential (TRP) channels and calcium release-activated calcium channel protein 1 (ORAI) are stimulated by ROS, which induce  $\text{Ca}^{2+}$  entry into ECs and cause PKC $\alpha$  activation. PKC $\alpha$  can be activated by three major pathways. First, p120-catenin dissociated from VE-cadherin after phosphorylation by PKC $\alpha$  causes disruption of adhesion junction and transmigration of

PMNs. Second, activation of Src phosphorylates VE-cadherin and  $\beta$ -catenin cause adhesion junction destabilized. Besides, TNF- $\alpha$  also activates this pathway (110). Third, the cooperation between activated PKC $\alpha$  and myosin light chain kinase (MLCK) inhibits activation of Rho A and reorganization of actin leading to endothelial barrier dysfunction. Moreover, ROS also activate the surface adhesion molecules such as intracellular adhesion molecule 1 (ICAM1), which can induce NF- $\kappa$ B activation. The binding between ICAM1 and integrin of PMNs induce NOX activation leading to ROS generation, which is the feedback loop in barrier dysfunction (111, 112). Loss of the barrier function of ECs induces cell inflammation and inflammatory cytokine release, causing coagulation and cardiovascular diseases (113).

#### 2.2.2.3. Excessive of angiogenesis

Angiogenesis is an important role to generate new blood vessels. In contrast, higher activation of this process can generate new blood supplies for the tumor cells. ROS and inflammation can activate redox signaling (Src, Akt, eNOS, and MAPK) and transcription factor (HIF-1, NF- $\kappa$ B, and AP-1) via TLRs and VEGFR induced angiogenic factor production, resulting in new blood vessel formation and angiogenesis. Moreover, ROS also activate NOX and other ROS sources that showing a positive feedback loop in tumor angiogenesis (114-116).

#### 2.2.2.4. Endothelial cells death and inflammation

ECs injury and death are the cause of endothelial dysfunction via death signaling pathways (apoptosis and necrosis). The apoptosis signaling kinase 1 (ASK1) is activated by ROS, then it activates JNK/p38 MAPK, inducing cell apoptosis (117). The apoptosis pathways include the two major pathways. First intrinsic pathway, mitochondrial oxidative stress is the cause of this pathway, in which ROS induce apoptogenic factors generation. Apoptogenic factors activate the caspase-independent pathway via activation of apoptosis-inducing factor (AIF) leading to DNA fragmentation and cell death. In the caspase-dependent pathway, the inhibitor of apoptosis proteins (IAPs) is inhibited by the second mitochondria-derived activator of caspases (Smac) while pro-apoptotic proteins (Bcl-2 family) are activated leading to cytochrome c

released and activated caspase 9 and then caspase 3, resulting in cell apoptosis. In the extrinsic pathway, the death family receptor (TNFR, Fas, and TRAIL-R) binding with their ligands induces the formation of the death-inducing signaling complex leading to caspase 8 activation and cell apoptosis (Figure 14) (9). ROS also induce endothelial cell inflammation via MAPK and NF- $\kappa$ B inflammatory pathways leading to endothelial cell inflammation and death. ECs injury and death induce endothelial dysfunction, finally atherosclerosis and CVDs (118).

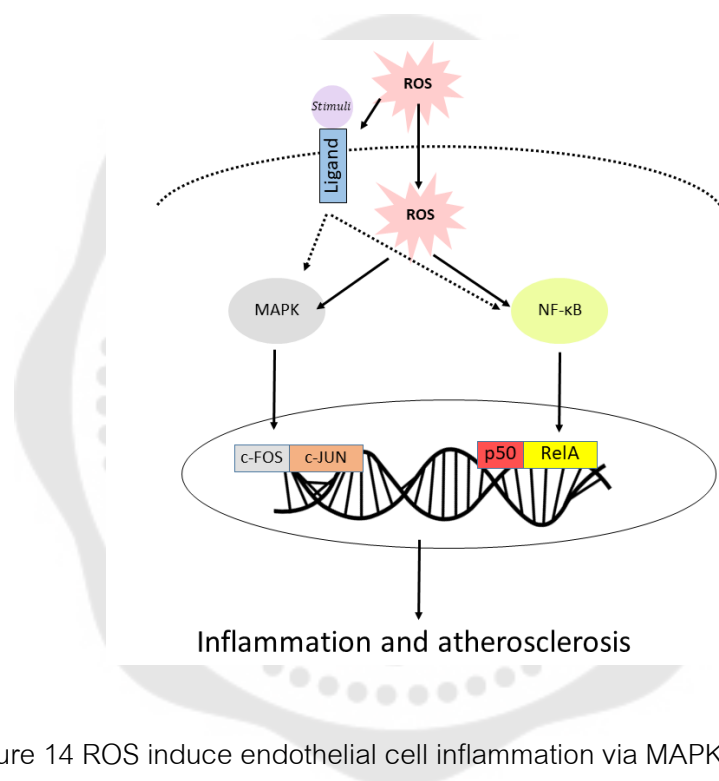


Figure 14 ROS induce endothelial cell inflammation via MAPK/c-Jun and NF $\kappa$ B pathways.

Source: Li Y, Cifuentes-Pagano E, DeVallance ER, and et al. (2019). NADPH oxidase 2 inhibitors CPP11G and CPP11H attenuate endothelial cell inflammation & vessel dysfunction and restore mouse hind-limb flow: *Redox Biology* p. 22.

#### 2.2.2.5 Endothelial dysfunction associated with cardiovascular disease (CVD)

Cardiovascular disease has been a major cause of death worldwide. Endothelial dysfunction is the main cause of this disease. Oxidative stress also induces CVD by damage to the cellular biomolecules consisting of DNA, protein, and lipid, cause tissue damage. Under the inflammatory conditions, PMNs are attached to the endothelium surface and transmigrated to subendothelial space, and differentiated into macrophages. ROS are generated by macrophages, ECs, and smooth muscle cells (SMC). ROS can convert LDL into Ox-LDL, which activates lectin-like oxidized LDL receptor 1 (LOX-1), MCP-1, and cell adhesion molecules (ICAM-1 and VCAM-1) inducing adhesion of monocyte on the endothelial surface. LOX-1 and CD36 expressed on macrophage induce internalization of Ox-LDL into macrophage that inducing foam cell generation causes atherosclerosis formation. Foam cells can release pro-inflammatory cytokines, which induce lots of macrophages moved into subendothelial space and increased inflammation. Accumulation of Ox-LDL can induce foam cell apoptosis and necrosis causing cell injury occurring the plaque formation. Ox-LDL also induces SMC proliferation and migration via platelet-derived growth factor (PDGF) and basic fibroblast growth factor (bFGF) from the extracellular matrix then fibrous cap cover and developing plaque forming in the necrotic core. The platelet activation is induced via Ox-LDL and endothelial dysfunction, in which Ox-LDL binding to CD36 and LOX-1 promotes activated platelets. The activated platelets adhere to ECs induced thrombus formation on the plaque rupture that blocking and narrowing blood flow, causing cardiovascular disease (24, 119, 120). Therefore, ROS are a key hallmark of CVDs via endothelial cell inflammation and death, which antioxidants might be improved risks of CVDs.

#### 2.2.3 Prevention of endothelial dysfunction and antioxidant

The antioxidant enzymes are the main mechanism for eliminating ROS in the ECs, which activated NRF2 induces intracellular antioxidant enzyme production including CAT, SOD, and GPX to protect against oxidative damage (6, 95). Non-enzymatic antioxidants including ascorbic acid,  $\alpha$ -tocopherol, glutathione, carotenoids,



flavonoids and other metabolites have been reported to scavenge ROS that protecting endothelial dysfunction from oxidative damage (4, 121). N-acetylcysteine (NAC) is an antioxidant that inhibiting ROS and pro-inflammatory cytokines by activation of ERK and inhibition of the NF $\kappa$ B pathway leading to cell survival. The eNOS modulators including L-arginine, statin, folic acid, BH<sub>4</sub>, and eNOS transcription enhancer can prevent eNOS uncoupling. L-arginine and BH<sub>4</sub> are important components of eNOS, which are eNOS substrates and co-factor that normalized ADMA and BH<sub>2</sub> prevent against uncoupled eNOS. Statin increases BH<sub>4</sub> levels via GTP cyclohydrolase (GTPCH) and BH<sub>4</sub> synthesis that reducing NOX upregulation and ROS production. Statin also upregulates eNOS increases NO production (122). Besides, the antioxidant effect of vegetables, herbs, and fruit prevent against ROS had been reported (123). The previous report showed that *Phyllanthus emblica* fruit extract protected against hydrogen peroxide-induced ECs cell oxidative stress by decreases of intracellular ROS and activation of the Akt pathway (30). Curcumin attenuates oxidative damage and cell death in H<sub>2</sub>O<sub>2</sub> induced ECs via Akt/mTOR and apoptosis pathways (29). The *Leonussibicus* herb extract suppresses adhesion molecules (ICAM and VCAM) and LOX1 expression in TNF $\alpha$  induced human umbilical vein endothelial cells (HUVECs) where hypercholesterolemia in rat showed beneficial effects on atherosclerosis (124). Moreover, the natural components of plant had been shown antioxidant effects against ECs damage, death and endothelial dysfunction. Alicin and resveratrol prevent apoptosis in H<sub>2</sub>O<sub>2</sub>-induced HUVECs by activating antioxidant enzymes and inhibiting apoptotic pathways by the decreased number of apoptosis cells (31, 32). Isoquercitrin reduces H<sub>2</sub>O<sub>2</sub>-induced apoptosis in EA hy926 by decreased apoptosis cascade (cleaved 3 and 9) and activated PIK3/Akt/GSK3 $\beta$  pathway (33). Ginsenoside Rb1 stimulates the sirtuin-1 pathway to prevent HUVECs senescence (34). In a clinical trial, green tea improves endothelial dysfunction in the smoker by reducing oxidative stress, inflammation, endothelial dysfunction, and CVD marker. Green tea also increases forearm blood flow and NO production that prevents endothelial dysfunction and the risk of CVD (125, 126). Moreover, green tea reduces LDL oxidation decreasing the risk of CVD (127).

Supplementation of the pure flavonoids epicatechin and quercetin reduce endothelial dysfunction and inflammation markers in (pre) hypertensive adults (128). Therefore, enzymatic and non-enzymatic antioxidants have an important role to protect ECs damage, reduce endothelial dysfunction and cardiovascular disease via signaling pathway of oxidative protection.

## 2.3 *Carica papaya*

### 2.3.1 Background

*Carica papaya* is a native tropical plant that can be found around the world. Papaya belongs to class Magnoliopsida, phylum Streptophyta, and family Caricaceae. It is a single-stemmed herbaceous perennial tree and palmately leaves. The male and female flowers are produced on different plants. However, papaya in cultivation is the hermaphrodite form that has both male and female flowers on the same plants. The papaya fruit is matured in 5-9 months. These fruits are oval shape and have a large central seed cavity. Papaya can pollinate by three methods including self-pollination, pollen from the same plant but the different flowers, and pollens from the different plants (129). Each different part of papaya has high and different nutrition. UCP contains vitamins, which can eliminate ROS by the donated electron to free radicals. Vitamin C and E also involve in thiol cycles, which eliminate ROS via antioxidant enzymes. Moreover, UCP also contains terpenoids, alkaloids, flavonoids, glycosides, saponins, steroids, papain, phenolic acid, and mineral (35). These nutrients of papaya can prevent oxidation reaction. However, antioxidant activity and phytochemical properties of papaya fruit are changed in the different ripening stages. The ripening stage of papaya fruit in RS5 (20 weeks) has higher antioxidant activity than RS4 (18 weeks), RS3 (16 weeks), RS2 (14 weeks), and RS1 (12 weeks), respectively (Table 4 and 5) (130).

Table 3 Appearance of papaya fruit in different ripening stages

Group	Ripening stages (weeks)	Skin color	Flesh color	Seed color
RS1	12	Green	White	White
RS2	14	Green	Pale yellow	Brown
RS3	16	Green	Yellow	Pale black
RS4	18	Trace of yellow	Orange	Black
RS5	20	More yellow	Reddish orange	Black

Table 4 Antioxidant capacity of papaya fruit in different ripening stages

Group	TPC mg/100g FW	TFC mg/100g FW	FRAP mg/100g FW	DDPH%	ABTS%
RS1	11.13 ± 0.17e	18.45 ± 0.46e	19.27 ± 0.20e	12.25 ± 0.45e	24.01 ± 0.02e
RS2	21.48 ± 0.31d	23.46 ± 0.40d	58.84 ± 0.05d	22.42 ± 0.46d	35.59 ± 0.01d
RS3	33.38 ± 0.99c	25.96 ± 0.61c	85.57 ± 0.16c	30.02 ± 0.21c	43.11 ± 0.01c
RS4	38.33 ± 0.63b	31.72 ± 1.88b	96.85 ± 0.40b	35.74 ± 0.20b	49.34 ± 0.01b
RS5	42.97 ± 0.21a	36.26 ± 0.58a	114.71 ± 0.13a	41.06 ± 0.67a	62.22 ± 0.02a

Source: Zuhair RA, Aminah, A., Sahilah, A.M. and Eqbal, D. (2013). Antioxidant activity and physicochemical properties changes of papaya (*Carica papaya* L. cv. Hong Kong) during different ripening stage: International Food Research Journal p.1653-9.

### 2.3.2 Medical research

Many parts of papaya have been widely studied. Papaya has antioxidant and antimicrobial activity that is different in each part and solvent extraction (35). Previous studies reported the medical property of papaya. Many parts of papaya affect inflammation and immune modulation by decreasing pro-inflammatory cytokine

generation and increasing antioxidant enzyme production (40). The medical research in a different part of papaya has been reported.

#### **2.3.2.1 Leaf extract**

The papaya leaf aqueous extract has a high antioxidant capacity and scavenging activity (131). The papaya leaf extract has a high antioxidant capacity and reduces H<sub>2</sub>O<sub>2</sub>-induced erythrocyte damage by reducing lipid peroxidation and hemolysis (132). Papaya leaves extract also has an anti-inflammatory effect in the ovalbumin-induced allergic asthma mouse model by down-regulated IL-4, IL-5, TNF $\alpha$ , iNOS, and NF-KB (133). Moreover, the papaya leaf juice significantly increased the rate of platelet count among patients with dengue fever(42). Therefore, papaya leaf shows a beneficial role in medical research

#### **2.3.2.2 Seed extract**

The papaya seed extract has a high antioxidant capacity (134). Papaya seeds contain polyphenols, flavonoids, alkaloids, tannins, and saponins, in which the seed extract of papaya protects against oxidative stress in H<sub>2</sub>O<sub>2</sub>-induced HepG2 cells oxidative stress (135). The ethanolic extract of papaya seed significantly decreases the wound healing area in Sprague-Dawley rats using the excision wound model(136). Moreover, papaya seed extract has an antibacterial effect, which protects against bacterial pathogens isolated from the wound, urine, and stool(137).

#### **2.3.2.3 Latex extract**

Papaya latex contains papain, vitamin, and alkaloids, which are antioxidants (35). The papaya latex hydrogel increase wound healing rate in mice burn model likely the standard (silver sulphadiazine and chlorhexidine gluconate cream; 1.0% w/w) when compared with control(138).

#### **2.3.2.4 Unripe fruit extract**

The unripe fruit shows a therapeutic effect on the diabetic rat and burns mice model by increasing the rate of the wound closer and resistant to oxidants and microorganisms (139, 140). Besides, oral administration of green and ripe papaya epicarp extract increased the rate of wound healing in pregnant mice's excised skin model. However, green papaya extracts reduced the bodyweight of live pups (141).

Short-term supplementation of fermented papaya can reduce the risk of CVD in Mauritian neo-diabetic subjects by reducing oxidative stress and inflammation (142). Moreover, the 8 hydroxyl-2'-deoxyguanosine (8-OHdG) oxidative marker in patients with Alzheimer's disease is also reduced in the fermented papaya intake group (43).

Therefore, previous studies have shown applications of papaya in medical research, which are of interest in the pharmacological and medical property. However, the prevention of endothelial cell death by papaya has not been reported.



## CHAPTER 3

### RESEARCH METHODOLOGY

#### 3.1 Chemicals and Equipment

##### 3.1.1 Chemicals

EA hy926 cell line	ATCC
6-Hydroxy-2,5,7,8-tetramethylchroman-2-carboxylic acid (Trolox)	Sigma-Aldrich
2-Deoxy-D-ribose	Sigma-Aldrich
Ethylenediaminetetraacetic acid (EDTA) trisodium salt	Sigma-Aldrich
Iron (III) chloride (FeCl <sub>3</sub> )	Sigma-Aldrich
L-Ascorbic acid sodium salt	Sigma-Aldrich
30% Hydrogenperoxide	Sigma-Aldrich
2-Thiobarbituric acid (TBA)	Sigma-Aldrich
Formaldehyde	Sigma-Aldrich
4-Amino-3-hydrazino-5-mercapto-1,2,4-triazole (Purplad)	Sigma-Aldrich
Potassium periodate	Sigma-Aldrich
Non-fat dry milk	Sigma-Aldrich
Potassium chlorite (KCl)	Sigma-Aldrich
Glutathione (GSH)	Sigma-Aldrich
Glutathione reductase (GR)	Sigma-Aldrich
Glutathione peroxidase (GPX)	Sigma-Aldrich
Nicotinamide adenine dinucleotide phosphate (NADPH)	Sigma-Aldrich
Sodium hypochlorite solution (NaOCl)	Sigma-Aldrich
Sodium borohydride	Sigma-Aldrich
5,5'-dithiobis(2-nitrobenzoic acid) (DTNB)	Sigma-Aldrich
Phenazine methosulfate (PMS)	Sigma-Aldrich
Nicotinamide adenine dinucleotide (NADH)	Sigma-Aldrich
Nitro blue tetrazolium (NBT)	Sigma-Aldrich
Homovalinic acid (HVA)	Sigma-Aldrich
Horseradish peroxidase (HRP)	Sigma-Aldrich



2,4,6-Tri(2-pyridyl)-s-triazine (TPTZ)	Sigma-Aldrich
Hydrochloric acid (HCl)	Sigma-Aldrich
Acetic acid	Sigma-Aldrich
2',7'-dichlorofluorescein diacetate (DCFH-DA)	Sigma-Aldrich
SOD assay kit (19160 sigma)	Sigma-Aldrich
Iron (II) sulfate ( $\text{FeSO}_4$ )	Sigma-Aldrich
Fluorescein	Sigma-Aldrich
Acrylamide	Sigma-Aldrich
Trisma base	Sigma-Aldrich
Sodium chlorite (NaCl)	Sigma-Aldrich
Triton x 100	Sigma-Aldrich
Sodium deoxycholate	Sigma-Aldrich
Disodium hydrogen phosphate ( $\text{Na}_2\text{HPO}_4$ )	Sigma-Aldrich
Dimethylsulfoxide (DMSO)	Sigma-Aldrich
Sodium bicarbonate	Sigma-Aldrich
Acetonitrile	Merck
Ammonium thiocyanate	Merck
Quercetin	Merck
Chlorogenic acid	Merck
Ellagic acid	Merck
Sodium hydroxide	Merck
Sodium phosphate, monobasic, monohydrate ( $\text{NaH}_2\text{PO}_4 \cdot \text{H}_2\text{O}$ )	Merck
Trichloroacetic acid (TCA)	Merck
2,2'-azobis(2-amidino-propane) dihydrochloride (AAPH)	Merck
Sulfuric acid	Merck
Methanol	Merck
Sodium phosphate, dibasic dehydrate ( $\text{Na}_2\text{HPO}_4 \cdot 2\text{H}_2\text{O}$ )	Unilab
Potassium phosphate, dibasic dehydrate ( $\text{K}_2\text{HPO}_4 \cdot 2\text{H}_2\text{O}$ )	Unilab
Potassium phosphate, monobasic, monohydrate ( $\text{KH}_2\text{PO}_4 \cdot \text{H}_2\text{O}$ )	Unilab

Cayman NRF2 transcription factor kit (No. 600590)	Cayman Chemical
Cayman Nuclear extraction kit (No. 10009277)	Cayman Chemical
Dulbecco's modified Eagle medium (DMEM)	Gibco BRL
Fetal bovine serum (FBS)	Gibco BRL
Penicillin-streptomycin	Gibco BRL
2.5% Trypsin	Gibco BRL
Bis-Acrylamide	Gibco BRL
Sodium lauryl sulfate	Scharlau
MTT(3-(4,5-dimethylthiazol-2-yl)-2,5-diphenyltetrazolium bromide)	Bio Basic inc.
Ammonium sulfate	Bio basic inc.
TEMED (Tetramethylethylenediamine)	Bio basic inc.
Bovine serum albumin (BSA) fraction V	Bio basic inc.
Propidiumiodide (PI)	Cell Signaling Technology
Hoechst	Cell Signaling Technology
Monoclonal antibodies against p38 and p-p38	Cell Signaling Technology
Monoclonal antibodies against AKT and phospho-p-AKT	Cell Signaling Technology
Monoclonal antibodies against JNK and p-JNK	Cell Signaling Technology
Monoclonal antibodies against NRF2	Cell Signaling Technology
Monoclonal antibodies against NF-kB	Cell Signaling Technology
Monoclonal antibodies against beta-actin	Cell Signaling Technology
Horseradish peroxidase conjugated anti-rabbit IgG Ab	Cell Signaling Technology
Horseradish peroxidase conjugated anti-mouse IgG Ab	Cell Signaling Technology
Enhanced chemiluminescence (ECL) detection agent	GE Healthcare
Polyvinylidene difluoride (PVDF)	GE Healthcare
Bradford reagent	Bio-Rad

### 3.1.2 Equipment

Analytical balance model A200S	Sartorius
Micropipette 10-10 $\mu$ L	Socorex
Micropipette 10-100 $\mu$ L	Rainin



Micropipette 100-1000 $\mu\text{L}$	Rainin
Multichannel pipette 20-200 $\mu\text{L}$	Rainin
Pipette controller	Rainin
Non-sterile 96-well plates	SPL/Nunc
pH meter	Utech
Water bath	Hetotherm
Vortex mixer model G560E (Vortex-Genie 2)	Scientific industries
Multimode microplate reader Synergy HT	BioTek
CO <sub>2</sub> water-jacketed incubator model NU-4750	Nuaire
Class II biological safety cabinet model NU-440 400E	Nuaire
Light microscope model CKX41	Olympus
Fluorescence microscope DP73+IX71	Olympus
Refrigerated centrifuge model Z32HK	Hermle
Sterile centrifuge tube 15 mL and 50 mL	Corning/Nunc
Sterile 75 cm <sup>2</sup> cell culture flask	Corning/Nunc
Sterile 25 cm <sup>2</sup> cell culture flask	Corning/Nunc
Sterile 60 mm cell culture dish	Corning
Sterile 35 mm cell culture dish	Corning
Sterile 100 mm cell culture dish	Corning
6-well cell culture plate	Corning
24-well cell culture plate	Corning
96-well cell culture plate	Corning
Hot plate stirrer	HS-115
Mini Rocker MR-1	Biosan
Mini-Gel apparatus	Biorad
Electrophoresis Chamber	Biorad
Power supply	Biorad
Wet tank blotting system	Biorad
Gel electrophoresis system and Power supplied	Bio-Rad

Gel documentation Syngene bio imagine	Gene genome
Flowcytometer	Guava
High performance liquid chromatography	Shimadzu
Nylon membrane	Merck
Filter paper	Merck
Milli-Q® Type 1 Ultrapure Water Systems	Merck
Microplate reader M2e	Spectra Max
Juice extractor	Sharp
Laboratory filtration equipment	Merck

### 3.2 Preparation of unripe *Carica papaya* fruit juice extraction

The unripe *Carica papaya* fruit (UCP) was purchased from the local market in Bangkok, Thailand. Papaya fruits were washed through sterile water to remove dirt and latex. This experiment was controlled under the semi-sterile condition. Papaya fruits were peeled the skin and discarded seeds. Then unripe-fleshed papayas were sliced into small pieces and adding into the compact juice extractor to crush their pieces and extract fruit juice. The degradation of the sensitive compounds and biomolecules in the extracted-fresh juices was avoided by keeping a beaker of juice on ice throughout the experiment. The sterile qualitative paper (1#whatman) with laboratory filtration equipment was used to filtrate fresh juice three times. The extracted-juice was dried into powder using freeze-drying or lyophilization. The dried-powders were stored at – 40 °C until used in the experiment.

### 3.3 The chemical components analysis of UCP using High-performance liquid chromatography (HPLC)

We review literature about the antioxidant phytochemical components in several fruits and select the effective chemical standards that might be a composed chemical of UCP. The effective phytochemical components including ascorbic acid, gallic acid, ellagic acid, chlorogenic acid, and quercetin were verified using HPLC (Shimadzu,

Japan) under different analytical conditions, which depended on each standard. The C-18 HPLC column was used in our analytical method.

### 3.3.1 Analysis of ascorbic acid

Preparation of experiment, standard ascorbic acid was dissolved in the ultrapure (Type 1) water at a concentration of 10 mg/mL. The stock solution was filtered through 0.45  $\mu\text{m}$  nylon membrane and diluted the concentration to 100, 50, 25, 12.5, and 6.25  $\mu\text{g/mL}$ , respectively, kept on ice until used. As well as ascorbic acid, the UCP sample was dissolved in ultrapure water at a concentration of 10 mg/mL and sonicated. Then the solution was filtered through a 0.45  $\mu\text{m}$  nylon membrane and kept on ice until used. 20 mM phosphate buffer (pH 2.5) was used as a mobile phase of this method. The flow rate was set at 0.4 mL/min and started the process at the wavelength at 243 nm.

### 3.3.2 Analysis of ellagic acid

UCP and standard ellagic acid powders were dissolved in 0.1 M NaOH at a concentration of 10 mg/mL. The UCP solution was sonicated following by filtered through the 0.45  $\mu\text{m}$  nylon membrane. Then the filtered-standard solution was diluted to the concentration of 100, 50, 25, 12.5, and 6.25  $\mu\text{g/mL}$  using 50% v/v of MeOH in ultrapure water. This assay mobile phase is composed of 20 mM phosphate buffer (pH 2.5) (A) and acetonitrile (B) at a ratio of 70:30 v/v. The flow rate of the mobile phase in this system was set at 1.0 mL/min whereas UV absorbance was monitored at 253 nm.

### 3.3.3 Analysis of gallic acid

The standard gallic acid stock solution was prepared by dissolving 10 mg/mL of their chemical powder in 100 % MeOH and filtered through a 0.45  $\mu\text{m}$  nylon membrane. Then linear standard curved was prepared at a concentration of 100, 50, 25, 12.5, and 6.25  $\mu\text{g/mL}$ , respectively by diluting with 1:1 MeOH and ultrapure water. UCP was dissolved in 1:1 MeOH, and filtered through a 0.45  $\mu\text{m}$  nylon membrane. The mobile phase of this experiment consisted of 20 mM PB (pH 2.5) (A) and acetonitrile (B) at 95:5 and the flow rate of the mobile phase was set at 1.5 mL/min. UV absorbance was monitored at 272 nm in this running system.

### 3.3.4 Analysis of chlorogenic acid and quercetin

The standard chlorogenic acid and quercetin stock solutions were prepared by dissolving 10 mg/mL of their chemical powders in 100 % MeOH and filtered through a 0.45  $\mu\text{m}$  nylon membrane. Then the solution was diluted at a concentration 100, 50, 25, 12.5, and 6.25  $\mu\text{g/mL}$  by diluting with 1:1 MeOH and ultrapure water, which standard curve was prepared following by these concentrations. UCP was dissolved in 1:1 MeOH, and filtered through a 0.45  $\mu\text{m}$  nylon membrane. The mobile phase is composed of 20 mM PB (pH 2.5) (A) and acetonitrile (B), The flow rate was set at 1.5 mL/min. The detection system was monitored the UV absorbance for quercetin and chlorogenic acetonitrile acid at 270 and 325 nm, respectively. The gradient elution was prepared to detect these chemicals following table 6.

Table 5 The gradient elution of quercetin and chlorogenic acid in HPLC detection

Standard	Mobile phase	
Quercetin	20 mM PB (pH 2.5)	(A)
Chlorogenic acid	Acetonitrile	(B)
	Times	%(B)
	0-3 min	10%B
	4-15 min	0-90%B
	16-21 min	90%B
	21-30 min	10%B

## 3.4 Antioxidant scavenging capacity of *Carica papaya* fruit juice extraction

### 3.4.1 Evaluation of hydroxyl radical scavenging activity

This assay based on the Fenton reaction is a catalyzed process to convert  $\text{H}_2\text{O}_2$  into highly reactive  $\text{OH}^\cdot$  via the oxidation of  $\text{Fe}^{2+}$  into  $\text{Fe}^{3+}$ . The reaction between 2-

deoxy-2-ribose and generated-OH<sup>•</sup> produce malonaldehyde bis (dimethyl acetal) (MDA). MDA reacts with thiobarbituric acid (TBA) under acid conditions leading to MDA-TBA adduct production. The MDA-TBA pink chromogen can detect at an absorbent wavelength of 532 nm using a spectrophotometer. The fading of the pink color chromogen is a direct variation with the scavenging potential of the sample. The scavenging activity of the sample can estimate by the linear plotted curve of percent inhibition and sample concentration.

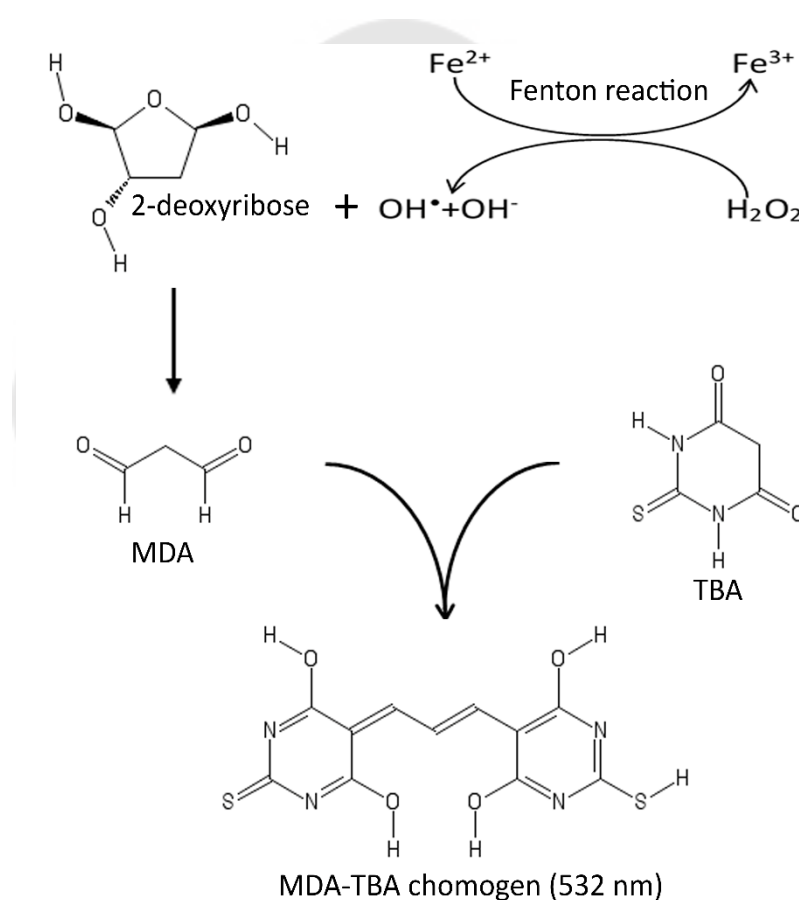


Figure 15 The reaction of hydroxyl radical scavenging activity

The preparation of this assay is based on the previous method by Mandal S. et al 2011 (143) and Birasuren B. et al 2013 (144). The UCP sample and Trolox standard were dissolved in 0.1 M potassium phosphate buffer ( $\text{KH}_2\text{PO}_4$ ) pH 7.4. Diluted sample and standard solutions were mixed with reaction mixture (EDTA,  $\text{FeCl}_3$ , 2-deoxy-2-

ribose,  $\text{H}_2\text{O}_2$ , and sodium L-ascorbate at 0.2, 0.1, 1.12, 0.2, and, 0.02 mM, respectively) incubated at 50 °C for 20 minutes. After incubation, the reaction was stopped by adding trichloroacetic acid (TCA) at a final concentration of 1.120% . TBA chromogen was added at a final concentration of 0.4 % and incubated at 95 °C for 15 minutes. The MDA-TBA adducts were measured at absorbance wavelength 532 nm using a spectrophotometer. The percent inhibition was calculated following the equation below. The linear regression curve of sample concentration and percent inhibition was plotted and evaluated  $\text{IC}_{50}$ .

$$\text{Percent inhibition} = \frac{(\text{Abs}_{\text{blank}} - \text{Abs}_{\text{sample}})}{\text{Abs}_{\text{blank}}} \times 100$$

### 3.4.2 Evaluation of hypochlorous acid scavenging activity assay

This assay is based on the reaction of 5,5-dithiobis (2-nitrobenzoic acid) (DTNB) is converted into 5-thio-2-nitrobenzoic acid (TNB) chromogens, which sodium borohydride ( $\text{NaBH}_4$ ) can convert DTNB into TNB to performing the assay. The dissolving of sodium hypochlorite ( $\text{NaOCl}$ ) in distilled water generates hypochlorous acid ( $\text{HOCl}$ ). TNB is transformed to DTNB (clear color) when reacted with  $\text{HOCl}$ , which this reaction used to evaluate the  $\text{HOCl}$  scavenging activity via measurement of TNB absorbance at wavelength 412 nm.

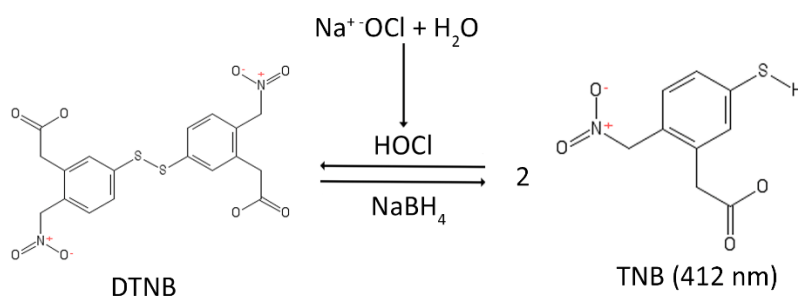


Figure 16 The reaction of hypochlorous acid scavenging activity

The preparation of this assay is based on the method described by Valentao P et al 2003 (145). Briefly, UCP and ascorbic acid standards were dissolved in 50 mM potassium phosphate buffer pH 6.6 and diluted to selective concentration. 40  $\mu$ M HOCl was freshly prepared by diluted NaOCl in distilled water to a final concentration at 0.1 % v/v and adjusted the pH to 6.2 with 0.6 M sulfuric acid ( $H_2SO_4$ ). The concentration of HOCl was further determined to close the true concentration using the molar absorption coefficient of HOCl at  $100 M^{-1}cm^{-1}$  at a measurement wavelength of 235 nm using a spectrophotometer. 40  $\mu$ M TNB was prepared by dissolving 1 mM solution of DTNB in 50 mM potassium phosphate buffer pH 6.0, containing 5 mM EDTA, and then mixed with 20 mM  $NaBH_4$  dissolved in distilled water at 5:1 fold. As well as HOCl, the TNB solution was determined and adjusted to closely the true concentration using the molar absorption coefficient of TNB at  $13,600 M^{-1}cm^{-1}$  at measurement wavelength 412 nm using a spectrophotometer. After preparation of the reaction solutions, UCP and ascorbic acid were mixed with TNB at a concentration of 40  $\mu$ M. Then absorbance wavelength at 412 nm was measured to prepared absorbance value before added HOCl ( $Abs_{before}$ ). Then the absorbance value after added HOCl ( $Abs_{after}$ ) was measured after added and incubated 40  $\mu$ M HOCl for 5 minutes. The linear regression curve of sample concentration and percent TNB remaining was plotted and IC50 value was calculated, which percent TNB remaining can calculate the following equation:

$$\text{Percent TNB remaining} = 100 - \frac{(Abs_{before} - Abs_{after})}{Abs_{before}} \times 100$$

### 3.4.3 Evaluation of superoxide anion scavenging activity

The oxygen is received electron via the reduction of phenazine methosulfate (PMS) into reduced form by nicotinamide adenine dinucleotide (NADH) generating superoxide anion radicals ( $O_2^{\bullet -}$ ). The produced  $O_2^{\bullet -}$  transfer electron to nitro blue tetrazolium (NBT). NBT formazan is generated after NBT is reduced. Determination of  $O_2^{\bullet -}$  scavenging activity evaluates via measurement of formazan absorbance at 560 nm

using a spectrophotometer. Which scavenger would decrease the yellow color of formazan by directly eliminate  $O_2^{\cdot-}$ .

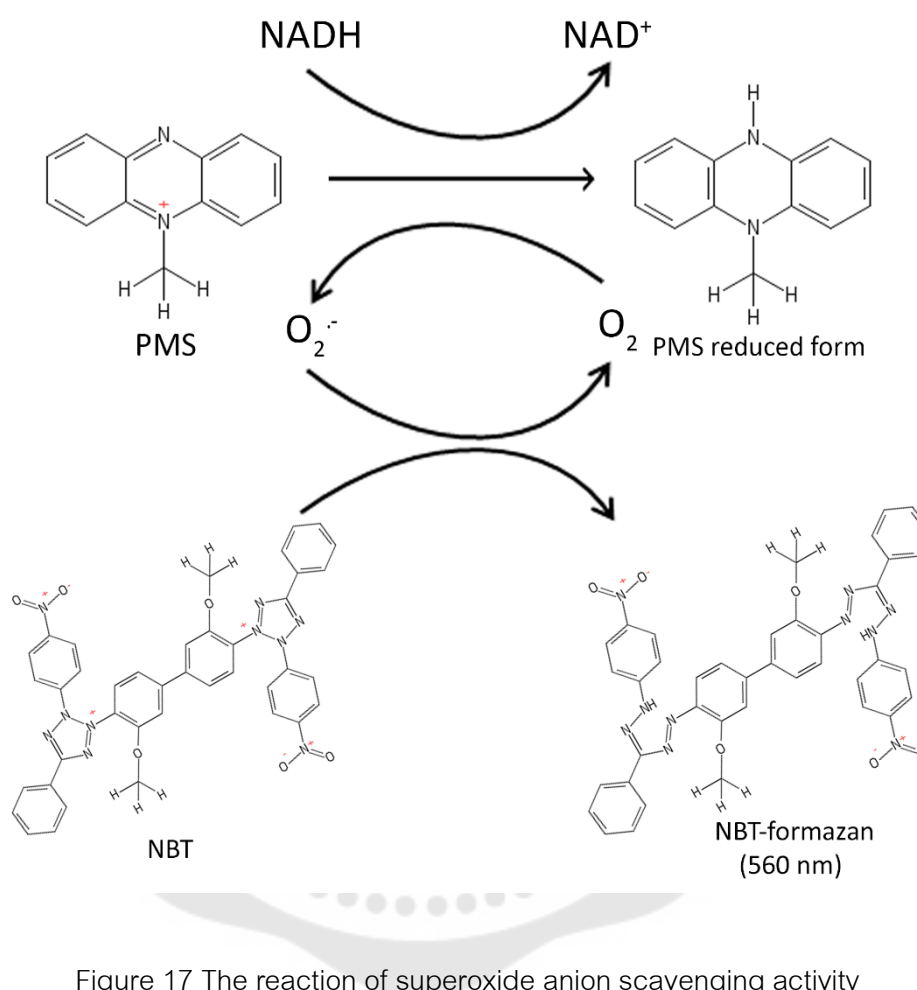


Figure 17 The reaction of superoxide anion scavenging activity

This method was prepared following the previous assay described by Kumar R. 2005. Et al (146). Various concentrations of UCP and standard (ascorbic acid) were mixed with 90  $\mu$ M NADH and 77.4  $\mu$ M NBT dissolved in 19 mM potassium phosphate buffer pH 7.4. Then PMS (9  $\mu$ M) in 19 mM potassium phosphate buffer pH 7.4 was mixed for start reaction. The reaction mixture was incubated at 25  $^{\circ}$ C for 3 minutes and measured absorbance wavelength at 560 nm using a spectrophotometer. The linear regression curve of sample concentration and percent inhibition was plotted



and IC50 value was calculated, which percent inhibition can calculate the following equation:

$$\text{Percent inhibition} = \frac{(\text{Abs}_{\text{blank}} - \text{Abs}_{\text{sample}})}{\text{Abs}_{\text{blank}}} \times 100$$

#### 3.4.4 Evaluation of hydrogen peroxide scavenging activity

The hydrogen peroxide scavenging activity is determined via the dimerization of homovalinic acid (HVA). The fluorescent dimers of HVA at an excitation wavelength at 315 nm and emission wavelength at 425 nm are generated after HVA monomer catalyzed by horseradish peroxidase (HRP) and  $\text{H}_2\text{O}_2$ , which it can measure using a spectrophotometer. Therefore,  $\text{H}_2\text{O}_2$  scavenger would inhibit the dimerization of HVA leading to fluorescent fading.

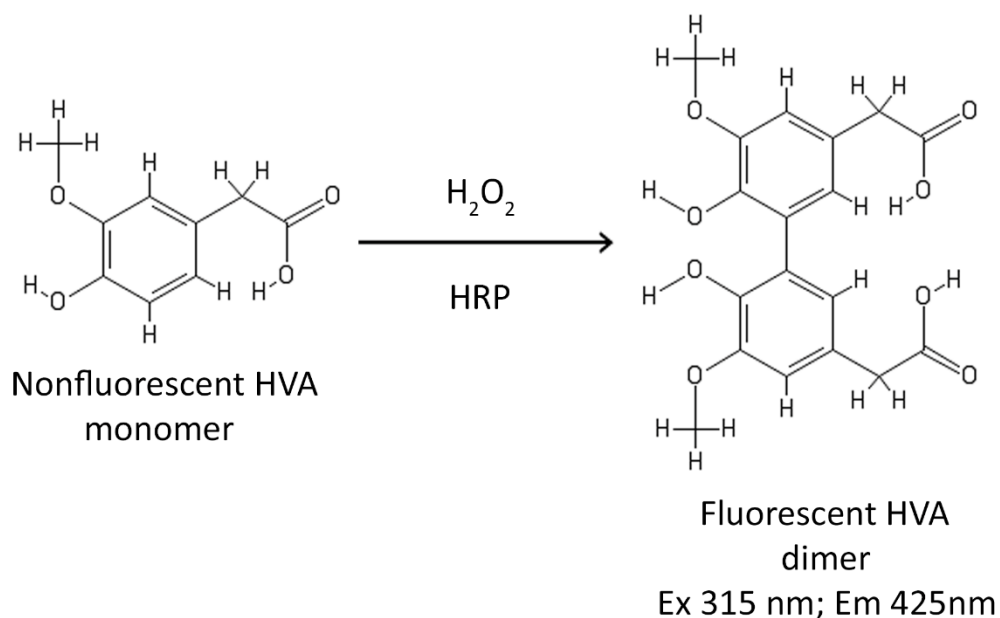


Figure 18 The reaction of hydrogen peroxide scavenging activity

The preparation of this assay is based on the previous method reported by Paital B .2014 (147). HVA and HRP were dissolved in 50 mM potassium phosphate buffer pH 7.4 at a concentration of 125  $\mu$ M and 0.1 U, respectively to prepare the reaction mixtures. Various concentrations of UCP and standard (Trolox) were mixed with the mixture in 96 well plates and added 30  $\mu$ M H<sub>2</sub>O<sub>2</sub> incubated for 60 minutes at room temperature with gentle shaking on the shaker. Then measured the fluorescence intensity at an excitation and emission wavelength at 315 and 425 nm using a spectrophotometer. Linear regression curve of sample concentration and percent inhibition was plotted and IC50 value was calculated, which percent inhibition can calculate the following equation;

$$\text{Percent inhibition} = 100 - \frac{(\text{RFU}_{\text{blank}} - \text{RFU}_{\text{sample}})}{\text{RFU}_{\text{blank}}} \times 100$$

### 3.5 Ferric reducing antioxidant power (FRAP)

This method is commonly accepted uses for the determination of antioxidant potential. This assay is based on the reduction of Fe<sup>3+</sup>-TPTZ complex into the Fe<sup>2+</sup>-TPTZ complex (blue color). Which the donated-electron from antioxidant to Fe<sup>3+</sup> complex is a key of reaction. Therefore, the antioxidant potential is a direct variation with blue color brightness, which can measure at absorbance wavelength 593 nm using a spectrophotometer.

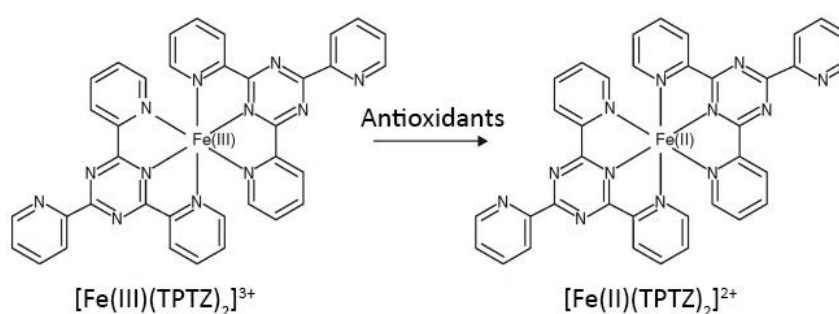


Figure 19 The reaction of FRAP assay

The preparation of this assay is based on the previous method reported by Benzie I. 1996 (148). 300 mM acetic acid, 20 mM  $\text{FeCl}_3$ , and 10 mM TPTZ in 40 mM HCl were mixed for preparation of FRAP reagent at a ratio of 1:1:10. The reaction was started after adding FRAP reagent into each well of samples the standard (ascorbic acid) in a 96-well plate. The absorbance at 593 nm was measured using a spectrophotometer. The antioxidant power in the FRAP unit (FRAP value) was calculated by using the standard  $\text{Fe(II)SO}_4$  linear plotted curve. In this assay, data were shown in FRAP value ( $\mu\text{M FeSO}_4$ ) of sample and standard equivalent.

### 3.6 Oxygen radical absorbance capacity (ORAC)

The ORAC is the commonly recommended assay to determine the antioxidant capacity of samples. The free radical initiator named 2,2'-azobis(2-amidino-propane) dihydrochloride (AAPH) generates peroxy radicals ( $\text{ROO}^\bullet$ ). Fluorescein is fluorescent probe tracer generating fluorescence that can detect at excitation 485 nm and emission wavelength 528 nm. The produced- $\text{ROO}^\bullet$  by AAPH can convert fluorescein into non-fluorescent, which this process is based on ORAC assay. Antioxidant would eliminate  $\text{ROO}^\bullet$  to inhibit the transforming of fluorescein, which would slowly fade down depending on the antioxidant potential.

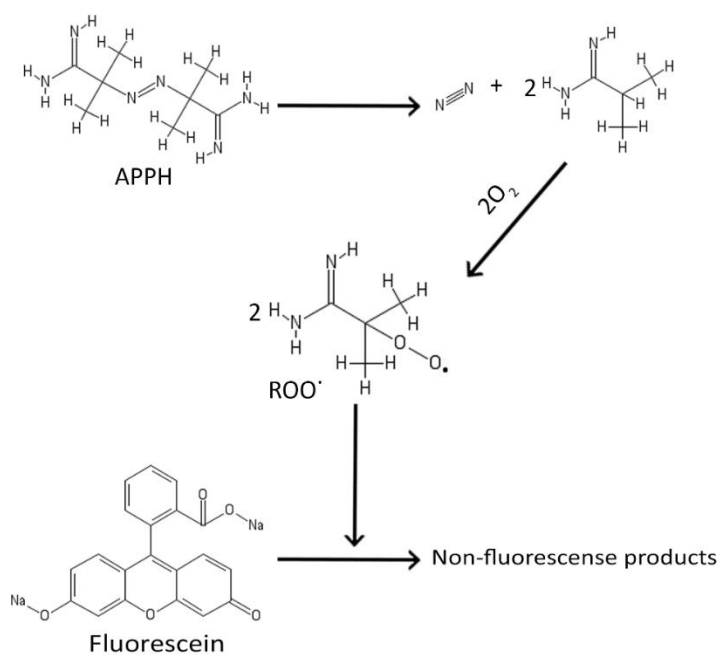


Figure 20 The reaction of ORAC assay

The preparation of this is based on the previous report by Thaipong K. 2006 (149). The reaction mixture containing 10 nM fluorescein and samples or standard dissolved in 75 mM potassium phosphate buffer pH 7.4 were incubated at 37 °C for 5 min (protect from light until the end of the experiment). Then 165 mM AAPH was added starting the reaction. The fluorescence intensity at excitation and emission wavelength 485 nm and 528, respectively were measured in a 1-minute interval for 60 min using a spectrophotometer. The kinetic data and area under the curve were calculated to follow equation or using Graphpad Prism software.

$$AUC = 1 + RFU_1/RFU_0 + RFU_2/RFU_0 + RFU_3/RFU_0 + \dots + RFU_n/RFU_0$$

RFU<sub>0</sub> = relative fluorescence units at time point zero

RFU<sub>n</sub> = relative fluorescence units at time points (eg. RFU<sub>5</sub> is the relative fluorescence value at minute five)

Evaluation of antioxidant capacity, Net AUC values were calculated following equation; and plotted linear curve

$$\text{Net AUC} = \text{AUC}_{\text{sample}} - \text{AUC}_{\text{blank}}$$

In this assay, the antioxidant potential of the sample was shown in standard (Trolox) equivalent values.

### 3.7 Ferric thiocyanate (FTC) assay

The FTC method was used to determine the effect of UCP on linoleic acid oxidation (lipid peroxidation). This assay is based on the described method by Takao T, Kitatani F, and Wanatabi N (1994) and Mihaljevic, Katusin-razem, and Razem, (1996) (150, 151). Linoleic acid is a carboxyl functional group (ROOH) that can receive an electron from  $\text{Fe}^{2+}$  converting to alkoxy ( $\text{RO}^{\cdot}$ ) and lipid peroxy radical ( $\text{ROO}^{\cdot}$ ),  $\text{Fe}^{3+}$  also produce in this reaction. Linoleic radicals also despoil electrons from  $\text{Fe}^{2+}$  to generate  $\text{Fe}^{3+}$ . The produced- $\text{Fe}^{3+}$  reacts with thiocyanate (SCN) generating ferric thiocyanate ( $\text{Fe}(\text{SCN})_5^{2-}$ ) that can measure at absorbance wavelength 500 nm.

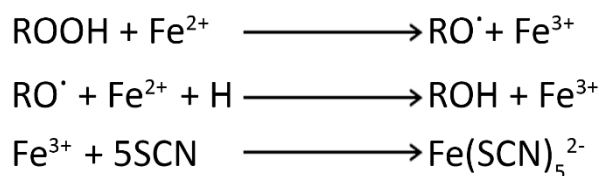
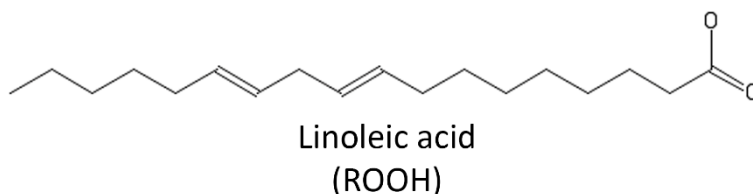


Figure 21 The reaction of FTC assay

Briefly, UCP and standard Trolox dissolved in 50 mM potassium phosphate buffer pH 7.0 were mixed with the linoleic solution (0.5 % final concentration). The solution mixtures were incubated at 40 C° in the dark. Each solution was aliquoted every 24 hours for the detection method. The aliquot of each sample was mixed with a solution mixture containing 3 mL of 75 % ethanol, 0.1 mL of 30% NH<sub>4</sub>SCN and 0.1 mL of 4.5 mM FeSO<sub>4</sub> in 0.02 M HCl incubated for 3 minutes. After incubation, the mixture was added in each well of 96 well plates and measured absorbance at 500 nm using a spectrophotometer. The linear regression curve of absorbance at 500 nm and times (day) were plotted whereas percent inhibition was calculated following the equation below, and plotted. The inhibition effect of UCP on linoleic acid peroxidation was compared with control (excluded linoleic acid).

$$\text{Percent inhibition} = \frac{(\text{Abs}_{\text{blank}} - \text{Abs}_{\text{sample}})}{\text{Abs}_{\text{blank}}} \times 100$$

### 3.8 Cell culture and treatment

Human endothelial cell line EA hy926 (ATCC® CRL-2922™) was used to determine the protective effect of UCP in this study. The EA hy926 was grown in Dulbecco's modified eagle medium (DMEM) contained 10% of fetal bovine serum (FBS), 1% of 10000 U/mL penicillin, and 10000 µg/mL streptomycin (Thermo Fisher Scientific, Massachusetts, USA) humidified with 5% CO<sub>2</sub> at 37 °C in the incubator. Fresh media was changed every 3 days when the cell growth to 80-90 % confluence, were trypsinized using 0.25% trypsin EDTA. Preparation for the experiment, EA hy926 cells were plated for 18 – 24 hours. Then the cells were pretreated with fresh media with or without various concentrations of UCP incubated for 48 hours. After that, cells were induced oxidative stress by 1mM H<sub>2</sub>O<sub>2</sub> for 2 hours and analyzed the following method of each experiment.

### 3.9 Cell viability assay

In this study cell viability of EA hy926 cells was determined 3-(4,5-dimethylthiazol-2-yl)-2,5-diphenyltetrazolium bromide (MTT) assay. MTT assay is the currently acceptable method to preliminarily evaluate cell viability, which is based on the catalyzed-MTT (yellow color) by the mitochondrial dehydrogenase enzyme in living cells, converting MTT into insoluble purple formazan crystal. These crystals were dissolved in 100% DMSO, which can measure at absorbance wavelength 550 nm using a spectrophotometer.

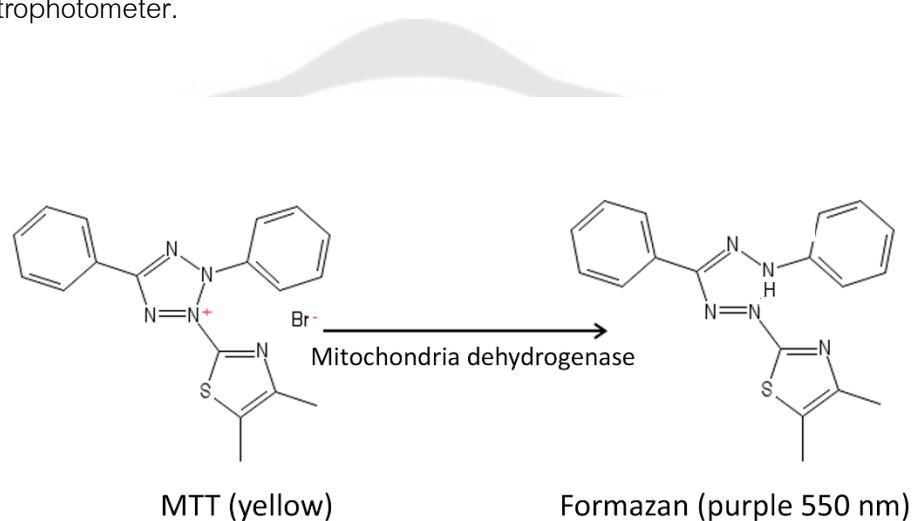


Figure 22 The reaction of MTT assay

Preparation of cell viability assay,  $5 \times 10^3$  cells were plated in 96-well cell culture plate for 18-24 hours. Then cells were pretreated with or without UCP at concentrations 10, 100, and 1000  $\mu\text{g}/\text{mL}$  incubated at 37 °C for 48 hours. Then media was removed and washed twice with fresh media. Cells were replaced with fresh media containing with or without 1 mM  $\text{H}_2\text{O}_2$  incubated for 2 hours. MTT was used to determine cell viability, in which 0.25 mg/mL of MTT was incubated for 3 hours. In each well, media was removed and formazan crystals were dissolved by adding 100% DMSO. The purple solutions were measured at an absorbance wavelength of 550 nm using a spectrophotometer. The cell viability sample was compared with the control group.

### 3.10 Measurement of intracellular ROS by flow cytometry assay

Intracellular ROS of EA hy926 cells is induced by  $H_2O_2$ . The cell-permeable 2',7'-dichlorodihydrofluorescein diacetate (DCFH-DA) is a non-fluorescent compound that most widely used probe for detecting intracellular ROS. DCFH-DA permeate through the cell membrane into the cell, which it is deacetylated by intracellular esterase to 2',7'-dichlorodihydrofluorescein (DCFH). DCFH is oxidized by intracellular ROS converting into 2',7'-dichlorofluorescein emitting fluorescent light at excitation and emission wavelength at 495 nm and 529 nm that can detect by fluorescence microscope or flow cytometer.

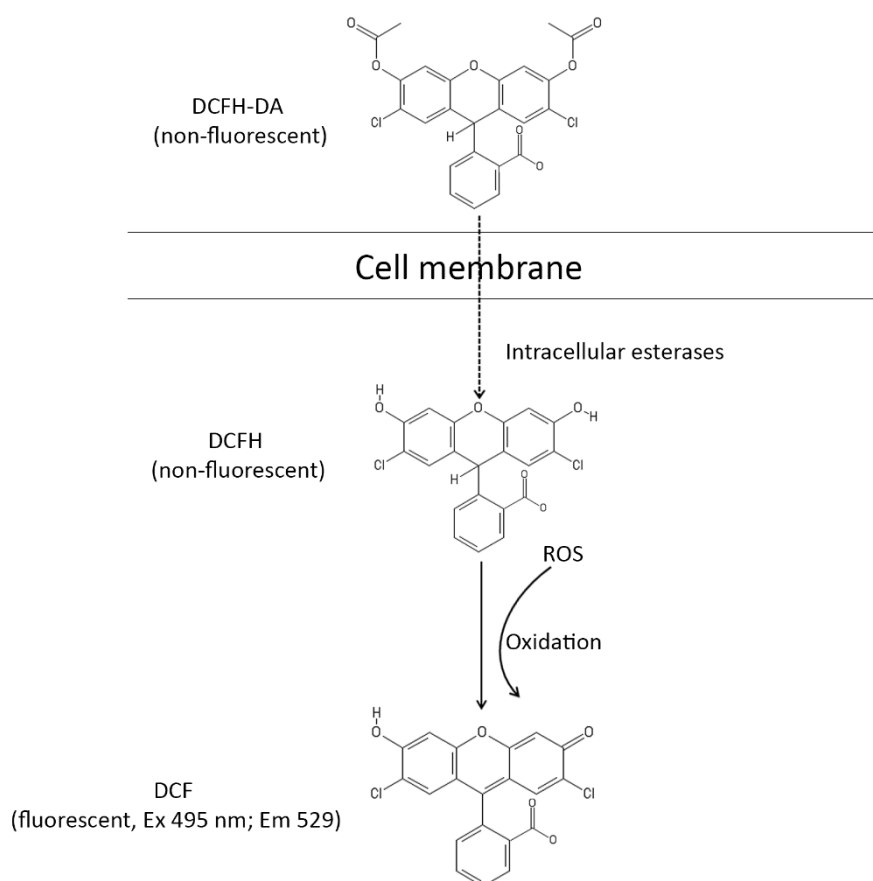


Figure 23 The reaction of DCFH-DA staining



$1.5 \times 10^5$  of EA hy926 cells were plated in a 60 mm cell culture plate for 18 -24 hours incubation. Then fresh media with or without various concentrations of UCP were replaced and incubated for 48 hours. After incubation, cells were treated 1 mM  $H_2O_2$  and washed with 1 x PBS twice times after 2 hours incubation. Then phenol red-free media containing 0.025 mg/mL DCFH-DA dissolved in 100% DMSO were replaced and incubated for 30 minutes. The media was removed and washed with 1 x PBS twice. Then cells were trypsinized using 0.05 % trypsin and neutralized 1:1 fresh media containing 10 % FBS centrifuged at 125 g for 5 minutes. The supernatant was removed and washed with 1 x cold PBS centrifuged at 125 g for 5 minutes twice times. Cell concentration was adjusted to 300 – 500 cells/ $\mu$ L before analyzed by the flow cytometer. Intracellular ROS were evaluated and analyzed using a flow cytometer (Guava ® easyCyte).

### 3.11 Measurement of apoptotic cells

The fluorescent nucleic acid stain dye, Hoechst can be permeated into the cell nucleus and attached to DNA emitting blue fluorescence. Different from Hoechst, propidium iodide (PI) cannot through the cell membrane of living cells. Ruptured of the cell membrane in an apoptotic cell lead to the PI through into the cell and attach to nuclear DNA emitting red fluorescent light. Which late apoptotic and necrotic cells are tagged by PI stain. These commonly nuclear-stained methods can detect by fluorescence microscope and flow cytometer.

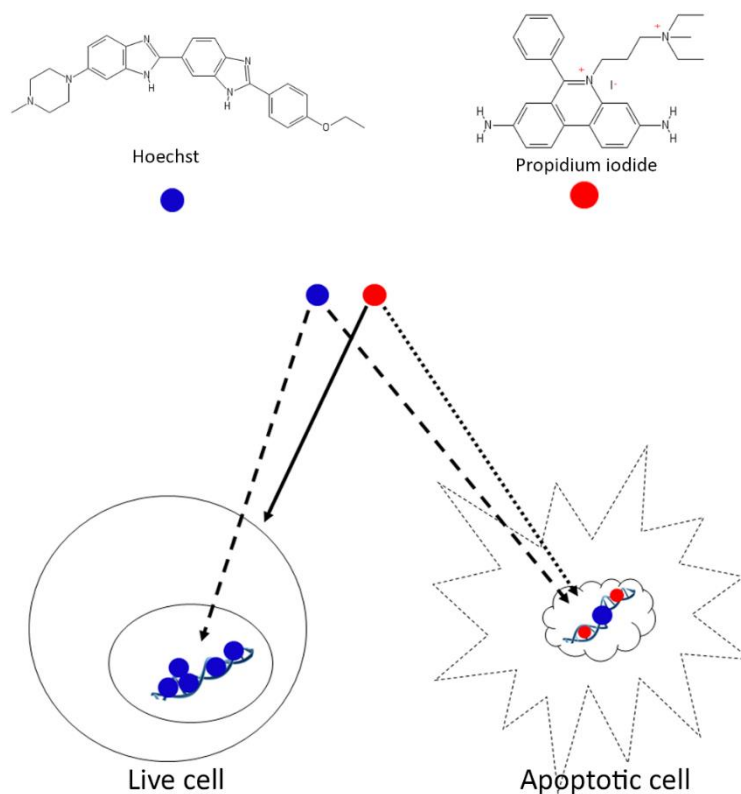


Figure 24 The reaction of Hoechst and PI staining

In the preparation for this method,  $4 \times 10^4$  of EA hy926 cells were plated in a 35 mm cell culture dish for 18-24 hours. Cells were pretreated with fresh media containing with or without various concentrations of UCP for 48 hours. After that, 1 mM  $H_2O_2$  was replaced and incubated for 4 hours. Media were replaced with fresh DMEM containing 1  $\mu\text{g}/\text{mL}$  Hoechst incubated for 15 min. After incubation, cells were washed and stained PI at a concentration of 1  $\mu\text{g}/\text{mL}$  for 15 min. cells were washed and cover the cell surface with adding 1 x PBS. The fluorescent staining cells were observed under a fluorescence microscope. The three randomized field images were used to analyze using image J software avoiding bias by add-in color threshold. Percent apoptotic cell was calculated following equations;

$$\text{Percent of apoptotic cells} = \frac{\text{Number of apoptotics cells}}{\text{Number of total cells}}$$

### 3.12 Measurement of superoxide dismutase activity

In our study, the SOD assay kit (19160 sigma) was used to determine the SOD activity of EA hy926 cells after treatment. The reaction of this assay kit is based on generated  $O_2^{\cdot -}$  by the catalyzation of  $O_2$  by xanthine oxidase. Scramble of the electron from water-soluble tetrazolium salt ( 2-( 4-Iodophenyl) - 3-( 4-nitrophenyl) -5-( 2,4-disulfophenyl)-2H-tetrazolium, monosodium salt (WST-1) by produced- $O_2^{\cdot -}$  generates a WST-1 formazan, which can measure at absorbance wavelength 440 nm using a spectrophotometer.

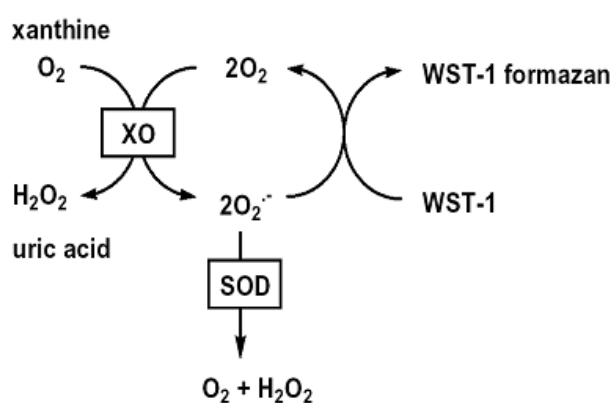


Figure 25 The reaction of SOD ELISA kit

The preparation of this method followed the SOD assay kit protocol. Briefly, 20  $\mu$ L of protein samples, blank 1 (without samples), blank 2 (without enzyme working solution), and blank 3 (without samples and enzyme working solution) were added in 96 well plates. Then each well was added 200  $\mu$ L of WST working solution well. The reaction was started by adding 20  $\mu$ L of enzyme working solution in the sample and blank 1 well, whereas blank 2 and 3 adding only dilution buffer. Then reagents were mixed and incubated at 37 °C for 20 minutes. After incubation, absorbance was measured using a spectrophotometer at wavelength 440 nm. SOD activity of each sample was calculated following equation;

$$\text{SOD activity} = \left\{ \frac{[(\text{Abs}_{\text{blank1}} - \text{Abs}_{\text{blank3}}) - (\text{Abs}_{\text{sample}} - \text{Abs}_{\text{blank2}})]}{(\text{Abs}_{\text{blank1}} - \text{Abs}_{\text{blank3}})} \right\} \times 100$$

### 3.13 Measurement of catalase activity

This method is based on the catalase enzyme-producing formaldehyde via catalyzation of methanol and  $\text{H}_2\text{O}_2$ . Produced-formaldehyde reacts with 4-amino-3-hydrazino-5-mercapto-1,2,4-triazole (Purplad chromogen) converting to an uncolored intermediate compound. Which this compound is oxidized by potassium periodate ( $\text{KIO}_4$ ) producing the purple-colored oxidation product that can measure at absorbance wavelength 540 nm using a spectrophotometer.

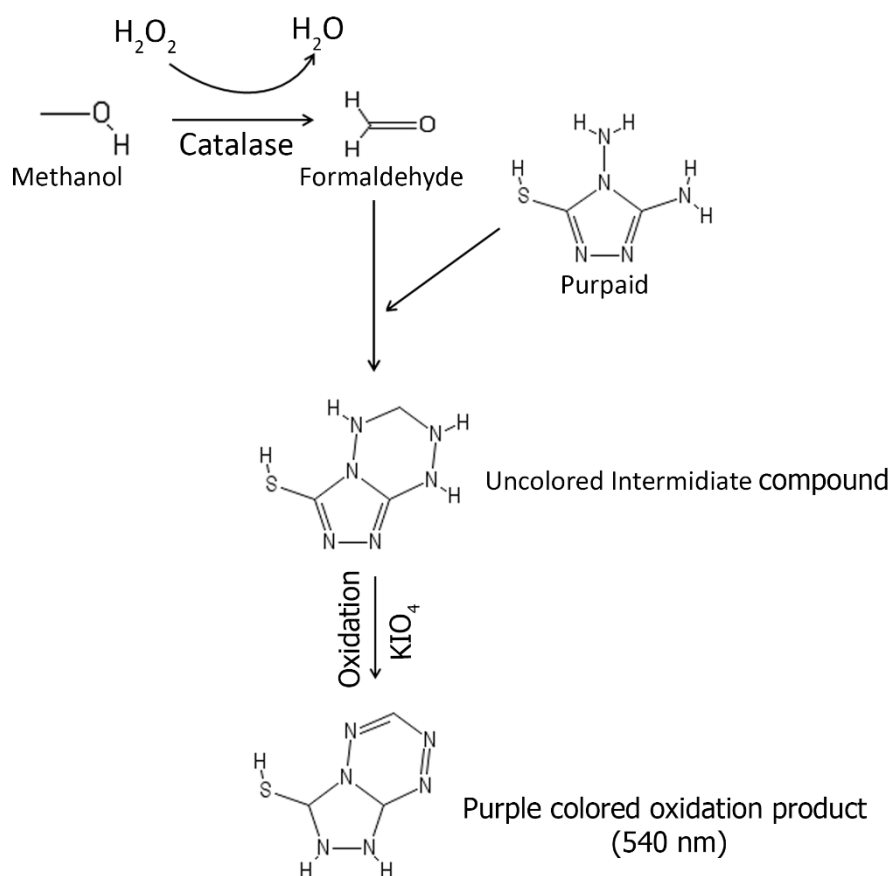


Figure 26 The reaction of CAT activity assay

The preparation of this assay is based on the basic method described by Johansson LH. 1988 (152). The various concentrations of formaldehyde (0-120  $\mu\text{M}$ ) were performed to standard in this assay. Test buffer containing 30% methanol in assay buffer (100 mM potassium phosphate buffer pH 7.0) was prepared. Protein lysates and standard formaldehyde 100 mM potassium phosphate buffer pH 7.5 supplementing 0.1% BSA and 1mM EDTA were added in a 96-well plate containing test buffer  $\text{H}_2\text{O}_2$  at a concentration of 35 mM was added to start the reaction. After incubation at room temperature for 20 minutes, 3mg/mL of Purpald dissolved in 0.5 M KCl was mixed incubating for 10 minutes with the gently shaking on the shaker. potassium periodate dissolved in 0.5 M KCl at a concentration of 65.2 mM was mixed into each well. After 5 minutes, the absorbance wavelength at 540 nm was measured using a spectrophotometer. The formaldehyde concentration and CAT activity were calculated following equation;

$$\text{Formaldehyde } (\mu\text{M}) = \left\{ \frac{[\text{Abs}_{\text{sample}} - (\text{y-intercept})]}{\text{Slope}} \times \frac{\text{Total volume (0.17 mL)}}{\text{volume (0.02 mL)}} \right\} \quad (152)$$

$$\text{CAT activity (nmol/min/mL)} = \left[ \left( \frac{\text{Formaldehyde } (\mu\text{M})}{\text{Reaction time (20 min)}} \right) \times \text{Dilution factor} \right]$$

### 3.14 Measurement of glutathione peroxidase activity

Determination of GPX activity based on the redox reaction of glutathione. GPX is a catalytic enzyme that eliminates intracellular ROS collaborating with GSH, which is converting to GSSG. Glutathione reductase cooperating with NADPH cofactor catalyzes GSSG reversing into GSH. As well as, in this assay, ROOH is catalyzed by GPX reaction into ROH leading to converting of GSH into GSSG. The generated-GSSG is reversed into GSH by NADPH and GR. NADPH is a key chemical compound of this method that can measure at absorbance wavelength 340 nm. When the reaction is started, NADPH will decrease with increasing time. Thus, the performing of this method is on the kinetic assay.

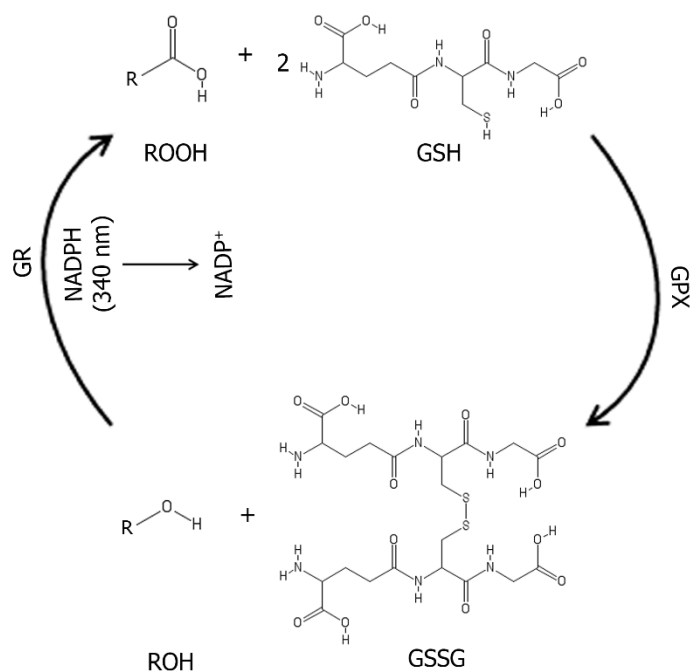


Figure 27 The reaction of GPX activity assay

This method is prepared following a previous study by Weydert C.J 2010. (153). The protein lysate samples and standard GPX in buffer (1 mM EDTA and 1mg/mL BSA dissolved in 100 mM KH<sub>2</sub>PO<sub>4</sub> pH 7.4) were mixed with 100 mM KH<sub>2</sub>PO<sub>4</sub> pH 7.4 accommodating 1mM EDTA). The co-substrate mixture was prepared by mixing 5 units/mL GR, 0.4 mg/mL GSH, and 0.6 mg/mL NADPH and then adding in each well. 15 mM of cumene hydroperoxide was added to start the reaction. The absorbance wavelength was quickly measured for 1 hour 1-minute interval at 340 nm. The GPX activity was calculated to follow the equation;

$$\text{Slope} \left( \frac{\Delta A_{340}}{\text{min}} \right) = \frac{|\Delta A_{340} (\text{Time}_2) - \Delta A_{340} (\text{Time}_1)|}{\text{Time}_2 - \text{Time}_1}$$

$$\text{GPX activity} = \left( \frac{\text{Slope} \times \text{Total volume} \times \text{Dilution factor}}{\text{NADPH extinction coefficient} \times \text{Sample volume}} \right)$$

### 3.15 Measurement of intracellular total glutathione levels

Likely GPX activity assay, total GSH (tGSH) is based on the glutathione redox cycle. However, the reaction solution of this method is without GSH. GSSG in the sample is a source of GSH, in which GSSG is catalyzed by GR cooperating with NADPH into GSH. The produced-GSH can transform non-colored DTNB into yellow-colored TNB that can measure at absorbance wavelength 412 nm.

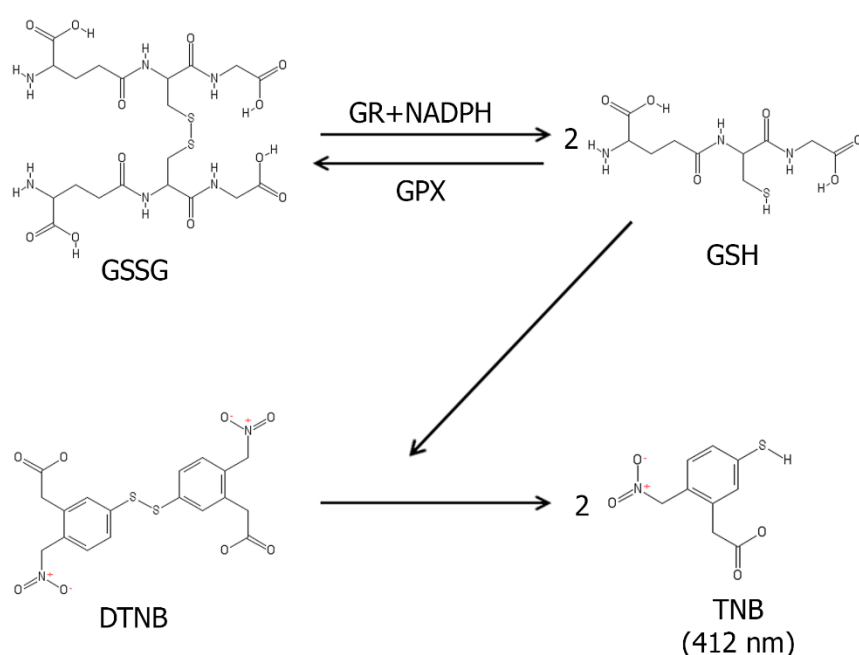


Figure 28 The reaction of tGSH levels assay

tGSH level is based on a previous method described by L. Chularojmontri, 2013 (154). Briefly, various concentrations of standard GSH (0-20  $\mu\text{M}$ ) and samples (10, 100, and 1000  $\mu\text{g/mL}$ ) at a volume of 50  $\mu\text{L}$  were added in each well of the 96-well plate. DTNB solution (0.5 mg/mL DTNB dissolved in 100 mM  $\text{K}_2\text{HPO}_4$  containing 1 mM EDTA pH 7.4) was added at a volume 50  $\mu\text{L}$  and mixed. 50  $\mu\text{L}$  of glutathione oxidoreductase solution (1 unit/mL of glutathione reductase dissolved in 100 mM  $\text{K}_2\text{HPO}_4$  with 1 mM EDTA and 1 mg/mL bovine serum albumin (BSA) pH 7.4) was added and incubated for

10 minutes at room temperature. After that, 0.3 mg/mL NADPH<sub>2</sub> dissolved in 100 mM K<sub>2</sub>HPO<sub>4</sub> with 1 mM EDTA pH 7.4 was added at a volume of 50 µL. The formation of color product (TNB) was monitored at absorbance wavelength 412 nm. The amount of tGSH level in the cell lysate sample was calculated using GSH standard curves and equalized each sample by normalized to 1 mg protein.

### 3.16 Measurement of an Nrf2 transcription factor

The 600590 Nrf2 transcription factor ELISA kit (Cayman Chemical) was used to examine this incident. Each well of 96 well plates in this kit is coated with a consensus dsDNA sequence. Which NRF2 transcription factor in the nucleus extract samples has specifically bound with the coated dsDNA. Primary antibody and secondary HRP antibody are used for detecting in this kit. The developing reagent activates HRP-conjugated on the secondary antibody, which can detect the signals at absorbance wavelength 450 nm using a spectrophotometer.



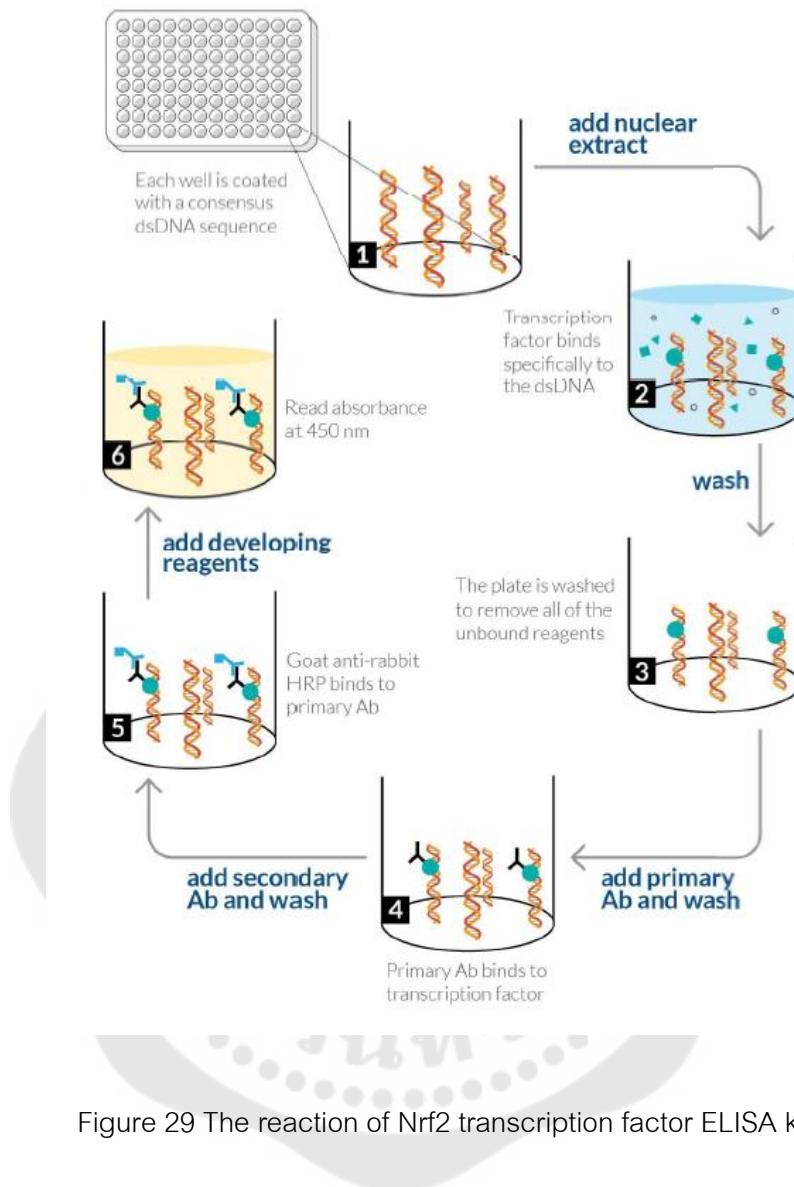


Figure 29 The reaction of Nrf2 transcription factor ELISA kit

The nuclear extraction kit (Cayman No. 10009277) was used to gather the nuclear extraction lysate samples for this assay detection. In the preparation, 96-well coated plate and buffer were equilibrated at room temperature. Complete transcription factor binding (CTFB) was prepared and mixed with or without samples, competitor, and positive control in each coated well and incubated overnight at 4 °C or one hour at room temperature without agitation. Each well was washed five times with 1 x wash buffer. Then diluted NRF2 primary antibody was added and incubated for one hour at room temperature without agitation. Each well was washed five times with 1 x wash buffer and

added diluted-NRF2 secondary antibody. Then incubated for one hour at room temperature without agitation. After that, each well was washed and replaced with a developing solution incubated for 15 – 45 minutes with gentle agitation. The stop solution was added and the absorbance wavelength at 450 nm was measured using a spectrophotometer. The analytical data were shown the percent, Nrf2 expression relative, with the control group.

### 3.17. Western blot analysis

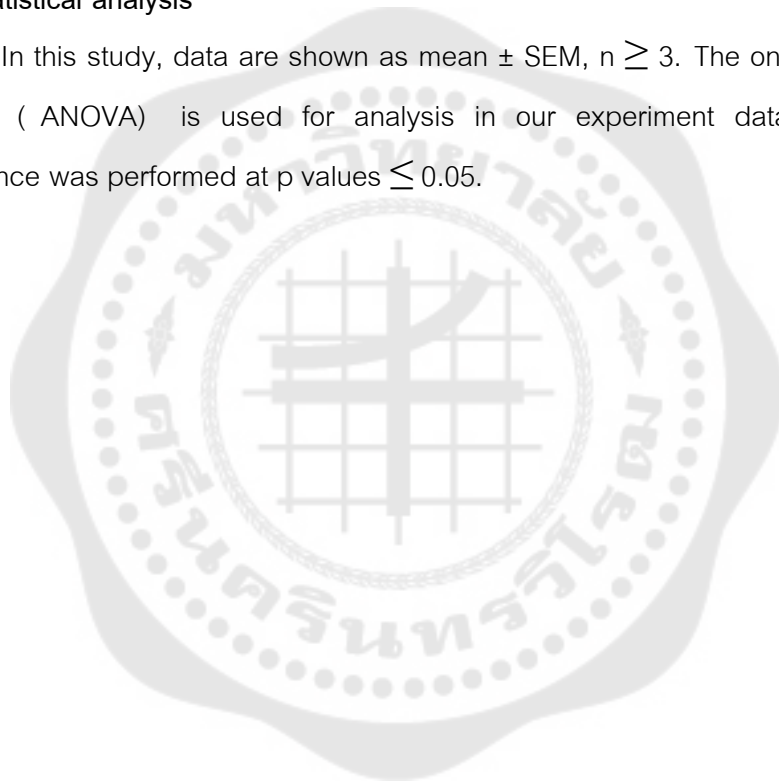
Western blot is an analytical technique to detect specific proteins. Protein lysate samples are separated by SDS-poly acrylamide gel electrophoresis (PAGE), which separates on protein size and charge. Separated proteins are transferred to polyvinylidene difluoride (PVDF) membranes and probed with primary specific antibodies. The HRP-conjugated secondary antibody is attached to the primary antibody. HRP substrate or developer adding induce HRP to promote signal. The protein quantification is evaluated by measured chemiluminescence signals using a gel documentation system.

In this assay, whole protein lysates were collected by RIPA buffer (50 mM Tris-HCl, 150 mM NaCl, 1% Triton X-100, 1% sodium deoxycholate, 0.1% SDS, 30 mM Na<sub>2</sub>HPO<sub>4</sub>, 50 mM NaF and 5 mM EDTA) and nuclear lysates were collected by nuclear extraction kit (Cayman No. 10009277). Both protein lysates were mixed with 6 x loading dye and separated by SDS-PAGE at 100 V for 90 min. After that, separated proteins were transferred into the Amersham™ Hybond™ 10600023 PVDF membrane using the Bio-Rad Mini-PROTEAN Tetra system at 100 V 120 minutes. PVDF membranes were blocked with a blocking agent (5% BSA or 5% non-fat dry milk in 1X Tris buffer saline containing 0.1% Tween (TBST)) and incubated at room temperature for one hour. Then primary antibodies including 1:1000 phospho-Akt, Akt, phospho-p38, p38, phospho-JNK, JNK, Nrf2, NF-κB, or beta-actin in TBST were incubated at 4 °C overnight. After incubation, membranes were washed three times with 1X TBST for 10 minutes. Then membranes were probed with 1:3000 anti-rabbit IgG or anti-mouse IgG, HRP-linked

secondary antibodies, and incubated at room temperature for one hour. After that, washed with 1X TBST for 10 minutes three times. To detect protein bands, the HRP-substrate reagent was added and the chemiluminescence signal of each protein band was detected under the gel documentation system. The quantification of the western blot protein band was measured by Image J software. Data were showed at the relative ratio of comparative protein.

### 3.18. Statistical analysis

In this study, data are shown as mean  $\pm$  SEM,  $n \geq 3$ . The one-way analysis of variance (ANOVA) is used for analysis in our experiment data, that statistical significance was performed at p values  $\leq 0.05$ .



## CHAPTER 4

### RESULT

#### 4.1 Phytochemical constituent of UCP

The phytochemical constituent of UCP was measured by the HPLC technique. The chromatography and standard curve of ascorbic acid were shown in Figure 53. The area under the curve of the chromatographic peak of standard ASC at a concentration of 100 µg/mL was approximately 10,000,000. The retention time of ascorbic acid peak was presented at 9.796 minutes under a flow rate of 0.5 mL/min at wavelength 243 nm (Figure 30a). The ascorbic acid chromatographic peak had been found in the chromatography diagram of UCP under the HPLC method (Figure 30b). The standard ascorbic acid showed the dose-dependent manner of their concentration and area under the curve of chromatographic peaks. The linear regression equation was used to evaluate the ascorbic acid concentration of UCP, which was found as  $39.67 \pm 2.40$  µg/mL in a 10 mg/mL UCP sample (Figure 30c).

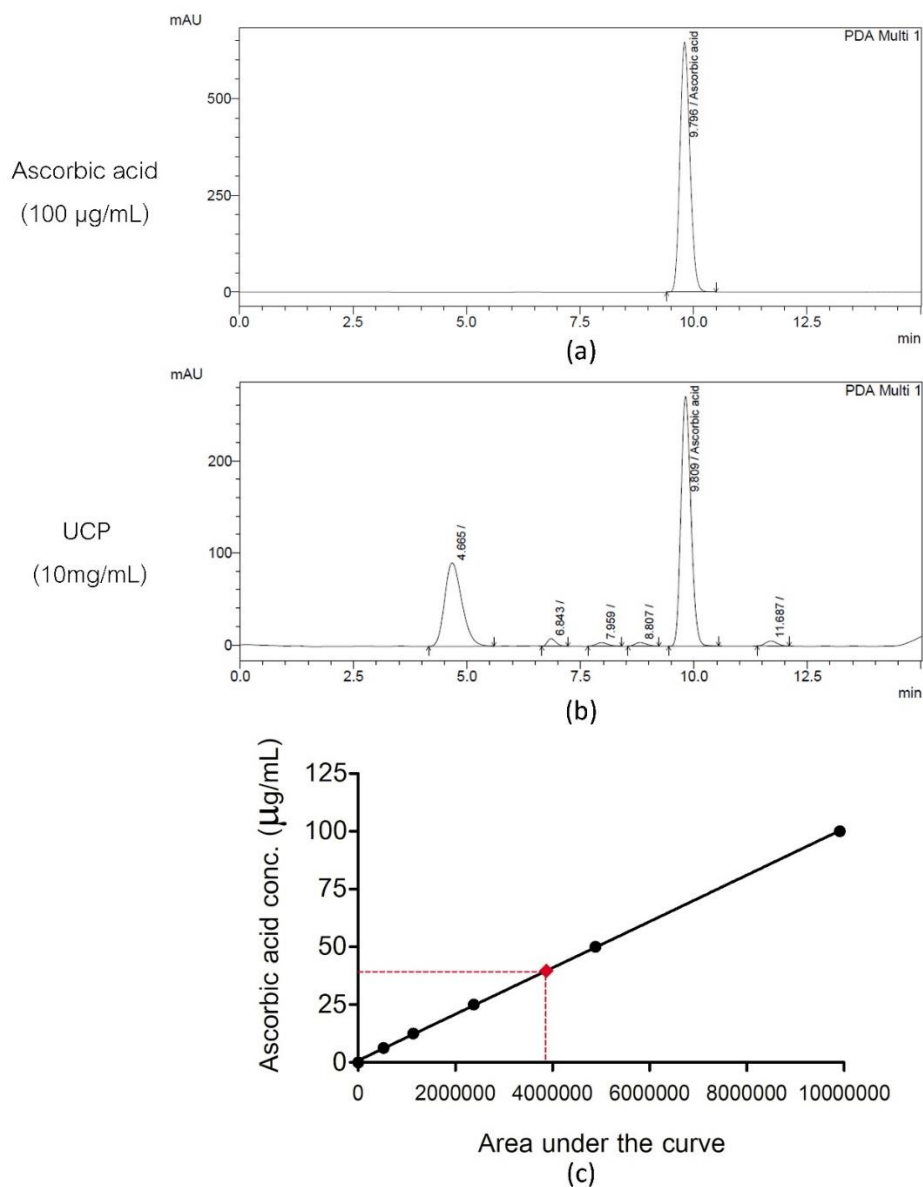
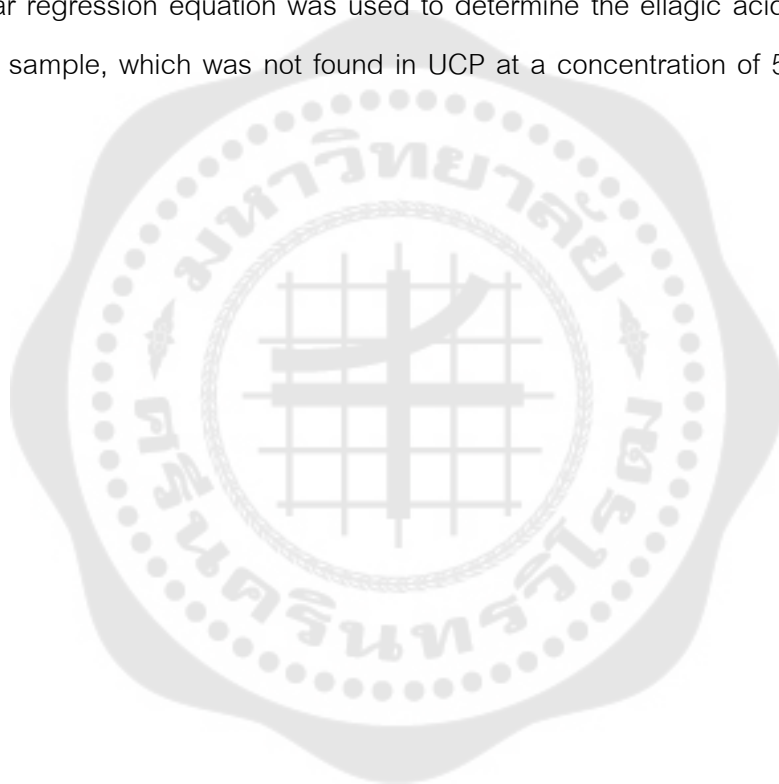


Figure 30 The HPLC analytical chromatography graph of ascorbic acid. The standard ascorbic acid chromatography graph under a flow rate of the mobile phase at 0.5 mL/min and detection wavelength at 243 nm. (b) The chromatography graph of UCP. (c) The interpolated point of standard ascorbic acid of UCP on the linear regression curve. Data are shown as mean  $\pm$  SEM ( $n \geq 3$ ).

The area under the curve of the ellagic acid standard chromatographic peak was approximately 4,500,000 at a concentration of 50  $\mu\text{g/mL}$ . The retention time of the ellagic acid peak was 4.808 minutes under the mobile phase flow rate of 1 mL/min at detection wavelength 253 nm (Figure 31a). The ellagic acid had not been found in the chromatographic peak in the UCP loading sample at the same retention time with standard on flow diagram (Figure 31b). The concentration of ellagic acid showed a dose-dependent manner with an area under the curve of their chromatographic peak. The linear regression equation was used to determine the ellagic acid concentration in the UCP sample, which was not found in UCP at a concentration of 50 mg/mL (Figure 31c).



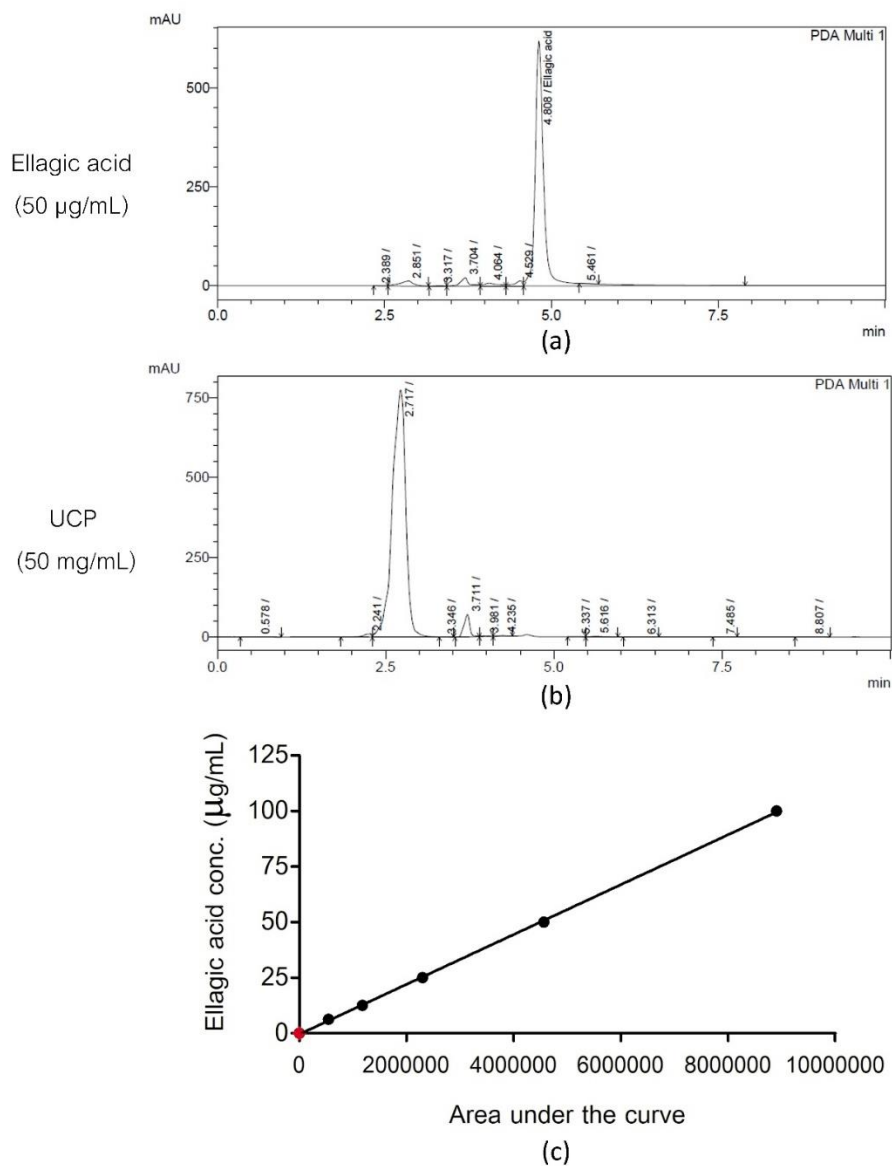
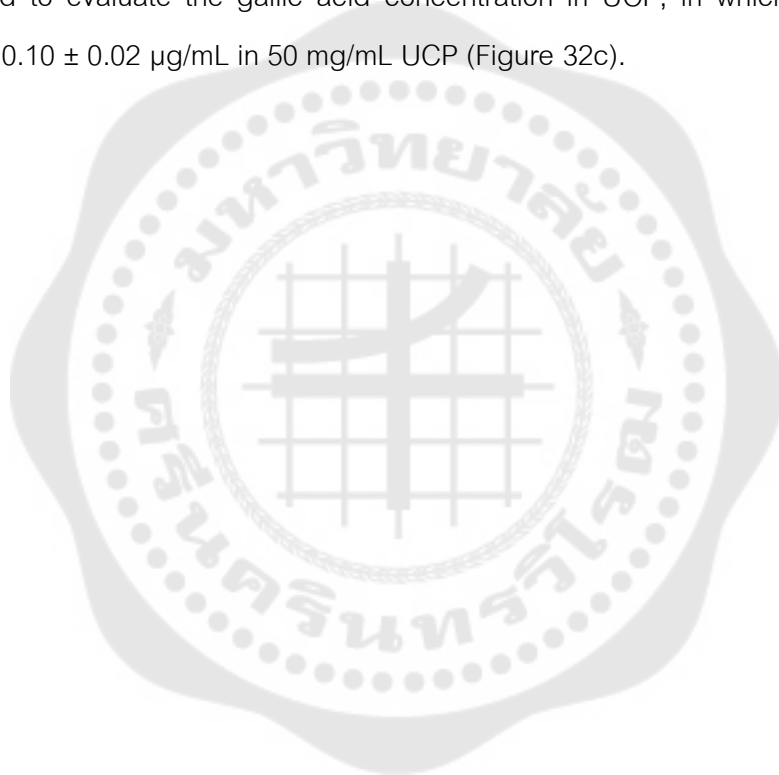


Figure 31 The HPLC analytical chromatography graph of ellagic acid. The standard ellagic acid chromatography graph under a flow rate of the mobile phase at 1 mL/min and detection wavelength at 254 nm. (b) The chromatography graph of UCP. (c) The interpolated point of UCP on the linear regression curve of standard ellagic acid. Data are shown as mean  $\pm$  SEM ( $n \geq 3$ ).

The area under the curve of the chromatographic peak of the gallic acid standard at a concentration of 50  $\mu\text{g/mL}$  approximately showed at 2,140,000. The retention time of the standard peak was 4.957 minutes under the mobile phase flow rate of 1.5 mL/min at a detection wavelength of 270 nm (Figure 32a). The gallic acid chromatographic peak had been found on the chromatography diagram of UCP (Figure 32b). The standard gallic acid showed the dose-dependent manner of concentrations with the area under the curve of a chromatographic peak. The linear regression equation was used to evaluate the gallic acid concentration in UCP, in which gallic acid was found at  $0.10 \pm 0.02 \mu\text{g/mL}$  in 50 mg/mL UCP (Figure 32c).





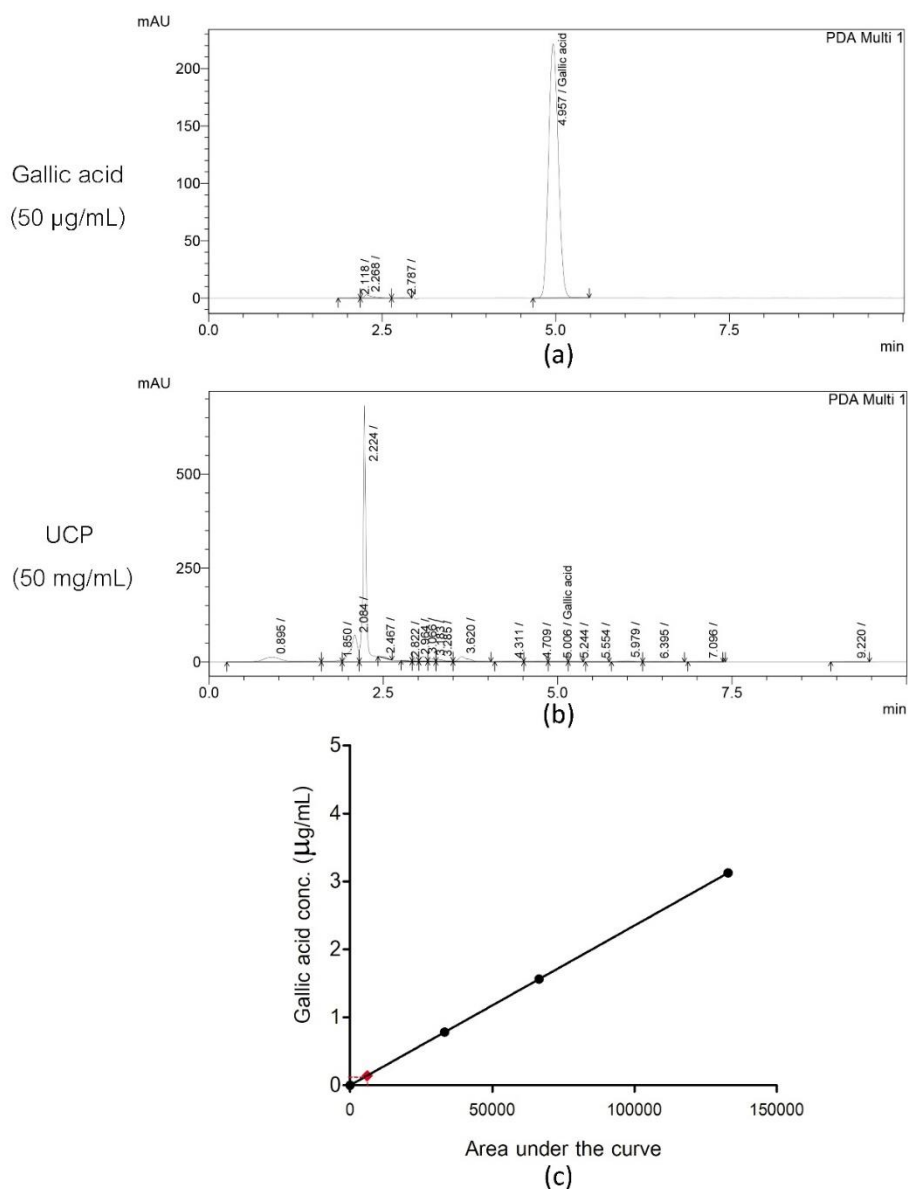


Figure 32 The HPLC analytical chromatography graph of gallic acid.

(a) The standard gallic acid chromatography graph under a flow rate of the mobile phase at 1.5 mL/min and detection wavelength at 270 nm. (b) The chromatography graph of UCP. (c) The interpolated point of UCP on the linear regression curve of standard gallic acid. Data are shown as mean  $\pm$  SEM ( $n \geq 3$ ).

The chromatographic peak of the area under the curve of the quercetin standard at a concentration of 100 µg/mL approximately was 4,500,000. The retention

time of the standard peak was 12.677 minutes under the mobile phase flow rate of 1.5 mL/min at detection wavelength 255 nm (Figure 33a). The quercetin chromatographic peak had been found in the UCP chromatography diagram (Figure 33b). The standard concentration showed a dose-dependent manner with the area under the curve of a chromatographic peak. The linear regression equation was used to evaluate the quercetin concentration in the UCP sample that quercetin was found  $0.09 \pm 0.002 \mu\text{g/mL}$  per 50 mg/mL of UCP (Figure 33c).



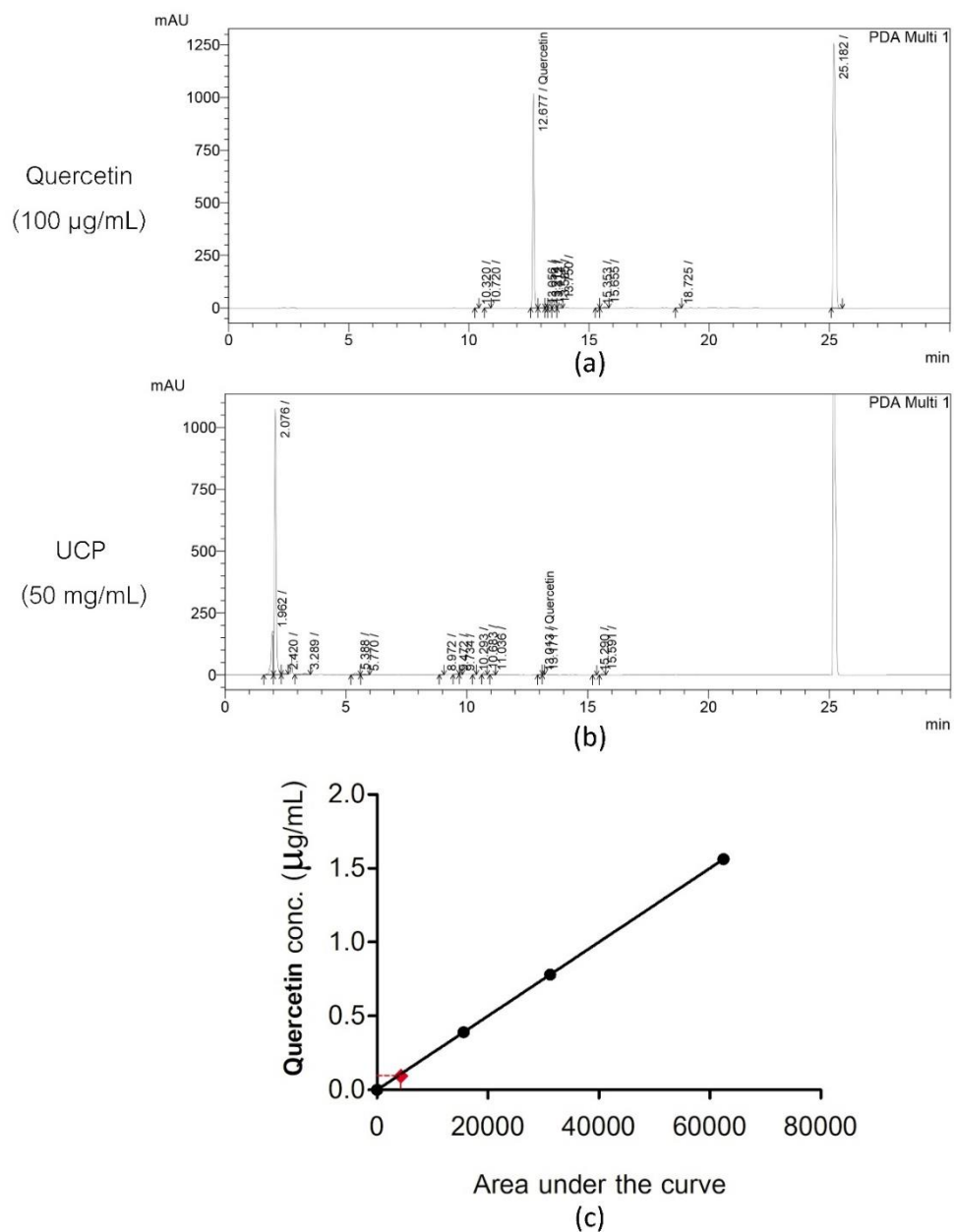


Figure 33 The HPLC analytical chromatography graph of quercetin.

(a) The standard quercetin chromatography graph under a flow rate of the mobile phase at 1.5 mL/min and detection wavelength at 255 nm. (b) The chromatography graph of UCP. (c) The interpolated point of UCP on the linear regression curve of standard quercetin. Data are shown as mean  $\pm$  SEM ( $n \geq 3$ ).

The chlorogenic acid standard at a concentration of 100  $\mu\text{g/mL}$  showed that the area under the curve of chromatographic peak approximated 4,500,000. The retention time of the standard peak was 8.626 minutes under the mobile phase flow rate of 1.5 mL/min at the detection wavelength of 325 nm (Figure 34a). The chlorogenic acid had not been found in the chromatography diagram of UCP (Figure 34b). The chlorogenic acid concentration showed the dose-dependent manner with an area under the curve of a chromatographic peak. The linear regression equation was used to evaluate the chlorogenic acid concentration in the UCP sample, which was not found (Figure 34c).



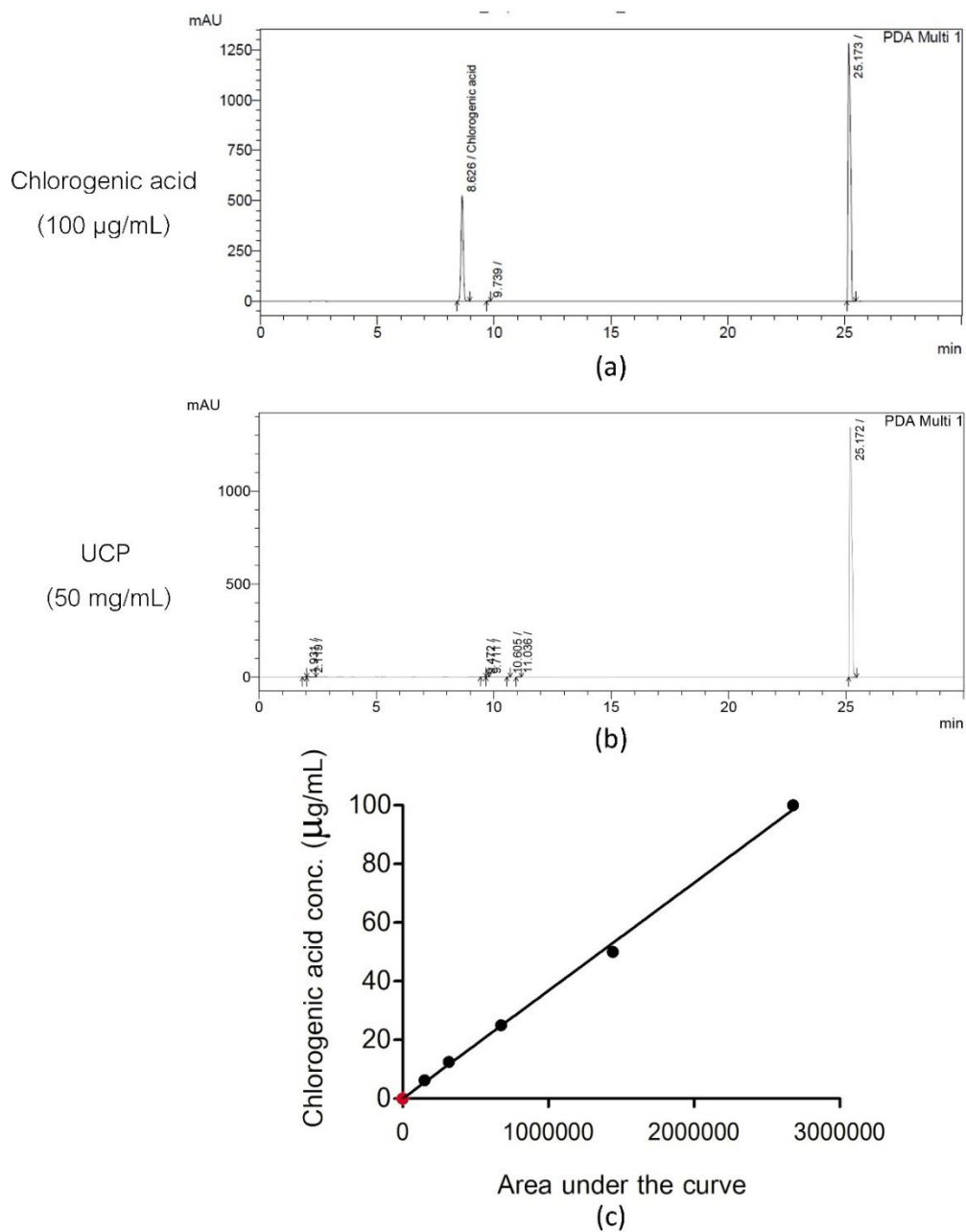


Figure 34 The HPLC analytical chromatography graph of chlorogenic acid. (a) The standard chlorogenic acid chromatography graph under a flow rate of the mobile phase at 1.5 mL/min and detection wavelength at 325 nm. (b) The chromatography graph of UCP. (c) The interpolated point of UCP on the linear regression curve of standard chlorogenic acid. Data are shown as mean  $\pm$  SEM ( $n \geq 3$ ).

## 4.2 Evaluation of the antioxidant potential of UCP

### 4.2.1 Determination of antioxidant scavenging activity

#### 4.2.1.1 Hydroxyl radical scavenging activity

The OH<sup>•</sup> scavenging activity assay was used to examine Trolox and UCP potential. The standard Trolox had been shown to the increasing of percent inhibition in a dose-dependent manner (Figure 35a). Regression equation and R square of Trolox were  $y = 49.93x - 22.93$  and 0.9892, respectively. While the IC<sub>50</sub> value was  $45.88 \pm 3.21$  µg/mL. In the same way, UCP also showed percent inhibition in a dose-dependent manner (Figure 35b). The regression and R square of UCP were  $y = 0.1151x + 17.24$  and 0.9866, respectively. IC<sub>50</sub> value was  $280.17 \pm 3.57$  µg/mL (Table 7).

Table 6 Linear regression and IC<sub>50</sub> values of Trolox and UCP on OH<sup>•</sup> scavenging activity

Sample	Linear regression equation	R square	IC <sub>50</sub> (µg/mL)
Trolox	$y = 49.93x - 22.93$	0.9892	$45.88 \pm 3.21$
UCP	$y = 0.1151x + 17.24$	0.9866	$280.17 \pm 3.57$

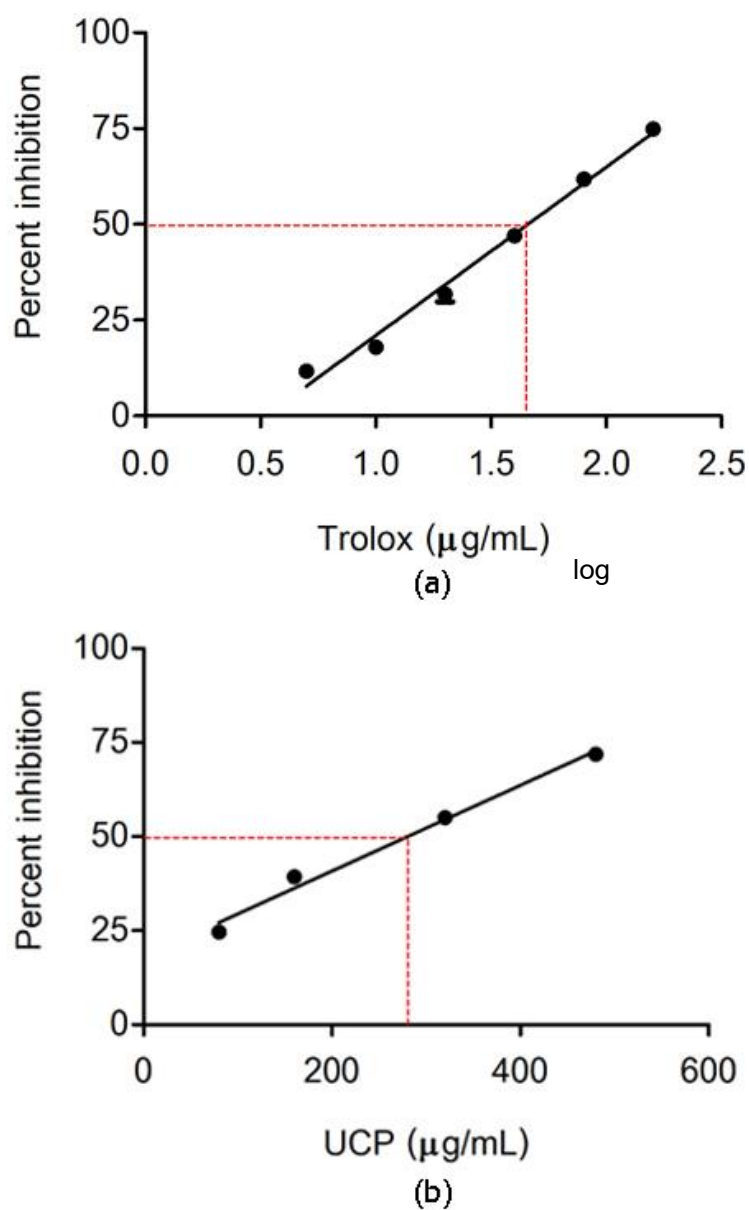


Figure 35 The  $\text{OH}^\cdot$  scavenging activity graph of standard Trolox and UCP.

The linear regression line of the concentrations and percent inhibition. (a) The linear regression curve of Trolox concentration and percent inhibition. (b) The linear regression curve of UCP concentration and percent inhibition. Data are shown as mean  $\pm$  SEM ( $n \geq$

3)

#### 4.2.1.2 Hypochlorous acid scavenging

The HOCl scavenging activity of standard ascorbic acid and UCP were evaluated using TNB remaining value. The various concentrations of ascorbic acid and UCP showed increasing of percent TNB remaining in a dose-dependent manner (Figure 36). The linear regression equations of ascorbic acid and UCP were  $y = 39.27x + 90.49$  and  $y = 35.76x + 2.951$ , respectively. R squares were 0.9875 and 0.9938 whereas IC50 values were  $93.93 \pm 5.34$  and  $1,316.63 \pm 21.78$   $\mu\text{g/mL}$ , respectively (Table 8.).

Table 7 Linear regression and IC50 values of ascorbic acid and UCP on HOCl scavenging activity

Sample	Linear regression equation	R square	IC50 ( $\mu\text{g/mL}$ )
Ascorbic acid	$y = 39.27x + 90.49$	0.9875	$93.93 \pm 5.34$
UCP	$y = 35.76x + 2.951$	0.9938	$1,316.63 \pm 21.78$



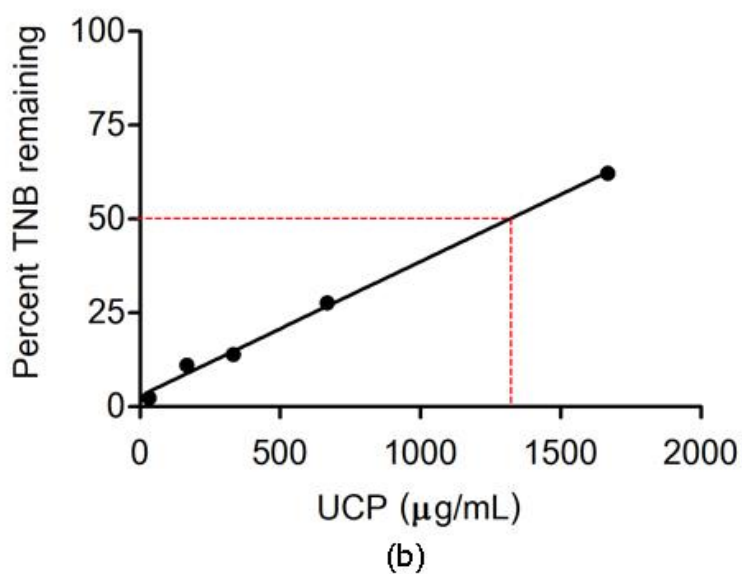
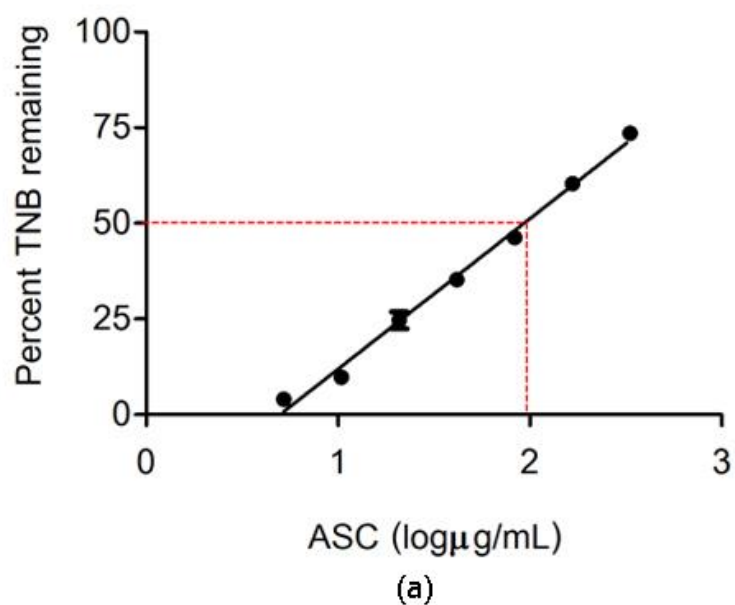


Figure 36 The HOCl scavenging activity graph of standard ascorbic acid and UCP. The linear regression curve shows the concentrations and percent TNB remaining. (a) The linear regression curve of ascorbic acid concentration and percent TNB remaining. (b) The linear regression curve of UCP concentration and percent TNB remaining. Data are shown as mean  $\pm$  SEM ( $n \geq 3$ )

#### 4.2.1.3 Superoxide anion scavenging activity

$O_2^{\cdot-}$  scavenging activity was determined by the reduction of NBT converting into formazan after received electron from  $O_2^{\cdot-}$ . The result showed that ascorbic acid increased the percent inhibition in a dose-dependent manner (Figure 37a). In the same way, UCP also increased the percent inhibition in a dose-dependent manner (Figure 37b). The linear regression equations of ascorbic acid and UCP were  $y = 0.1430x + 22.19$  and  $y = 0.0566x + 2.536$ , respectively. While R squares were 0.7785 and 0.9431, respectively. The IC50 values of ascorbic acid and UCP were  $241.02 \pm 19.71$  and  $846.53 \pm 40.16$   $\mu\text{g/mL}$ , respectively (Table 9).

Table 8 Linear regression and IC50 values of ascorbic acid and UCP on  $O_2^{\cdot-}$  scavenging activity

Sample	Linear regression equation	R square	IC50 ( $\mu\text{g/mL}$ )
Ascorbic acid	$y = 0.1430x + 22.19$	0.7785	$241.02 \pm 19.71$
UCP	$y = 0.0566x + 2.536$	0.9431	$846.53 \pm 40.16$

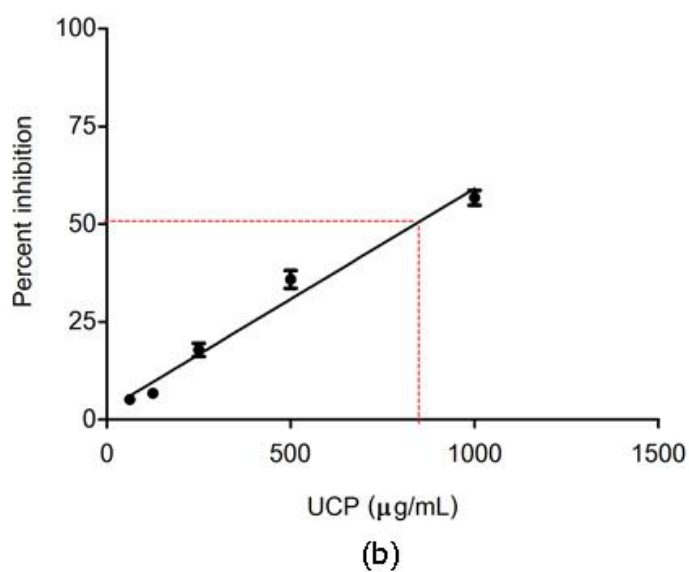
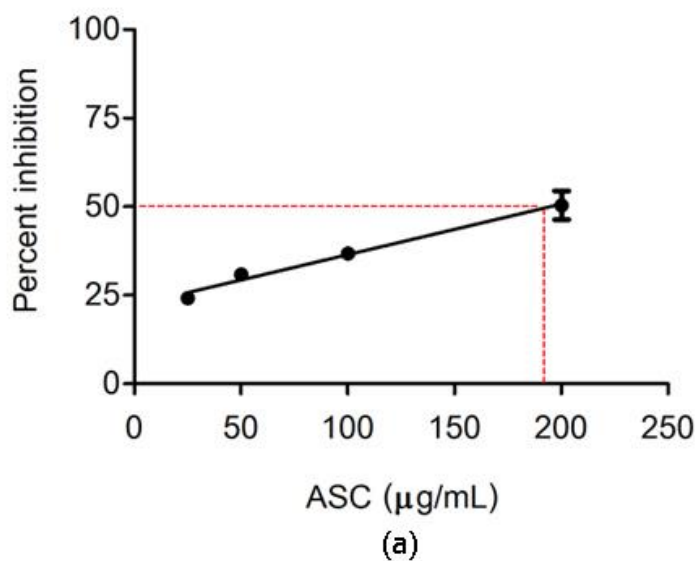


Figure 37 The  $\text{O}_2^{\cdot -}$  scavenging activity graph of standard ascorbic acid and UCP. The linear regression curve shows the concentrations and percent inhibition. (a) The linear regression curve of Trolox concentration and percent inhibition. (b) The linear regression curve of UCP concentration and percent inhibition. Data are shown as mean  $\pm$  SEM ( $n \geq 3$ )

#### 4.2.1.4 Hydrogen peroxide scavenging activity

The determination of this scavenging activity of UCP based on the dimerization of HVA after catalyzed by  $H_2O_2$  and HRP. Trolox increases the percent inhibition in a dose-dependent manner (Figure 38a). The linear regression curve of UCP also showed increasing of percent inhibition in a dose-dependent manner (Figure 38b). The linear regression equations of Trolox and UCP were  $y = 100.2x - 8.584$  and  $y = 0.3168x - 12.47$ , and R squares were 0.9517 and 0.9671, respectively. As a result, the IC50 values were  $0.579 \pm 0.046$  and  $196.39 \pm 7.36$ , respectively (Table 10).

Table 9 Linear regression and IC50 values of Trolox and UCP on  $H_2O_2$  scavenging activity

Sample	Linear regression equation	R square	IC50 ( $\mu\text{g/mL}$ )
Trolox	$y = 100.2x - 8.584$	0.9517	$0.579 \pm 0.046$
UCP	$y = 0.3168x - 12.47$	0.9671	$196.39 \pm 7.36$

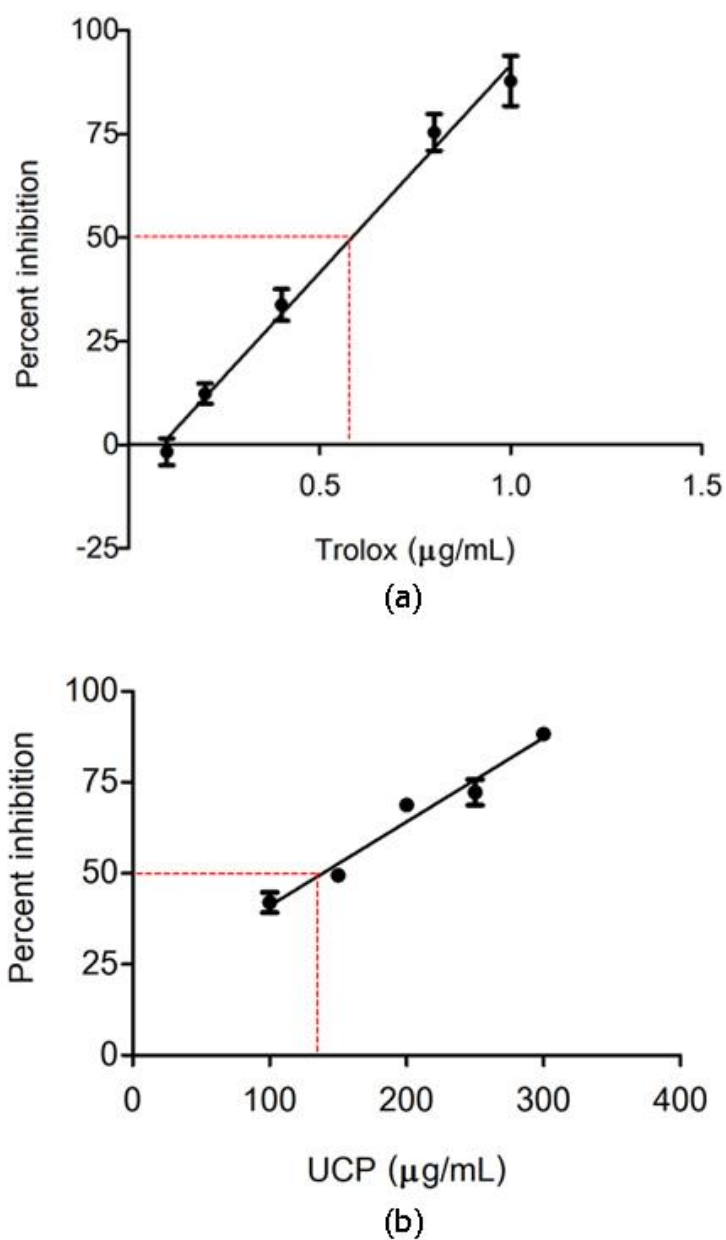


Figure 38 The H<sub>2</sub>O<sub>2</sub> scavenging activity graph of standard Trolox and UCP. The linear regression curve is plotted from the concentrations and percent inhibition. (a) The linear regression curve of Trolox concentration and percent inhibition. (b) The linear regression curve of UCP concentration and percent inhibition. Data are shown as mean ± SEM (n ≥ 3)

## 4.2.2 Determination of UCP capacity

### 4.2.2.1 Ferric Reducing Antioxidant Power

The reduction of  $[\text{Fe(III)(TPTZ)}_2]^{3+}$  complex into  $[\text{Fe(II)(TPTZ)}_2]^{2+}$  complex was used to evaluate the antioxidant power of UCP. The absorbance value at wavelength 593 nm was increased in a dose-dependent manner depending on the concentration of  $\text{FeSO}_4$  that was used to calculate the FRAP values of samples and standard (Figure 39a). The standard ascorbic acid and UCP also increased optical density values at 593 nm in a dose-dependent manner (Figure 39b and 39c). The FRAP values were calculated by the interpolation of absorbance value at 593 nm and  $\text{FeSO}_4$  concentration. The linear regression curve of ascorbic acid showed that 50  $\mu\text{g/mL}$  of ascorbic acid found the FRAP values at  $100.29 \pm 4.18 \mu\text{M}$  or  $2.01 \pm 0.08 \text{ mmol/g}$  (Figure 39d). The UCP linear regression curve demonstrated that the FRAP value of UCP was found at  $2.68 \pm 0.24 \mu\text{M}$  or  $26.79 \pm 2.43 \mu\text{mol/g}$  (Figure 39e). The ascorbic acid equivalent of UCP was calculated and interpolated via FRAP values. The UCP at a concentration of 100  $\mu\text{g/mL}$  had an ascorbic acid equivalent at  $0.67 \pm 0.04 \mu\text{M}$  or 6.65  $\mu\text{mol/g}$  (Figure 39f).

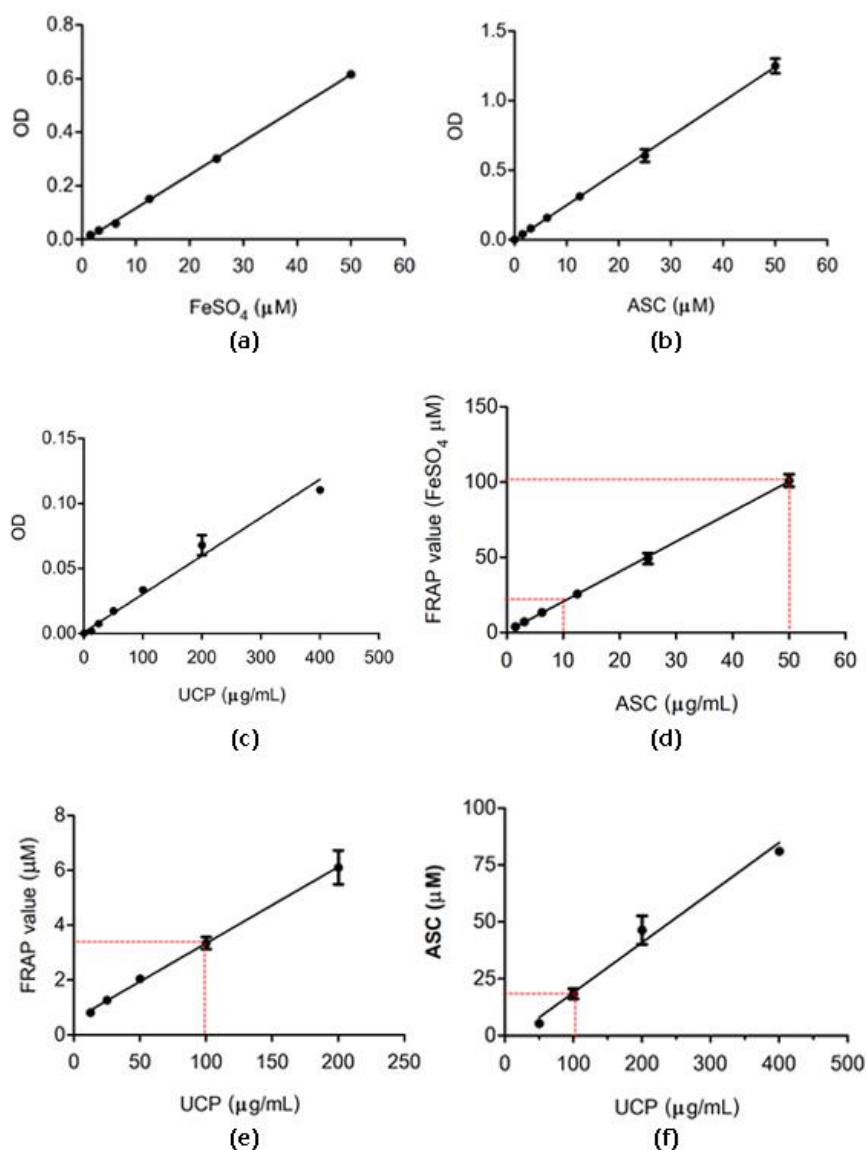


Figure 39 The linear regression curve data of FRAP assay.

(a) The linear curve of FeSO<sub>4</sub> concentration and optical density at wavelength 593 nm.

(b) Linear regression curve of ascorbic acid at absorbance wavelength 593 nm. (c)

Linear regression curve of UCP optical density at wavelength 593 nm. (d) Interpolation

of ascorbic acid at absorbance wavelength 593 nm to FRAP value. (e) The linear

regression curve of the FRAP value of UCP. (d) The interpolation curve of UCP to

ascorbic acid equivalent value via FRAP value. Data are shown as mean  $\pm$  SEM ( $n \geq 3$ )

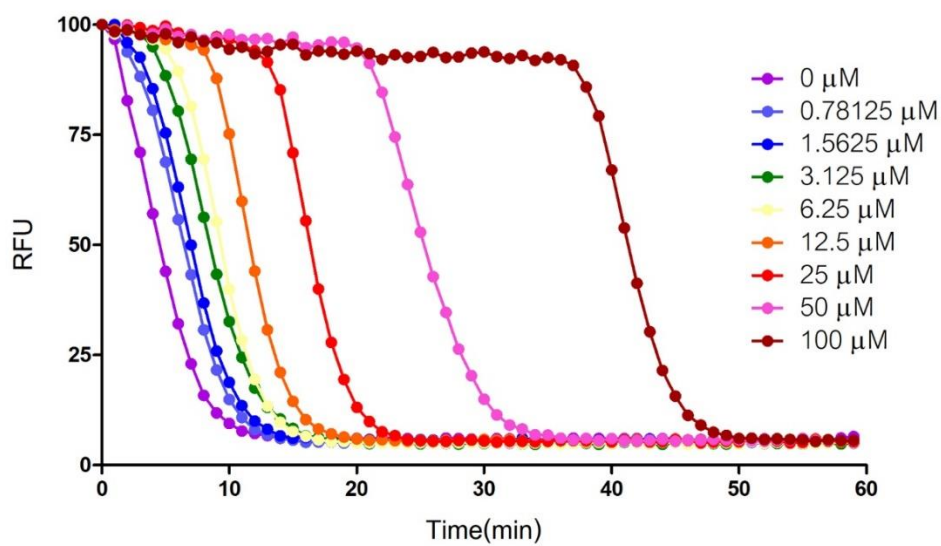
#### 4.2.2.2 Oxygen radical absorbance capacity

The antioxidant potential of UCP was evaluated by the ORAC assay. The relative fluorescence units (RFU) of standard Trolox were measured at excitation and emission wavelength 485 and 528 nm at 1-min intervals for 60 minutes. The RFU of fluorescein was decreased related to times, while antioxidant reduces the decline of fluorescein. The inhibition graph showed that the concentration of Trolox delayed the reduction of RFU in a dose-dependent manner (Figure 40a). While Net AUC of various concentrations of Trolox was increased (Figure 40b).

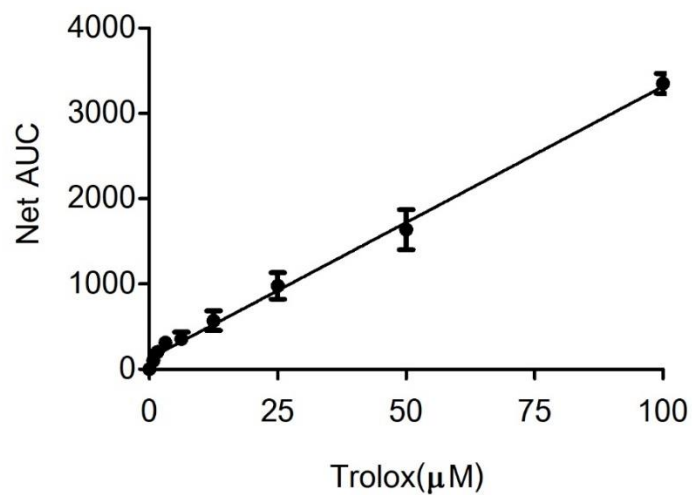
The various concentrations of UCP also delayed the decrease of the RFU in a dose-dependent manner (Figure 41a). Net AUC was increased depending on the UCP concentration in a dose-dependent manner (Figure 41b).

The Trolox equivalent of UCP was calculated by using the interpolation of Trolox Net AUC and UCP concentration. The linear regression curve showed that UCP at a concentration of 1 mg/mL had TE to  $56.03 \pm 7.52 \mu\text{M}$  of Trolox or  $\mu\text{mol/g}$  (Figure 42).





(a)



(b)

Figure 40 The ORAC assay graph data of standard Trolox.

(a) The inhibition curve of various concentrations of Trolox. (b) The linear regression curve of Net AUC varies with standard concentration. Data are shown as mean  $\pm$  SEM (n  $\geq$  3)

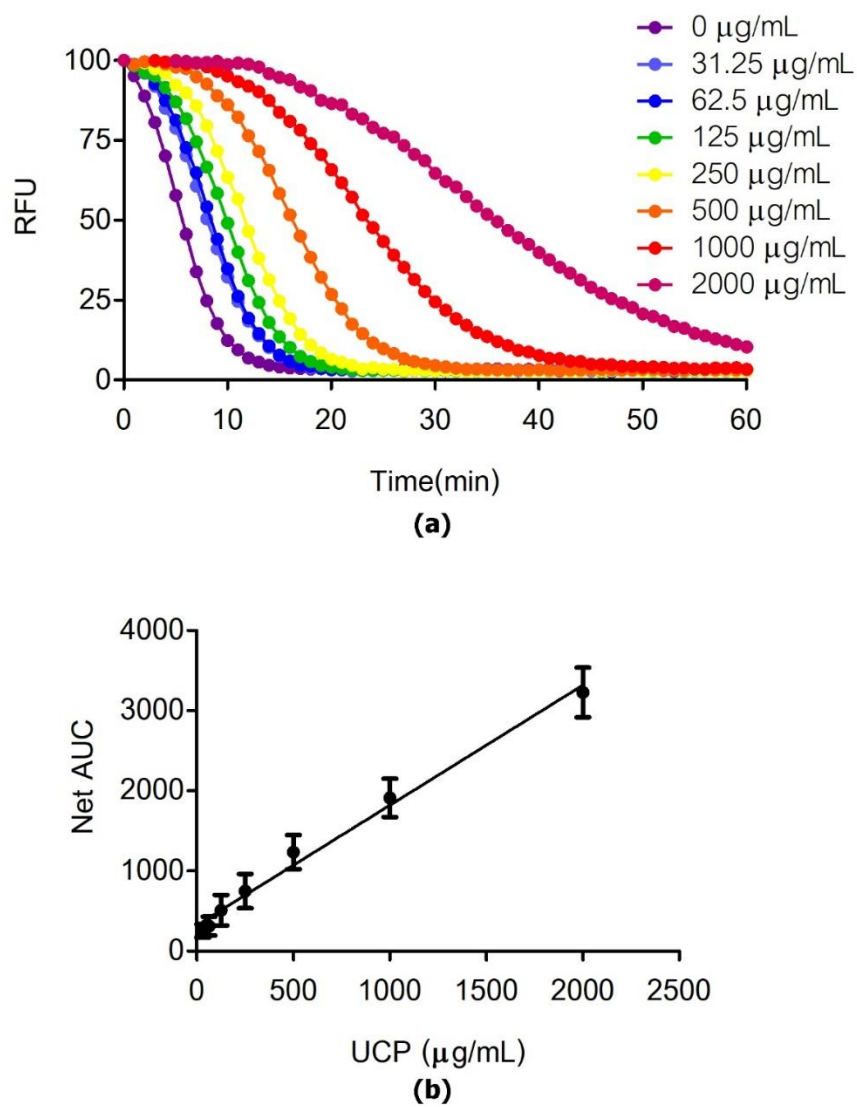


Figure 41 The ORAC assay curve of UCP.

(a) The inhibition curve of various concentrations of UCP. (b) The linear curve of Net AUC varies with UCP concentration in a dose-dependent manner. Data are shown as

mean  $\pm$  SEM ( $n \geq 3$ )

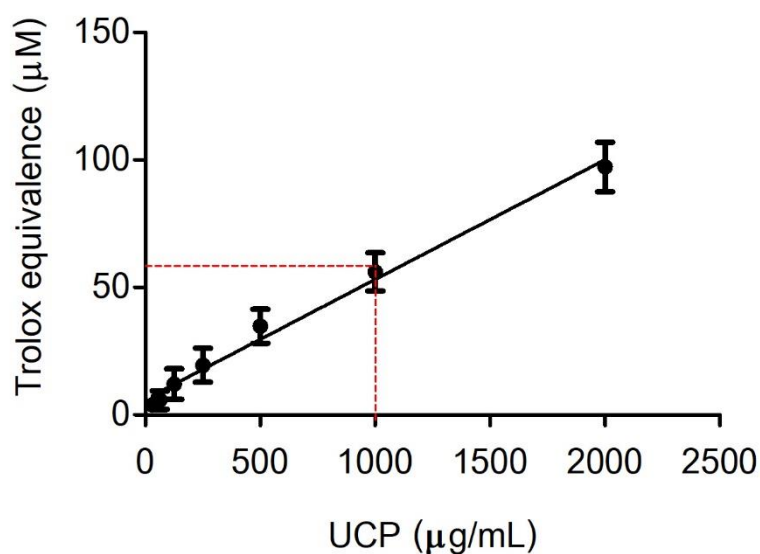


Figure 42 The linear regression curve of the Trolox equivalent of UCP. Data are shown as mean  $\pm$  SEM ( $n \geq 3$ )

#### 4.2.2.3 Ferric Thiocyanate

The antioxidant activity of UCP on lipid peroxidation was evaluated via the peroxidation of linoleic acid by FTC assay. The absorbance value at wavelength 500 nm was increased via the transformation of  $\text{Fe}^{3+}$  complex into  $\text{Fe}^{2+}$  complex by lipid radical. Trolox standard showed reduced absorbance values at wavelength 550 nm when compared with control. UCP also showed a trend to reduce absorbance value (Figure 43a). Percent inhibition of standard Trolox and UCP at a concentration 1 mg/mL were  $97.20 \pm 0.02\%$  and  $14.07 \pm 0.36\%$ , respectively. As a result, Trolox significantly inhibits lipid peroxidation in FTC assay at  $p < 0.001$ . Although, UCP showed a trend to inhibit lipid peroxidation even though no significantly (Figure 43b).

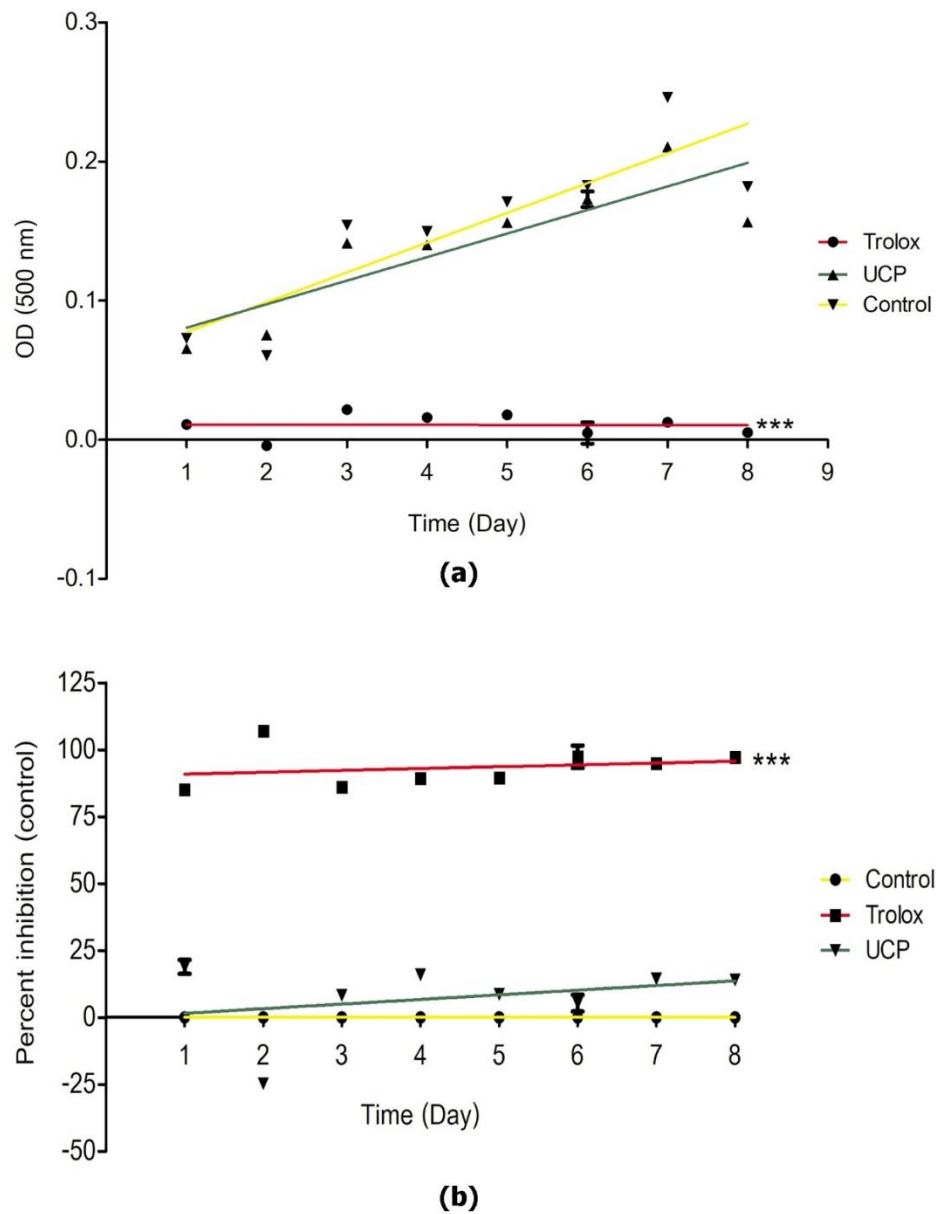


Figure 43 The linear regression curves of Trolox standard and UCP in FTC assay.

(a) The linear regression graph of absorbance value at wavelength 500 nm. (b) The percent inhibition of Trolox and UCP compare with the control group. Data are shown as mean  $\pm$  SEM ( $n \geq 3$ ). \*\*\*  $p < 0.001$  compared with control group.

#### 4.3 Preventive effect of UCP against H<sub>2</sub>O<sub>2</sub>-induced cell death

The H<sub>2</sub>O<sub>2</sub>-induced EA hy926 cells model was used to determine the preventive effect of UCP. H<sub>2</sub>O<sub>2</sub> challenged for 2 hours significantly reduced percent cell viability to  $77.61 \pm 1.02$ ,  $30.57 \pm 9.31$  and  $1.01 \pm 0.50$  %, at  $p < 0.01$  at a concentration 1000, 2000, and 4000, respectively when compared with the non-challenged group (Figure 44).

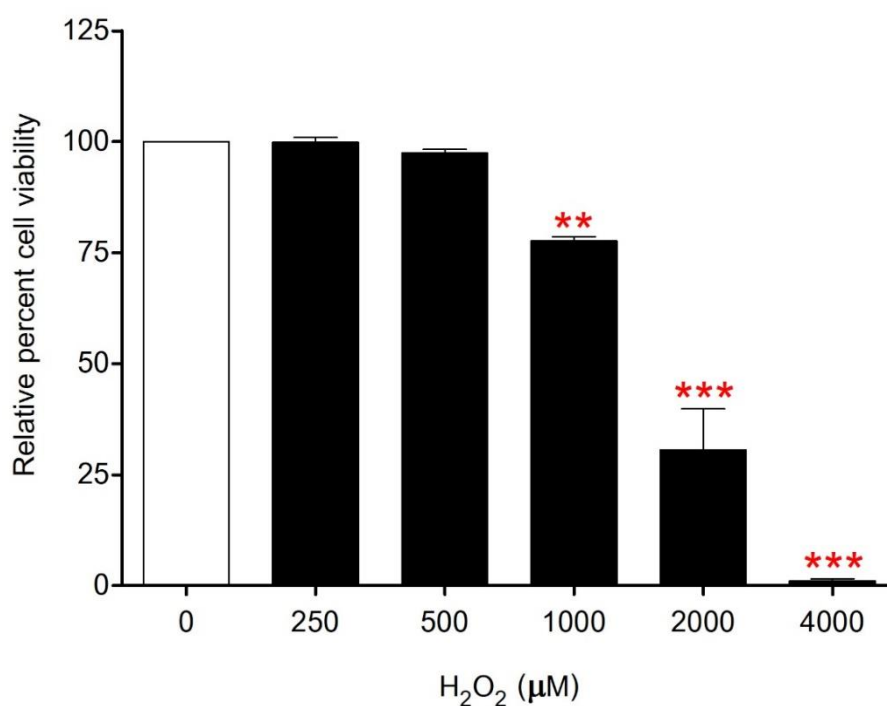


Figure 44 The histogram chart data of H<sub>2</sub>O<sub>2</sub> toxicity on EA hy926 cells.

Data are showed as mean  $\pm$  SEM ( $n \geq 3$ ). \*\*,  $p < 0.01$  and \*\*\*  $p < 0.001$  compared with control group.

UCP had no toxicity on EA hy926 cells after incubated for 48 hours, while 100 and 1000  $\mu\text{g/mL}$  of UCP significantly increased percent cell viability to  $108.26 \pm 1.85$  and  $112.45 \pm 1.27$  % at  $p < 0.05$ , respectively when compared with the vehicle-treated group. While EA hy926 cells exposed with 1 mM H<sub>2</sub>O<sub>2</sub> significantly decreased percent cell survival to  $76.99 \pm 2.00$  % when compared with the control group. 100 and 1000  $\mu\text{g/mL}$  UCP pretreated on H<sub>2</sub>O<sub>2</sub>-induced EA hy926 cells oxidative stress showed

significantly improved percent cell viability to  $84.69 \pm 2.34$  and  $89.14 \pm 3.57$  at  $p < 0.05$  and  $0.001$ , respectively when compared with the  $\text{H}_2\text{O}_2$  exposed group (Figure 45).

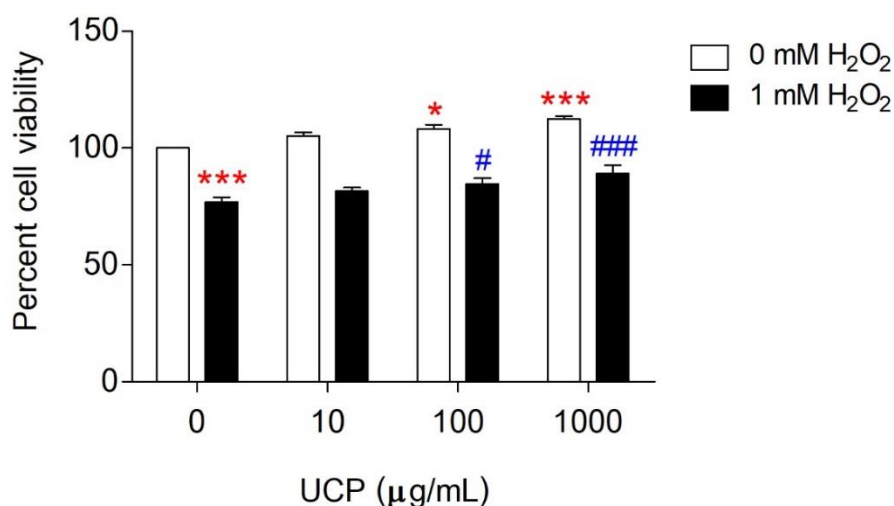


Figure 45 The histogram data of UCP preventive effect on  $\text{H}_2\text{O}_2$ -induced cell death. Data are shown as mean  $\pm$  SEM ( $n \geq 3$ ). \*,  $p < 0.05$  and \*\*\*  $p < 0.001$  compared with control group. #,  $p < 0.05$  and ###  $p < 0.001$  compared with  $\text{H}_2\text{O}_2$ -exposed group.

#### 4.4 Effect of UCP on $\text{H}_2\text{O}_2$ -induced EA hy926 cell apoptosis

The preventive effect of UCP on  $\text{H}_2\text{O}_2$ -induced EA hy926 cell apoptosis was determined by observation of Hoechst and PI staining under a fluorescent microscope. The  $\text{H}_2\text{O}_2$ -exposed cells after 2 hours showed high fluorescence intensity of Hoechst and PI stained, while UCP treatment had no significance when compared with vehicle treatment. The fluorescence intensity of Hoechst and PI stained were decreased after cell pretreatment UCP before challenged with  $\text{H}_2\text{O}_2$  (Figure 46).

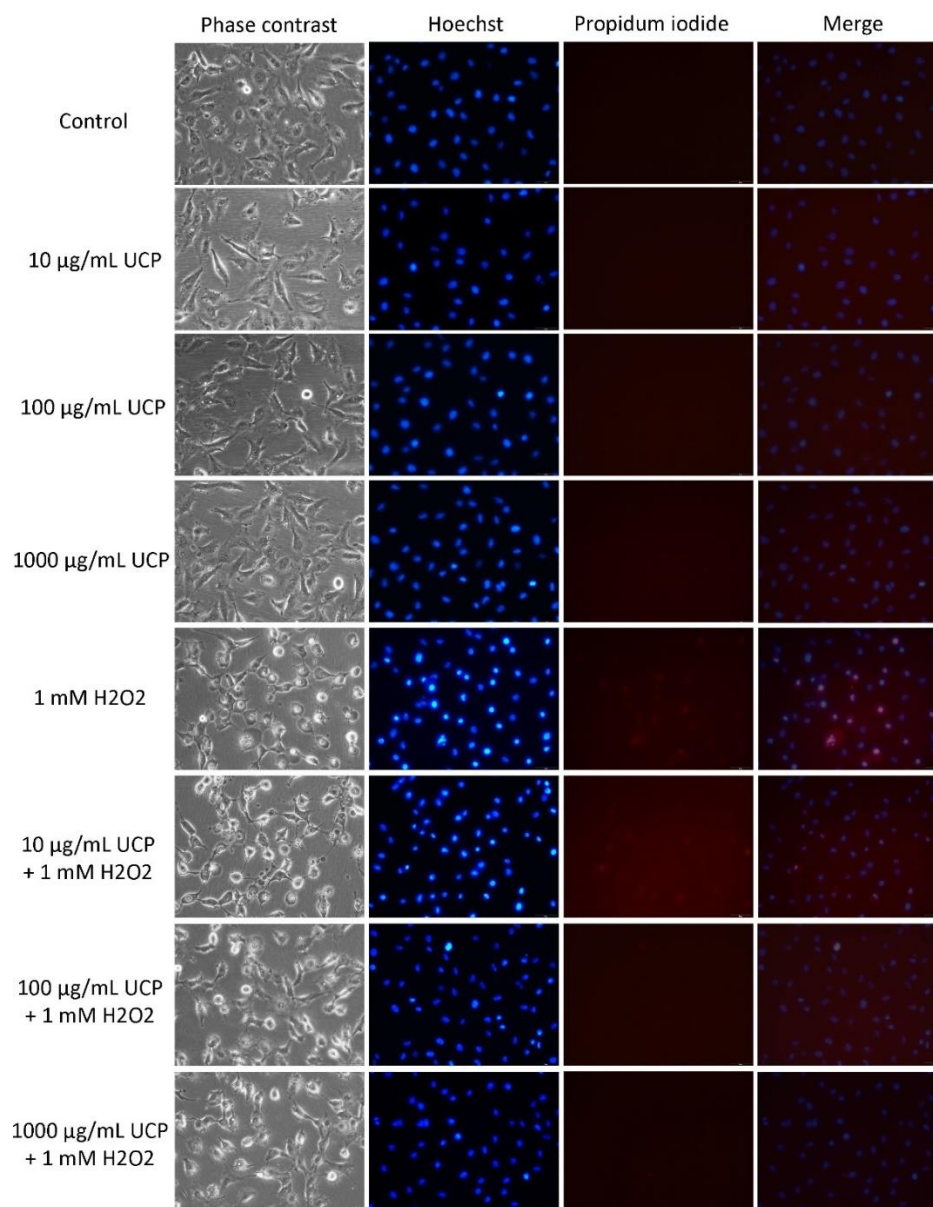


Figure 46 The apoptotic EA hy926 cells stained with Hoechst and PI under the fluorescence microscope.

To separate the normal and apoptotic cells, the Image J software plug-in on the color threshold was used to avoid bias.  $n \geq 3$  randomized pictures were used to count and calculate the percent of apoptotic cells.

The randomized pictures of Hoechst and PI stained EA cells ( $n \geq 3$ ) were used to calculate the percent apoptotic cell. UCP had no effect to induce apoptosis on EA hy926 cells when compared with the control group. Whereas  $H_2O_2$  exposed after 4 hours significantly elevated cell apoptosis to  $71.74 \pm 3.68\%$  at  $p < 0.001$ . UCP pretreatment 100 and 1000  $\mu\text{g/mL}$  of UCP on  $H_2O_2$ -induced cell apoptosis showed significantly decreased percent apoptotic cell to  $54.84 \pm 3.61$  and  $39.06 \pm 2.09$ , respectively when compared with the  $H_2O_2$ -exposed group (Figure 47).

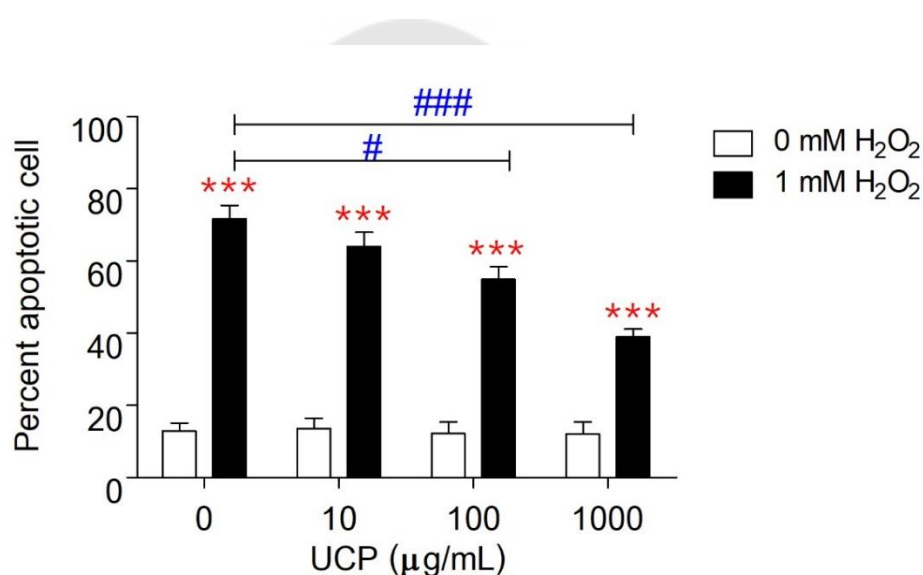


Figure 47 The histogram of percent apoptotic cells of EA hy926 cells after treatment. Three randomized pictures were used to count and calculate the percent apoptotic cell. To avoid bias, Image J software with a color threshold plug-in was used. Data are represented as mean  $\pm$  SEM ( $n \geq 3$ ). \*\*\*  $p < 0.001$  compared with vehicle treatment. #,  $p < 0.05$  and ###  $p < 0.001$  compared with  $H_2O_2$ -exposed group.

#### 4.5 Effect of UCP on intracellular ROS

The preventive effect on intracellular ROS was evaluated by DCFH-DA probe staining via flow cytometry assay. The flow cytometry graphs of each sample tagged with DCFH-DA was shown in figure 71a. To gating the ROS positive field, the unstained curve was prepared. UCP treated on EA hy926 cells showed the trend to decrease



intracellular ROS in a dose-dependent manner when compared with the vehicle-treated group. The EA hy926 cells exposed with H<sub>2</sub>O<sub>2</sub> for 2 hours showed the high intensity of green fluorescence that the graphs were shifted to the right side (ROS gating field) when compared with the control group. In the same way, UCP showed the efficacy to reduce the intracellular ROS on H<sub>2</sub>O<sub>2</sub>-induced EA hy926 cells in a dose-dependent manner when compared with the H<sub>2</sub>O<sub>2</sub>-exposed group (Figure 48a). As a result, UCP showed an inhibitory effect to decrease the percent fluorescence intensity of intracellular ROS of EA hy926 cells after incubated 48 hours to 84.02 ± 2.43, 79.15 ± 7.71, and 64.04 ± 14.00 % at a concentration 10, 100, and 1000 µg/mL, respectively when compared with the control group. H<sub>2</sub>O<sub>2</sub> is an oxidative stress inducer that significantly increased the percent fluorescence intensity to 233.04 ± 7.56 % when compared with the control group. While, 10, 100 and 1000 µg/mL UCP pretreated on H<sub>2</sub>O<sub>2</sub>-induced cells oxidative stress significantly decreased percent fluorescence intensity to 201.16 ± 9.01, 173.53 ± 10.68 and 151.18 ± 14.68 at p < 0.05, 0.01 and 0.001, respectively (Figure 48b).

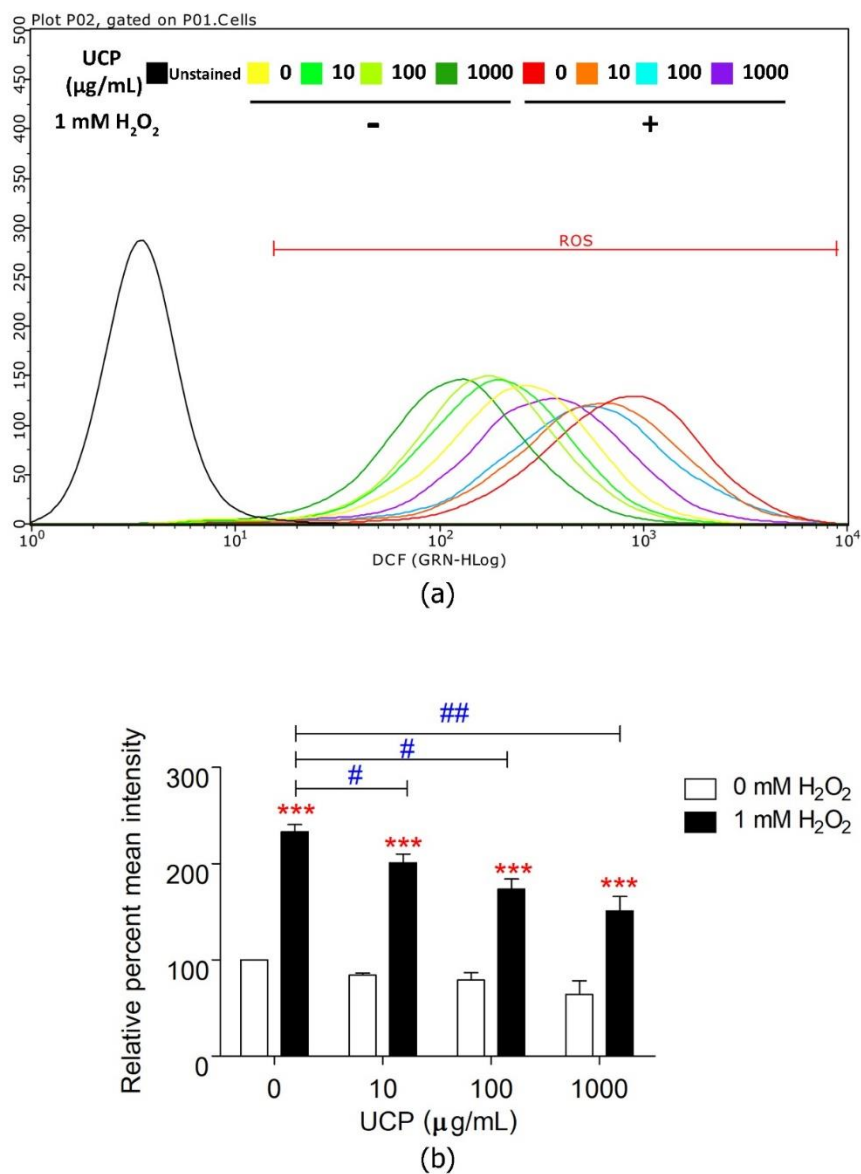


Figure 48 The UCP antioxidant effect on intracellular ROS of H<sub>2</sub>O<sub>2</sub>-induced cells oxidative stress.

a) The flow cytometry graph of the fluorescence intensity of DCFH-DA intracellular ROS probe. b) The percent mean intensity histogram of each sample. Data are presented as mean ± SEM (n ≥ 3). \*\*\* p < 0.001 compared with vehicle treatment. #, p < 0.05 and ## p < 0.01 compared with H<sub>2</sub>O<sub>2</sub>-exposed group.

#### 4.6 Effect of UCP on endogenous enzymatic antioxidant activity and glutathione levels

The effect of UCP on antioxidant enzymes was evaluated using SOD, GPX, and CAT enzyme activity assay.

##### 4.6.1 Effect of UCP on SOD activity

The SOD ELISA kit (Sigma) was used to determine the UCP effect on intracellular SOD activity of H<sub>2</sub>O<sub>2</sub>-induced cells oxidative stress. The percent inhibition of the SOD standard at a concentration 0-200 U/mL was used to plot the standard SOD inhibition curve (Figure 49a). Each sample was calculated the SOD activity (U/mL) by interpolated the percent inhibition with the standard curve. 1000 µg/mL of UCP treated on EA hy926 cells significantly increased SOD activity to  $3.91 \pm 0.17$  U/mL at  $p < 0.05$  when compared with vehicle-treated group ( $2.91 \pm 0.31$  U/mL). H<sub>2</sub>O<sub>2</sub>-exposed after 2 hours decreased activity to  $2.48 \pm 0.10$  U/mL when compared with the control group, while UCP pretreated on H<sub>2</sub>O<sub>2</sub>-induced EA hy926 cell oxidative stress had increased to  $3.00 \pm 0.24$  U/mL (Figure 49b).

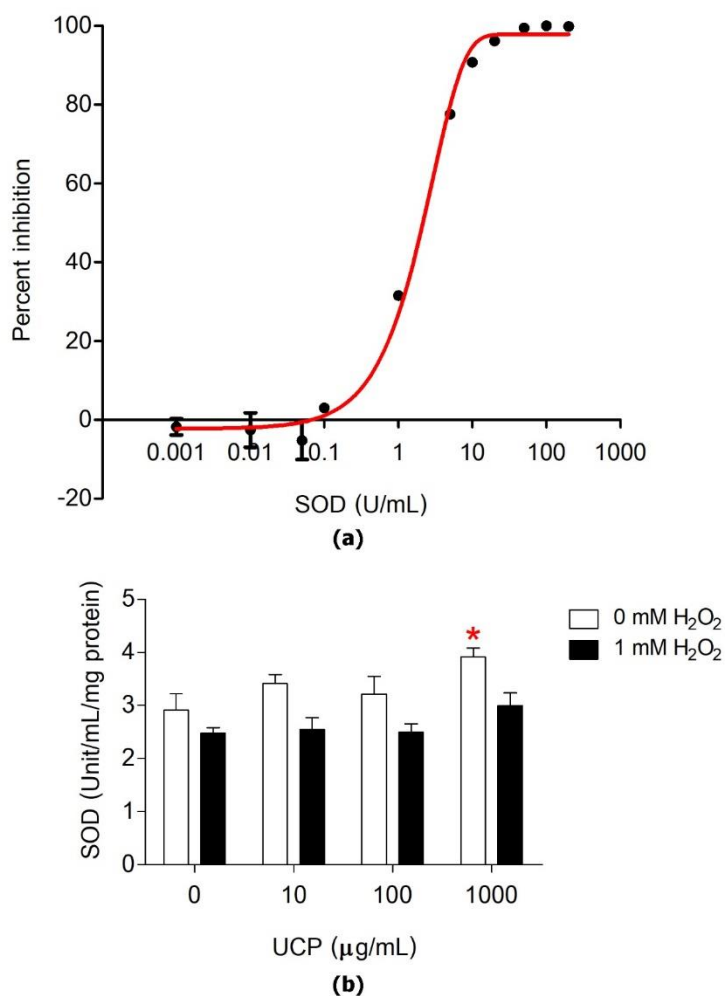


Figure 49 The effect of UCP pretreated on SOD activity.

a) The standard inhibition curve of SOD at a concentration 0-200 U/mL. b) The histogram data of UCP treated on EA hy926 cell W/WO exposed with  $\text{H}_2\text{O}_2$ . Data are shown as mean  $\pm$  SEM ( $n \geq 3$ ). \*  $p < 0.05$  when compared with the control group.

#### 4.6.2 Effect of UCP on CAT activity

The effect of UCP on CAT activity was determined by the CAT activity assay. The formaldehyde standard curve was used to calculate the CAT activity of each sample in this assay (Figure 50a). UCP treatment did not affect intracellular CAT activity in EA hy926 cells. While,  $\text{H}_2\text{O}_2$  exposed on EA hy926 cell showed significantly decreased CAT activity to  $13.53 \pm 2.09$  nmol/min/mL/mg protein at  $p < 0.05$  when

compared with control group ( $18.34 \pm 2.06$  nmol/min/mL/mg protein). UCP pretreated on  $H_2O_2$ -induced EA hy926 cells significantly improved CAT activity to  $19.01 \pm 2.15$  nmol/min/mL/mg protein at  $p < 0.05$ , when compared with  $H_2O_2$ , exposed group (Figure 50b).

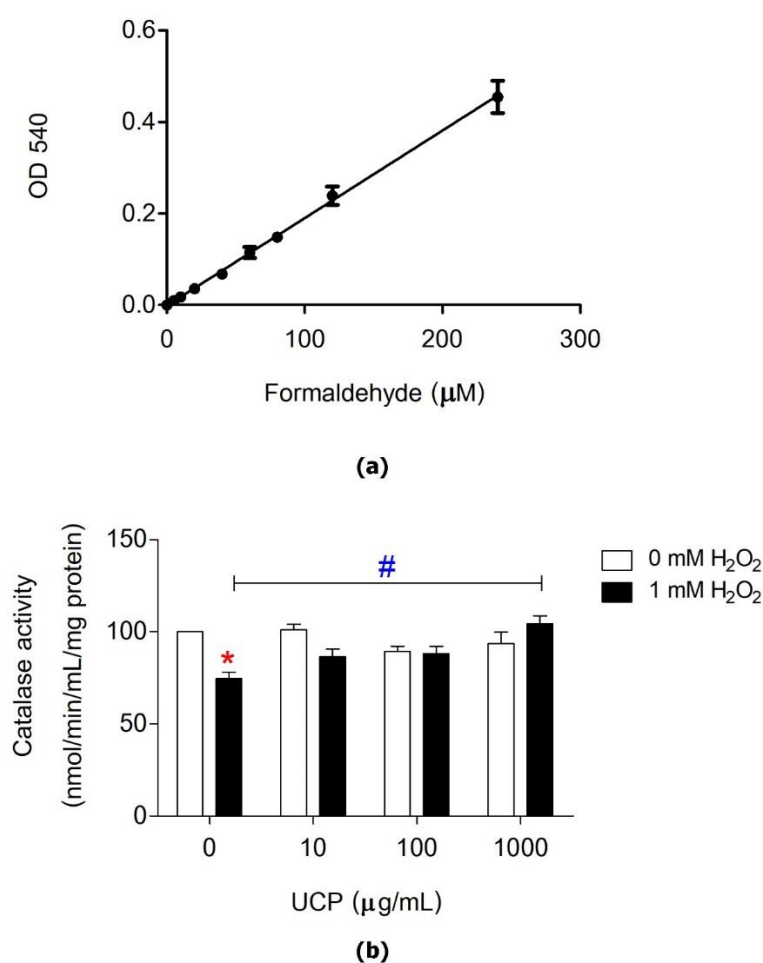


Figure 50 Effect of UCP on CAT activity.

a) Standard formaldehyde curve for calculating the CAT activity of each sample. b) The result data of UCP treated on EA hy926 cell W/WO exposed with  $H_2O_2$ . Data are shown as mean  $\pm$  SEM ( $n \geq 3$ ). \*  $p < 0.05$  when compared with the vehicle treatment. #  $p < 0.05$  when compared with the  $H_2O_2$ -exposed group.

#### 4.6.3 Effect of UCP on GPX activity

UCP effect on GPX activity was determined by the GPX activity assay. The absorbance of NADPH at wavelength 340 nm was used to evaluate GPX activity. The NADPH absorbance of GPX enzymatic standard at concentrations 0-40 mU/mL was plotted in 1-minute interval-time for 30 minutes to prepare the standard curve (Figure 51a). The standard curve of GPX activity of each concentration was calculated and plotted (Figure 51b). As the result, H<sub>2</sub>O<sub>2</sub> treated on EA hy926 cells did not change GPX activity. UCP pretreatment on H<sub>2</sub>O<sub>2</sub>-induced cells oxidative stress did not affect intracellular GPX activity (Figure 51c).



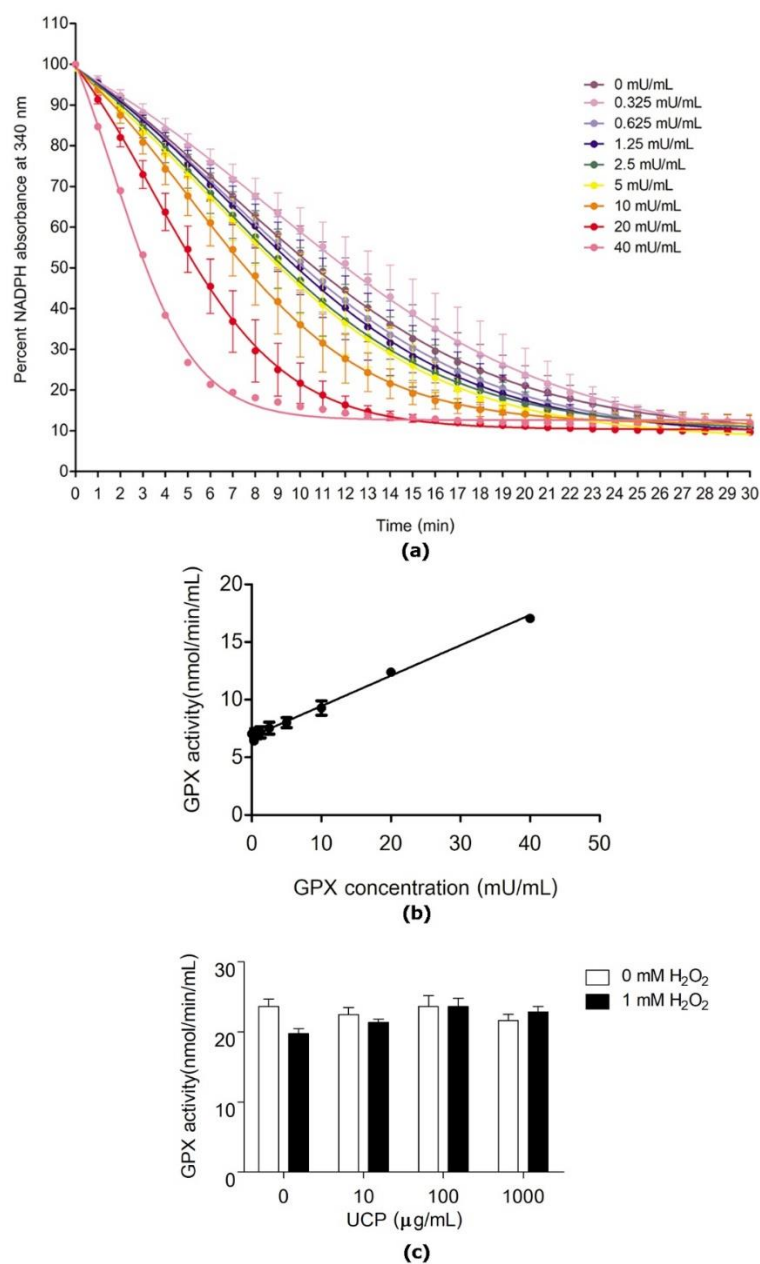


Figure 51 The UCP effect on GPX activity of  $\text{H}_2\text{O}_2$ -induced EA hy926 cell oxidative stress.

a) The reduction of NADPH absorbance at wavelength 450 nm of standard GPX at a concentration 0-40 mU/mL. b) The GPX activity standard curve. c) The effect of UCP treated on GPX activity of EA hy926 cell W/WO exposed with  $\text{H}_2\text{O}_2$ . Data are shown as

mean  $\pm$  SEM ( $n \geq 3$ )

#### 4.6.4 Effect of UCP on total GSH levels

The UCP effect on intracellular GSH levels was determined by the total GSH assay. The standard GSH curve at concentrations 0-20  $\mu\text{M}$  was prepared using an absorbance value at 415 nm (Figure 52a). UCP treated had no difference in each sample group. In the same way,  $\text{H}_2\text{O}_2$  also did not affect the GSH level when compared with the control group (Figure 52b).

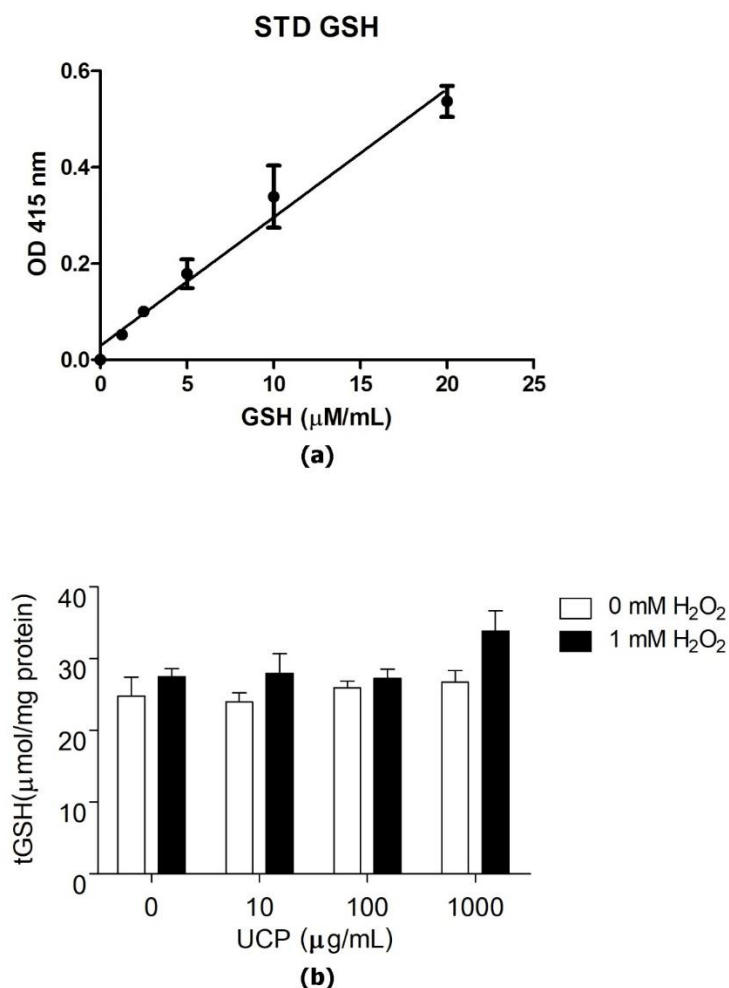


Figure 52 UCP effect on GSH level of  $\text{H}_2\text{O}_2$ -induced cell oxidative stress.

a) Standard curve of GSH concentration. b) Histogram of GSH level in each sample.

Data are shown as mean  $\pm$  SEM ( $n \geq 3$ )

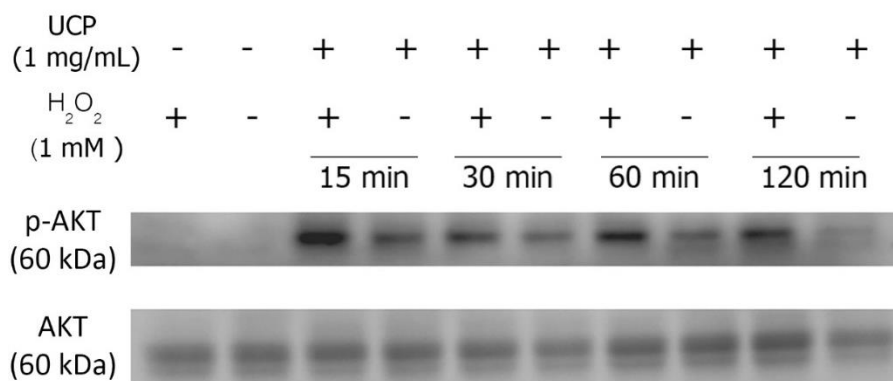


#### 4.7 Effect of UCP on the cell signaling pathways

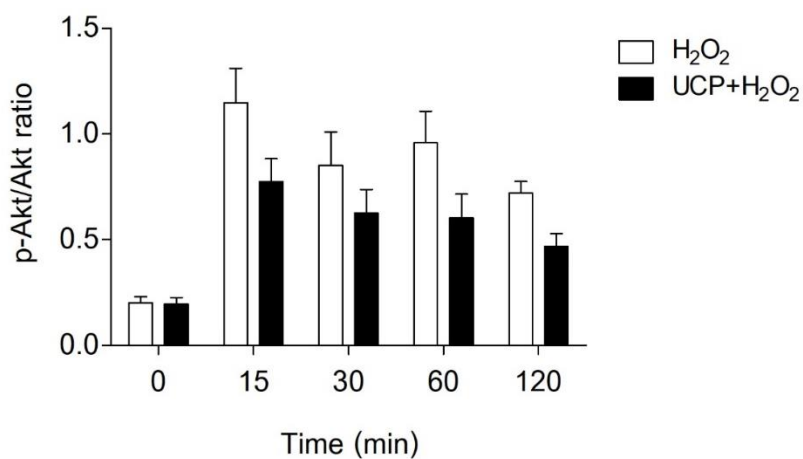
The UCP preventive effect on cell signaling pathways of H<sub>2</sub>O<sub>2</sub>-induced cell oxidative stress was evaluated by western blot. The Akt survival pathway and MAPK (JNK and p38) pathways were detected in whole protein lysates. While NF- $\kappa$ B and Nrf2 pathways were detected in nuclear lysates. Image J software was used to measure the intensity of protein bands. H<sub>2</sub>O<sub>2</sub> activation of the cell signaling pathway was observed for 120 min time-intervals.

##### 4.7.1 Effect of UCP on Akt phosphorylation

The effect of H<sub>2</sub>O<sub>2</sub> on the activation of Akt survival signaling protein was observed time-interval for 120 min. The phosphorylation of Akt after cell challenged 1 mM H<sub>2</sub>O<sub>2</sub> (Figure 53a). UCP preincubation did not affect Akt signaling protein when compared with the vehicle-treated group. P-Akt/Akt ratio had significantly increased after exposure with 1 mM H<sub>2</sub>O<sub>2</sub> for 15, 30, 60 and 120 minutes to  $1.15 \pm 0.16$ ,  $0.85 \pm 0.16$ ,  $0.96 \pm 0.15$  and  $0.72 \pm 0.06$  at  $p < 0.05$ , respectively when compared with vehicle-treated group ( $0.20 \pm 0.03$ ). UCP pretreated at a concentration 1 mg/mL on H<sub>2</sub>O<sub>2</sub>-EAhy926 cell decreased P-Akt/Akt ratio to  $0.77 \pm 0.11$ ,  $0.63 \pm 0.11$ ,  $0.60 \pm 0.11$  and  $0.47 \pm 0.06$  at each time-interval but did not significantly different in statistical analysis (Figure 53b).



(a)



(b)

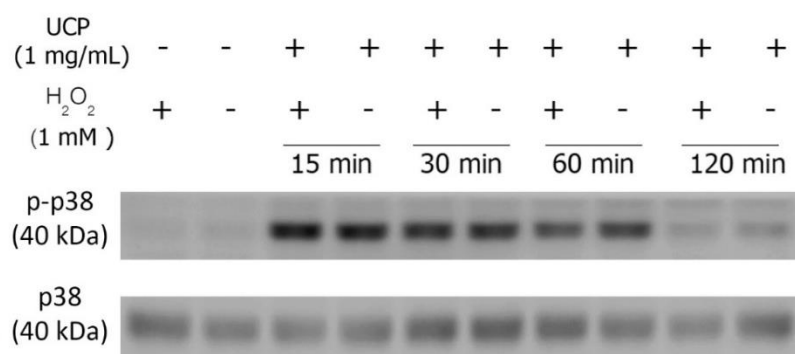
Figure 53 The Akt protein response to UCP pretreated on H<sub>2</sub>O<sub>2</sub>-induced EA hy926 cell oxidative stress.

a) Representative protein bands of P-Akt and Akt determined. b) The calculation of P-Akt/Akt protein ratio. Data are shown as mean  $\pm$  SEM ( $n \geq 3$ ). \*  $p < 0.05$  when compared with the control group

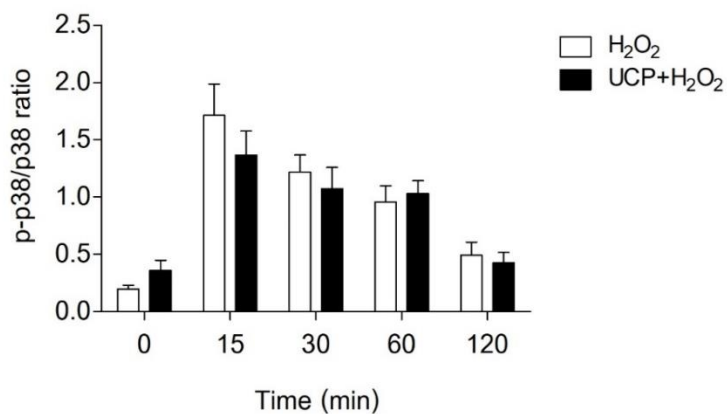
#### 4.7.2 Effect of UCP on p38 phosphorylation

The p38 activation was remarked for 120 minutes time-intervals by western blot analysis. Phosphorylation of p38 was increased for 15 minutes and descend until

120 minutes (Figure 54a). The P-p38/p38 ratio had significantly increased after exposed with 1 mM H<sub>2</sub>O<sub>2</sub> for 15, 30. and 60 minutes to  $1.71 \pm 0.28$ ,  $1.22 \pm 0.15$  and  $0.96 \pm 0.14$  at  $p < 0.05$ , respectively until descend at 120 minutes to  $0.49 \pm 0.11$  when compared with control group ( $0.20 \pm 0.03$ ). UCP preincubation on cells exposed W/WO H<sub>2</sub>O<sub>2</sub> did not influence P-p38 (Figure 54b).



(a)



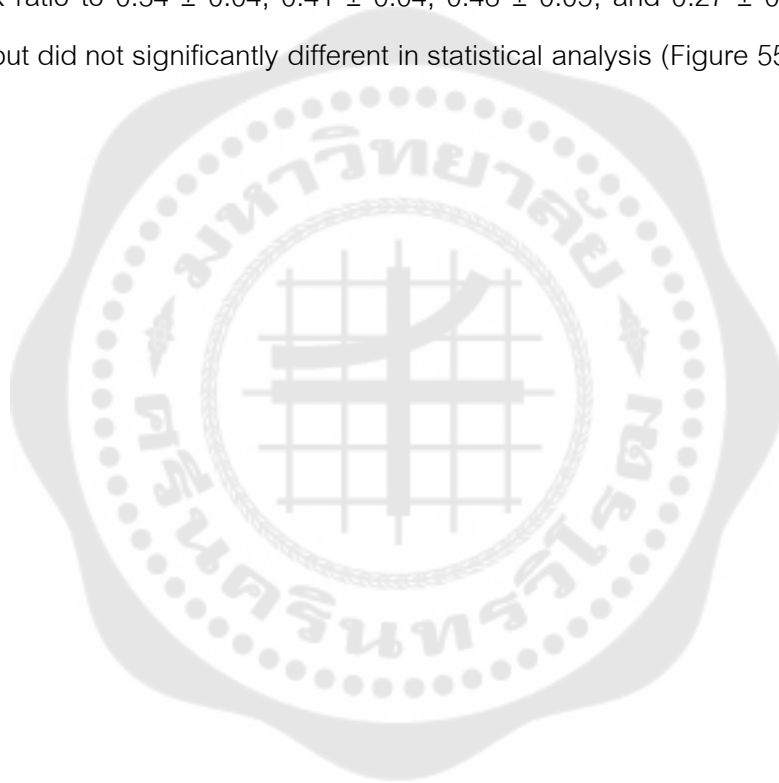
(b)

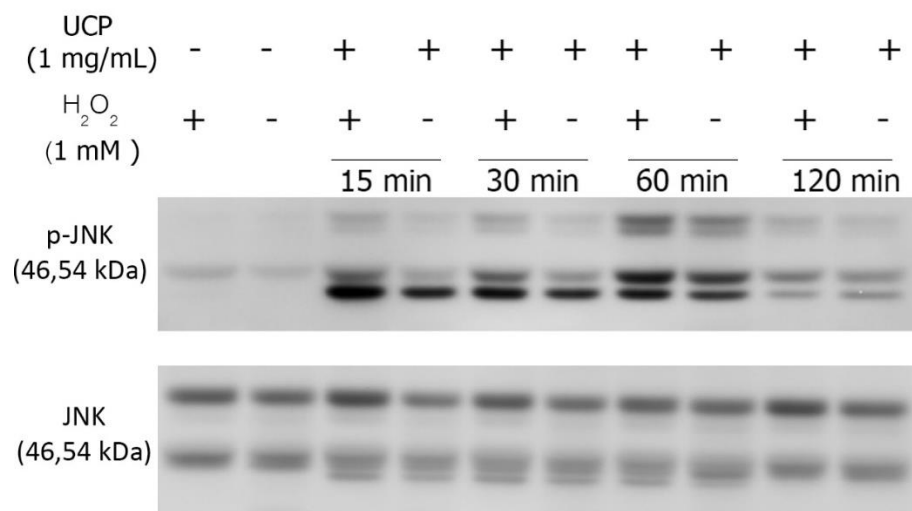
Figure 54 The p38 phosphorylation response of UCP pretreated on H<sub>2</sub>O<sub>2</sub>-induced cell oxidative stress.

a) Representative protein bands of P-p38 and p38 b) Calculation of P-p38/p38 Protein ratio. Data are shown as mean  $\pm$  SEM ( $n \geq 3$ ). \*  $p < 0.05$  when compared with the control group.

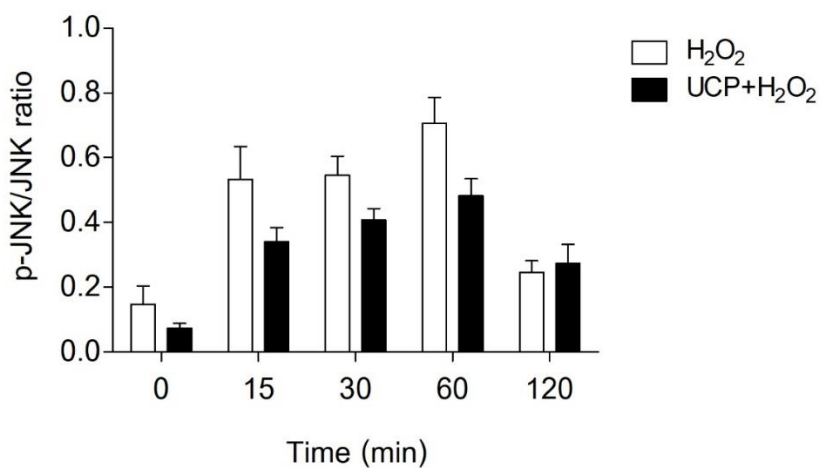
#### 4.7.3 Effect of UCP on JNK phosphorylation

The JNK phosphorylation was evaluated for a 120-minute time-interval by western blot analysis. Similarly, with P-p38, P-JNK was increased for 15 minutes and descend until 120 minutes (Figure 55a). 1 mM H<sub>2</sub>O<sub>2</sub> treated on EA hy926 cells showed significant increased of P-JNK/JNK ratio to  $0.53 \pm 0.10$ ,  $0.55 \pm 0.66$  and  $0.71 \pm 0.08$  at  $p < 0.05$ , respectively until decreased to  $0.25 \pm 0.04$  at 120 minutes when compared with control group ( $0.15 \pm 0.06$ ). UCP pretreated on H<sub>2</sub>O<sub>2</sub>-EA hy926 cell decreased P-JNK/JNK ratio to  $0.34 \pm 0.04$ ,  $0.41 \pm 0.04$ ,  $0.48 \pm 0.05$ , and  $0.27 \pm 0.06$  at each time-interval but did not significantly different in statistical analysis (Figure 55b).





(a)



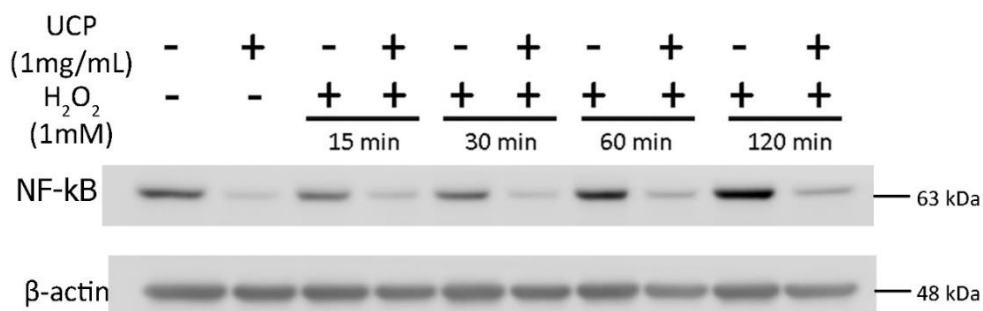
(b)

Figure 55 The JNK phosphorylation response to UCP pretreated on H<sub>2</sub>O<sub>2</sub>-induced cell oxidative stress.

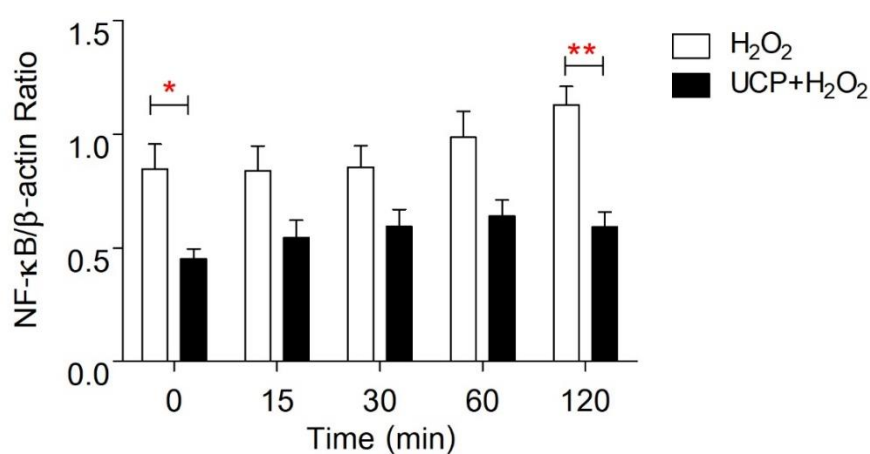
a) Representative protein bands of P-JNK and JNK b) Calculation of P-JNK/JNK Protein ratio. Data are shown as mean  $\pm$  SEM ( $n \geq 3$ ). \*  $p < 0.05$  when compared with the control group.

#### 4.7.4 Effect of UCP on NF- $\kappa$ B phosphorylation

NF- $\kappa$ B is an important signaling protein in inflammatory pathways. The effect of UCP pretreated on NF- $\kappa$ B signaling protein was observed for 120 minutes time-interval by western blot analysis (Figure 56a). UCP preincubation for 48 hours had significantly decreased NF- $\kappa$ B/ $\beta$ -actin ratio to  $0.44 \pm 0.04$  at  $p < 0.05$  when compared with control group ( $0.85 \pm 0.11$ ). Whereas  $H_2O_2$  exposed to EA hy926 cell for 60 and 120 minutes increased NF- $\kappa$ B/ $\beta$ -actin ratio to  $0.98 \pm 0.11$  and  $1.11 \pm 0.08$  but did not significantly different in statistical analysis. UCP pretreated on  $H_2O_2$ -induced EA hy926 cell oxidative stress showed decreased of NF- $\kappa$ B/ $\beta$ -actin to  $0.53 \pm 0.08$ ,  $0.57 \pm 0.06$ ,  $0.63 \pm 0.06$ , and  $0.57 \pm 0.05$  at 15, 30, 60, and 120 minutes, respectively when compared with their interval times. Only UCP preincubation on  $H_2O_2$ -treated EA hy926 cells for 120 minutes had significantly different at  $p < 0.05$  when compared with the  $H_2O_2$ -treated group (Figure 56b).



(a)



(b)

Figure 56 The NF- $\kappa$ B protein response of UCP pretreated on H<sub>2</sub>O<sub>2</sub>-induced EA hy926 cell oxidative stress.

Representative protein bands of NF- $\kappa$ B and  $\beta$ -actin determined by western blot. b) Protein ratio calculation of NF- $\kappa$ B/ $\beta$ -actin. Data are shown as mean  $\pm$  SEM ( $n \geq 3$ ). \*  $p < 0.05$ .

#### 4.7.5 Effect of UCP on Nrf2 phosphorylation and transcription factor

Nrf2 is a signaling protein in the antioxidant cascade. UCP preincubation on H<sub>2</sub>O<sub>2</sub>-induced cell oxidative stress for 120 minutes interval-time was observed by western blot analysis (Figure 57a). UCP treated on EA hy926 cells for 48 hours had no significance when compared with the vehicle-treated group. Whereas H<sub>2</sub>O<sub>2</sub> exposed for 120 minutes time-interval showed an increase of Nrf2/ $\beta$ actin ratio in a time-dependent

manner to  $0.98 \pm 0.20$ ,  $1.06 \pm 0.06$ ,  $1.41 \pm 0.21$  and  $1.70 \pm 0.21$  at 15, 30, 60, and 120 minutes, respectively, which only 120 minutes had significant differences when compared with the control group ( $0.84 \pm 0.20$ ). UCP pretreated on  $H_2O_2$ -exposed EA hy926 cells showed maintenance of the Nrf2/ $\beta$ actin ratio nearby to the control group. Moreover, UCP reduce  $H_2O_2$ -induced Nrf2 activation by reduce Nrf2/ $\beta$ actin to  $0.80 \pm 0.14$ ,  $0.73 \pm 0.09$ ,  $0.74 \pm 0.20$  and  $1.00 \pm 0.23$  when compared with each time interval groups (Figure 57b).

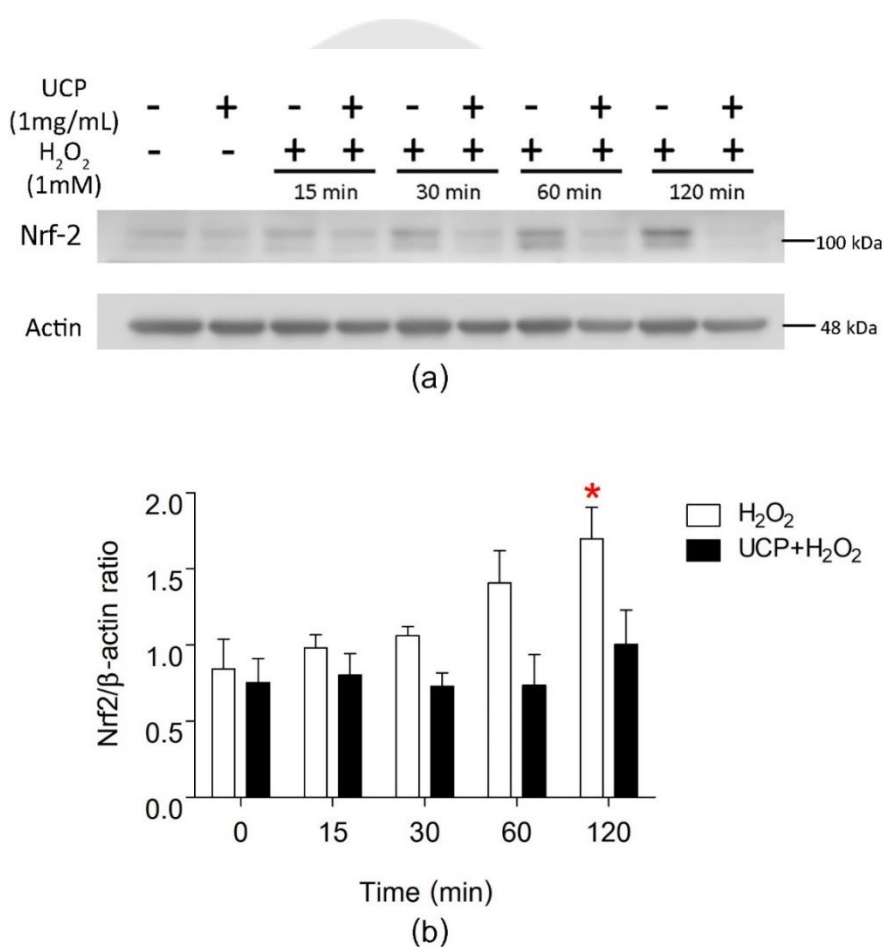


Figure 57 Effect of UCP preincubation to Nrf2 activation on  $H_2O_2$ -induced EA hy926 cell oxidative stress.

- a) Representative protein bands of Nrf2 and  $\beta$ -actin. b) Calculation of Nrf2/ $\beta$ -actin protein ratio. Data are shown as mean  $\pm$  SEM ( $n \geq 3$ ). \*  $p < 0.05$ .



The intracellular Nrf2 transcription factor in the EA hy926 cell nucleus was detected by the Nrf2 ELISA kit. To check the kits, transcription factor Nrf2 positive control was compared with their added competitor group. The result showed that the competitor completely inhibits the binding of the Nrf2 transcription factor and specific Nrf2 dsDNA for statistical significance at  $p < 0.001$  (Figure 58a).  $H_2O_2$ -exposed on EA hy926 cells significantly increased the Nrf2 transcription factor, whereas UCP pretreated showed the opposite effect. The competitive treated group showed a completely decreased absorbance at 450 nm when compared with the untreated group (Figure 58b). UCP (10, 100, and 1000  $\mu\text{g/mL}$ ) treated on EA hy926 cell had no significant difference when compared with the vehicle-treated group. Whereas, the  $H_2O_2$ -exposed group significantly increased relative percent absorbance at 450 nm to  $175.11 \pm 16.85$  % when compared with the control group (100 %). 10  $\mu\text{g/mL}$  of UCP pretreated on  $H_2O_2$ -exposed EA hy926 cell increased of absorbance to  $175.11 \pm 16.85$  %, whereas 100 and 1000  $\mu\text{g/mL}$  concentration reduced to  $145.61 \pm 8.79$  and  $142.65 \pm 13.22$ , respectively (Figure 81c).

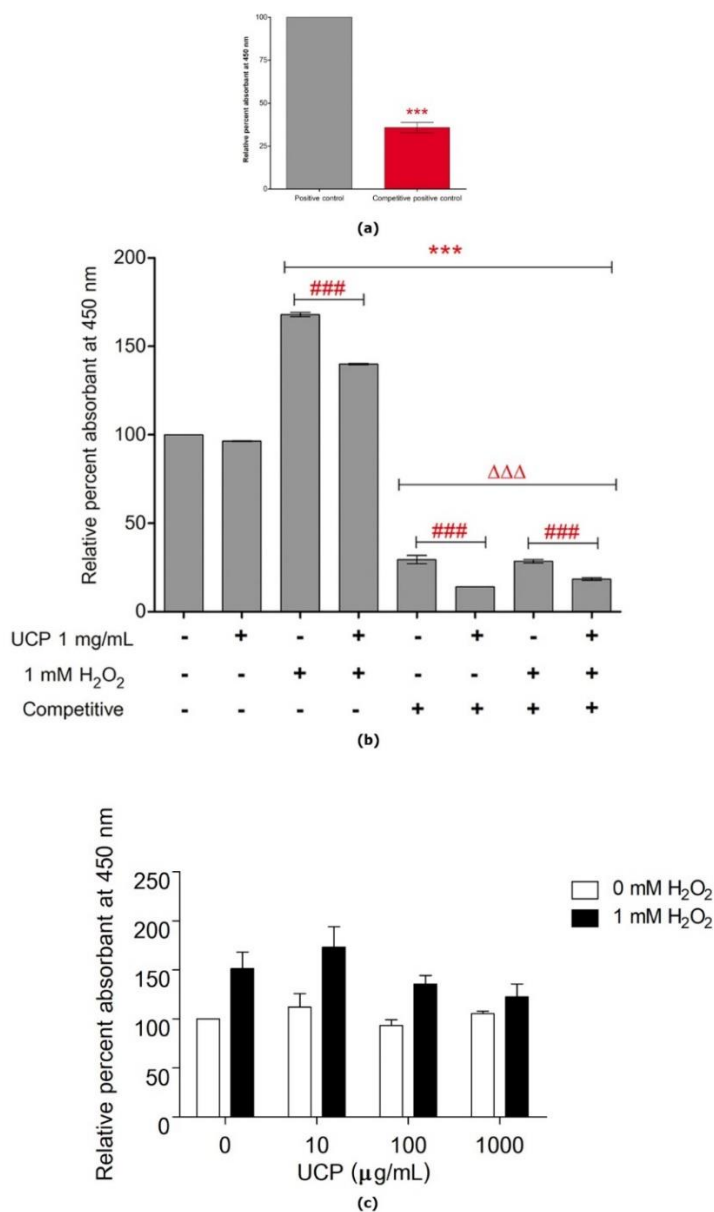


Figure 58 UCP pretreatment effect on the Nrf2 transcription factor on H<sub>2</sub>O<sub>2</sub>-induced EA hy926 cell oxidative stress.

a) positive and competitive test data. b) UCP pretreated on H<sub>2</sub>O<sub>2</sub>-exposed EA hy926 cell oxidative stress and their competitive treatment. c) Representative of UCP effect on Nrf2 transcription factor. Data are shown as mean ± SEM ( $n \geq 3$ ). \*  $p < 0.05$ , \*\*\*  $p < 0.001$  when compared with control group. ###  $p < 0.001$  when compared between group. ΔΔΔ  $p < 0.001$  when compared with the competitive group.

## CHAPTER 5

### SUMMARY DISCUSSION AND SUGGESTION

ROS are normally produced from the cellular mechanism in the living cell, which play many important roles in cell homeostasis and signaling pathways. Homeostatic imbalance of ROS can induce oxidative stress, leading to endothelial cell damage and death. Endothelial cell oxidative stress promotes atherosclerosis and CVDs via endothelial dysfunction and apoptosis. ROS are interrelated in cellular metabolism, which catalyze of  $O_2^{\bullet\bullet}$  by SOD to generate  $H_2O_2$ .  $H_2O_2$  can be eliminated by GPX and CAT and also can produce  $OH^\bullet$  via Fenton reaction. UCP has high scavenging activities against  $H_2O_2 > OH^\bullet > O_2^{\bullet\bullet} > HOCl$ , respectively. The scavenging activity of UCP on these ROS has a beneficial effect to protect against cellular oxidative stress. HOCl is produced by MPO to fight against the infection of pathogens (155). For this reason, the low scavenging activity of UCP on HOCl is useful to remain anti-infective effects of HOCl. Antioxidant compounds including ascorbic acid, quercetin, and gallic acid were found in UCP, which are phytochemical compounds to protect against ROS. FRAP value of UCP was found at  $2.68 \pm 0.24 \mu M$  ( $26.79 \pm 2.43 \mu mol/g$ ) in FRAP assay and UCP at a concentration of 1 mg/mL had Trolox equivalent to  $56.03 \pm 7.52 \mu M$   $\mu mol/g$  in ORAC assay. FRAP values of UCP is almost the same as green grape, mangosteen, and navel orange (156) whereas ORAC values nearly the same as green *Amaranthus mangostanus* and *Saccharum officinarum* (157). UCP also shows the antioxidant effect to reduce lipid peroxidation of linoleic acid in FTC assay. Lipid peroxidation by ROS can cause atherosclerosis, leading to CVDs (158), in which UCP might reduce these risks. Like Chinese medicine herbal formulation, Sailutong composing of *Panax ginseng*, *Ginkgo biloba*, and, *Crocus sativus* exhibit preventive effect on  $H_2O_2$ -induced EA hy926 oxidative stress (159), UCP also reduce intracellular ROS levels to defend cell death and injury, in which MTT assay showed that UCP increases percent cell viability of endothelial cell when compared with  $H_2O_2$ -treated group. The uncontrolled levels of ROS in the endothelial cell can induce cell death via apoptotic signaling pathways (160).

H<sub>2</sub>O<sub>2</sub> also induce endothelial cell apoptosis via mitochondrial oxidative stress, JNK, p38, and Fas pathways (161), in which UCP showed the antioxidant and antiapoptotic effect by direct eliminate ROS and show a trend to decrease the JNK signaling pathway on H<sub>2</sub>O<sub>2</sub>-induced EAhy926 cell death. Thus UCP is an antioxidant source to protect against H<sub>2</sub>O<sub>2</sub>-induced endothelial cell oxidative stress and death.

Exposure of H<sub>2</sub>O<sub>2</sub> activates Akt and ERK1/2 survival pathways, which can induce NO production via activation of eNOS (161). UCP did not affect on Akt survival pathway. NF- $\kappa$ B is the main signaling pathway to induce cell inflammation, H<sub>2</sub>O<sub>2</sub>-treated on EA hy926 also increase NF- $\kappa$ B signaling pathway induces endothelial cell inflammation and death, which under these circumstances play a key role to promote vascular inflammation and CVDs (162). Decrease in NF- $\kappa$ B by UCP can improve H<sub>2</sub>O<sub>2</sub>-induced endothelial cell inflammation that might reduce the risks of atherosclerosis. Nrf2 is the key important pathway to eliminate and balance intracellular ROS reducing oxidative damage via activation of enzymatic antioxidant production such as GPX, CAT, and, SOD (163). H<sub>2</sub>O<sub>2</sub>-exposed on endothelial cell increase Nrf2 in over time to respond elevating of intracellular ROS levels. While UCP pretreatment on H<sub>2</sub>O<sub>2</sub>-induced endothelial cell kept oxidative stress balance Nrf2 levels nearly control group. The elimination effect of UCP on intracellular ROS improved the Nrf2 levels leading to homeostasis balance of the cell.

In this study, we use H<sub>2</sub>O<sub>2</sub> to induce endothelial cell oxidative stress but the defencesive enzyme SOD is minimally involved in reducing oxidative stress. The SOD function is to convert O<sub>2</sub><sup>••</sup> into H<sub>2</sub>O<sub>2</sub>; UCP increases SOD activity is beneficial to eliminate excessive O<sub>2</sub><sup>••</sup> generated from cellular mitochondrial electron transport chain and offer sources. Although GPX and CAT are H<sub>2</sub>O<sub>2</sub> eliminators our results show that GPX activity and total GSH levels did not change whereas In fibroblast, CAT activity was decreased after exposure to H<sub>2</sub>O<sub>2</sub>. CAT plays a major role to eliminate exogenous H<sub>2</sub>O<sub>2</sub> leading to minimizing GPX activity and decreasing CAT activity (164). UCP pretreatment restores CAT activity to almost control, which provides defense of the antioxidant environment to reduce oxidative stress.

In summary, UCP has a high antioxidant property that can protect against  $H_2O_2$ -induced endothelial cell inflammation and death via the elimination of ROS and balancing of cell homeostasis leading to the restoration of CAT activity and reduction of NF- $\kappa$ B and Nrf2 protein signaling pathways. UCP might be a candidate for a dietary supplement on alternative complementary medicine to prevent risks of atherosclerosis and CVDs. The study of their effect on in vivo and clinical research are studies warranty.



## REFERENCES

1. Bhattacharya S. Reactive oxygen species and cellular defense system. In: Rani V, Yadav UCS, editors. Free Radicals in Human Health and Disease. New Delhi: Springer India; 2015. p. 17-29.
2. Turrens JF. Mitochondrial formation of reactive oxygen species. *The Journal of physiology*. 2003;552(Pt 2):335-44.
3. Yoboue ED, Sitia R, Simmen T. Redox crosstalk at endoplasmic reticulum (ER) membrane contact sites (MCS) uses toxic waste to deliver messages. *Cell Death & Disease*. 2018;9(3):331.
4. Birben E, Sahiner UM, Sackesen C, Erzurum S, Kalayci O. Oxidative stress and antioxidant defense. *The World Allergy Organization journal*. 2012;5(1):9-19.
5. Liu D, Xu Y. p53, oxidative stress, and aging. *Antioxidants & redox signaling*. 2011;15(6):1669-78.
6. Zhang J, Wang X, Vikash V, Ye Q, Wu D, Liu Y, et al. ROS and ROS-mediated cellular signaling. *Oxidative Medicine and Cellular Longevity*. 2016;2016:18.
7. Fang FC. Antimicrobial actions of reactive oxygen species. *mBio*. 2011;2(5).
8. Schieber M, Chandel NS. ROS function in redox signaling and oxidative stress. *Current biology : CB*. 2014;24(10):R453-62.
9. Circu ML, Aw TY. Reactive oxygen species, cellular redox systems and apoptosis. *Free radical biology & medicine*. 2010;48(6):749-62.
10. Klotz LO, Sánchez-Ramos C, Prieto-Arroyo I, Urbánek P, Steinbrenner H, Monsalve M. Redox regulation of FoxO transcription factors. *Redox Biology*. 2015;6:51-72.
11. Ma Q. Role of nrf2 in oxidative stress and toxicity. *Annual review of pharmacology and toxicology*. 2013;53:401-26.
12. Panth N, Paudel KR, Parajuli K. Reactive oxygen species: A key hallmark of cardiovascular disease. *Advances in Medicine*. 2016;2016:12.
13. Liou GY, Storz P. Reactive oxygen species in cancer. *Free radical research*. 2010;44(5):479-96.

14. Di Dalmazi G, Hirshberg J, Lyle D, Freij JB, Caturegli P. Reactive oxygen species in organ-specific autoimmunity. *Auto-immunity highlights*. 2016;7(1):11.
15. Rodrigues SF, Granger DN. Blood cells and endothelial barrier function. *Tissue barriers*. 2015;3(1-2):e978720.
16. Stamatovic SM, Keep RF, Andjelkovic AV. Brain endothelial cell-cell junctions: How to "open" the blood brain barrier. *Current Neuropharmacology*. 2008;6(3):179-92.
17. Lamalice L, Le Boeuf F, Huot J. Endothelial cell migration during angiogenesis. *Circulation research*. 2007;100(6):782-94.
18. Hermann M, Flammer A, Luscher TF. Nitric oxide in hypertension. *Journal of clinical hypertension (Greenwich, Conn)*. 2006;8(12 Suppl 4):17-29.
19. Bouwens EA, Stavenuiter F, Mosnier LO. Mechanisms of anticoagulant and cytoprotective actions of the protein C pathway. *Journal of thrombosis and haemostasis : JTH*. 2013;11 Suppl 1:242-53.
20. Absher E, Labarrere CA, Carter C, Haag B, Faulk WP. The endothelial heparan sulfate-antithrombin III natural anticoagulant pathway in normal and transplanted human kidneys. *Transplantation*. 1992;53(4):828-34.
21. Mai J, Virtue A, Shen J, Wang H, Yang XF. An evolving new paradigm: endothelial cells--conditional innate immune cells. *Journal of hematology & oncology*. 2013;6:61.
22. Karbach S, Wenzel P, Waisman A, Munzel T, Daiber A. eNOS uncoupling in cardiovascular diseases--the role of oxidative stress and inflammation. *Current pharmaceutical design*. 2014;20(22):3579-94.
23. Csiszar A, Wang M, Lakatta EG, Ungvari Z. Inflammation and endothelial dysfunction during aging: role of NF-kappaB. *Journal of applied physiology (Bethesda, Md : 1985)*. 2008;105(4):1333-41.
24. Madamanchi NR, Vendrov A, Runge MS. Oxidative stress and vascular disease. *Arteriosclerosis, thrombosis, and vascular biology*. 2005;25(1):29-38.
25. Breton-Romero R, Lamas S. Hydrogen peroxide signaling in vascular endothelial cells. *Redox Biology*. 2014;2:529-34.
26. Sadidi M, Lentz SI, Feldman EL. Hydrogen peroxide-induced akt phosphorylation

regulates bax activation. *Biochimie*. 2009;91(5):577-85.

27. Chen B, Lu Y, Chen Y, Cheng J. The role of Nrf2 in oxidative stress-induced endothelial injuries. *The Journal of endocrinology*. 2015;225(3):R83-99.

28. Yin J, Duan J, Cui Z, Ren W, Li T, Yin Y. Hydrogen peroxide-induced oxidative stress activates NF- $\kappa$ B and Nrf2 /Keap1 signals and triggers autophagy in piglets. *RSC Advances*. 2015;5(20):15479-86.

29. Guo S, Long M, Li X, Zhu S, Zhang M, Yang Z. Curcumin activates autophagy and attenuates oxidative damage in EA.hy9 2 6 cells via the Akt/mTOR pathway. *Molecular medicine reports*. 2016;13(3):2187-93.

30. Wongpradabchai S, Chularojmontri L, Phornchirasilp S, Wattanapitayakul SK. Protective effect of *Phyllanthus emblica* fruit extract against hydrogen peroxide-induced endothelial cell death. *Journal of the Medical Association of Thailand = Chotmaihet thangphaet*. 2013;96 Suppl 1:S40-8.

31. Chen S, Tang Y, Qian Y, Chen R, Zhang L, Wo L, et al. Allicin prevents H<sub>2</sub>O<sub>2</sub>-induced apoptosis of HUVECs by inhibiting an oxidative stress pathway. *BMC Complementary and Alternative Medicine*. 2014;14.

32. Liu L, Gu L, Ma Q, Zhu D, Huang X. Resveratrol attenuates hydrogen peroxide-induced apoptosis in human umbilical vein endothelial cells. *Eur Rev Med Pharmacol Sci*. 2013;17(1):88-94.

33. Zhu M, Li J, Wang K, Hao X, Ge R, Li Q. Isoquercitrin inhibits hydrogen peroxide-induced apoptosis of EA.Hy9 2 6 cells via the PI3 K/Akt/GSK3  $\beta$  signaling pathway. *Molecules*. 2016;21(3):356.

34. Song Z, Liu Y, Hao B, Yu S, Zhang H, Liu D, et al. Ginsenoside Rb1 prevents H<sub>2</sub>O<sub>2</sub>-induced HUVEC senescence by stimulating sirtuin-1 pathway. *PLoS one*. 2014;9(11):e112699.

35. Aravind G, Bhowmik D, S D, Harish G. Traditional and medicinal uses of *Carica papaya*. *J Med Plants Stud*. 2013;1:7-15.

36. Asghar N, Naqvi SA, Hussain Z, Rasool N, Khan ZA, Shahzad SA, et al. Compositional difference in antioxidant and antibacterial activity of all parts of the *Carica*



*papaya* using different solvents. Chemistry Central journal. 2016;10:5.

37. Panzarini E, Dwikat M, Mariano S, Vergallo C, Dini L. Administration dependent antioxidant effect of *Carica papaya* seeds water extract. Evidence-Based Complementary and Alternative Medicine. 2014;2014:13.

38. Nayak BS, Ramdeen R, Adogwa A, Ramsubhag A, Marshall JR. Wound-healing potential of an ethanol extract of *Carica papaya* (Caricaceae) seeds. International wound journal. 2012;9(6):650-5.

39. Mohamed Sadek K. Antioxidant and immunostimulant effect of *Carica papaya* linn. Aqueous extract in acrylamide intoxicated rats. Acta informatica medica : AIM : journal of the Society for Medical Informatics of Bosnia & Herzegovina : casopis Društva za medicinsku informatiku BiH. 2012;20(3):180-5.

40. Pandey S, Cabot PJ, Shaw PN, Hewavitharana AK. Anti-inflammatory and immunomodulatory properties of *Carica papaya*. Journal of Immunotoxicology. 2016;13(4):590-602.

41. Nguyen TTT, Shaw PN, Parat M-O, Hewavitharana AK. Anticancer activity of *Carica papaya*: A review. Molecular Nutrition & Food Research. 2013;57(1):153-64.

42. Subenthiran S, Choon TC, Cheong KC, Thayan R, Teck MB, Muniandy PK, et al. *Carica papaya* Leaves Juice Significantly Accelerates the Rate of Increase in Platelet Count among Patients with Dengue Fever and Dengue Haemorrhagic Fever. Evidence-Based Complementary and Alternative Medicine. 2013;2013:7.

43. Barbagallo M, Marotta F, Dominguez LJ. Oxidative stress in patients with Alzheimer's disease: effect of extracts of fermented papaya powder. Mediators of inflammation. 2015;2015:624801.

44. Zhao CN, Meng X, Li Y, Li S, Liu Q, Tang GY, et al. Fruits for Prevention and Treatment of Cardiovascular Diseases. Nutrients. 2017;9(6).

45. Phaniendra A, Jestadi DB, Periyasamy L. Free radicals: properties, sources, targets, and their implication in various diseases. Indian journal of clinical biochemistry : IJCB. 2015;30(1):11-26.

46. Lipinski B. Hydroxyl radical and its scavengers in health and disease. Oxidative

Medicine and Cellular Longevity. 2011;2011.

47. Muller F. The nature and mechanism of superoxide production by the electron transport chain: Its relevance to aging. *Journal of the American Aging Association*. 2000;23(4):227-53.
48. Paravicini TM, Touyz RM. NADPH oxidases, reactive oxygen species, and hypertension: clinical implications and therapeutic possibilities. *Diabetes care*. 2008;31 Suppl 2:S170-80.
49. Ayala A, Muñoz MF, Argüelles S. Lipid peroxidation: Production, metabolism, and signaling mechanisms of malondialdehyde and 4-hydroxy-2-nonenal. *Oxidative Medicine and Cellular Longevity*. 2014;2014:360438.
50. McBride AG, Borutaite V, Brown GC. Superoxide dismutase and hydrogen peroxide cause rapid nitric oxide breakdown, peroxynitrite production and subsequent cell death. *Biochimica et biophysica acta*. 1999;1454(3):275-88.
51. Mello Filho AC, Hoffmann ME, Meneghini R. Cell killing and DNA damage by hydrogen peroxide are mediated by intracellular iron. *Biochemical Journal*. 1984;218(1):273-5.
52. Di Marzo N, Chisci E, Giovannoni R. The role of hydrogen peroxide in redox-dependent signaling: Homeostatic and pathological responses in mammalian cells. *Cells*. 2018;7(10):156.
53. Veal EA, Day AM, Morgan BA. Hydrogen peroxide sensing and signaling. *Molecular Cell*. 2007;26(1):1-14.
54. Spickett CM, Jerlich A, Panasenko OM, Arnhold J, Pitt AR, Stelmaszynska T, et al. The reactions of hypochlorous acid, the reactive oxygen species produced by myeloperoxidase, with lipids. *Acta biochimica Polonica*. 2000;47(4):889-99.
55. Pullar JM, Vissers MC, Winterbourn CC. Living with a killer: the effects of hypochlorous acid on mammalian cells. *IUBMB life*. 2000;50(4-5):259-66.
56. McKenna SM, Davies KJ. The inhibition of bacterial growth by hypochlorous acid. Possible role in the bactericidal activity of phagocytes. *Biochemical Journal*. 1988;254(3):685-92.

57. Bhattacharyya A, Chattopadhyay R, Mitra S, Crowe SE. Oxidative stress: an essential factor in the pathogenesis of gastrointestinal mucosal diseases. *Physiological reviews*. 2014;94(2):329-54.
58. Zhang DX, Gutterman DD. Mitochondrial reactive oxygen species-mediated signaling in endothelial cells. *American journal of physiology Heart and circulatory physiology*. 2007;292(5):H2023-31.
59. Schrader M, Fahimi HD. Peroxisomes and oxidative stress. *Biochimica et Biophysica Acta (BBA) - Molecular Cell Research*. 2006;1763(12):1755-66.
60. Del Rio LA, Lopez-Huertas E. ROS generation in peroxisomes and its role in cell signaling. *Plant & cell physiology*. 2016;57(7):1364-76.
61. Fransen M, Nordgren M, Wang B, Apanasets O. Role of peroxisomes in ROS/RNS-metabolism: Implications for human disease. *Biochimica et Biophysica Acta (BBA) - Molecular Basis of Disease*. 2012;1822(9):1363-73.
62. Manivannan S, Scheckhuber CQ, Veenhuis M, van der Klei IJ. The impact of peroxisomes on cellular aging and death. *Front Oncol*. 2012;2:50-.
63. Zeeshan H, Lee G, Kim H-R, Chae H-J. Endoplasmic reticulum stress and associated ros. *International Journal of Molecular Sciences*. 2016;17(3):327.
64. Cao SS, Kaufman RJ. Endoplasmic reticulum stress and oxidative stress in cell fate decision and human disease. *Antioxidants & redox signaling*. 2014;21(3):396-413.
65. Di Meo S, Reed TT, Venditti P, Victor VM. Role of ROS and RNS sources in physiological and pathological conditions. *Oxidative Medicine and Cellular Longevity*. 2016;2016:44.
66. Azzam EI, Jay-Gerin JP, Pain D. Ionizing radiation-induced metabolic oxidative stress and prolonged cell injury. *Cancer letters*. 2012;327(1-2):48-60.
67. Valavanidis A, Vlachogianni T, Fiotakis K. Tobacco smoke: Involvement of reactive oxygen species and stable free radicals in mechanisms of oxidative damage, carcinogenesis and synergistic effects with other respirable particles. *International Journal of Environmental Research and Public Health*. 2009;6(2):445-62.
68. Schieber M, Chandel NS. ROS function in redox signaling and oxidative stress.

Current biology : CB. 2014;24(10):R453-R62.

69. Fukai T, Ushio-Fukai M. Superoxide dismutases: role in redox signaling, vascular function, and diseases. *Antioxidants & redox signaling*. 2011;15(6):1583-606.
70. Kirkman HN, Rolfo M, Ferraris AM, Gaetani GF. Mechanisms of protection of catalase by NADPH. Kinetics and stoichiometry. *The Journal of biological chemistry*. 1999;274(20):13908-14.
71. Lu J, Holmgren A. The thioredoxin antioxidant system. *Free radical biology & medicine*. 2014;66:75-87.
72. Kaźmierczak-Barańska J, Boguszewska K, Adamus-Grabicka A, Karwowski BT. Two faces of vitamin C-antioxidative and pro-oxidative agent. *Nutrients*. 2020;12(5):1501.
73. Zhou S-S. Vitamin paradox in obesity: Deficiency or excess? *World Journal of Diabetes*. 2015;6:1158.
74. Moussa Z, Judeh Z, Ahmed S. Nonenzymatic exogenous and endogenous antioxidants. 2019.
75. Anand David AV, Arulmoli R, Parasuraman S. Overviews of biological importance of quercetin: A bioactive flavonoid. *Pharmacogn Rev*. 2016;10(20):84-9.
76. Naveed M, Hejazi V, Abbas M, Kamboh AA, Khan GJ, Shumzaid M, et al. Chlorogenic acid (CGA): A pharmacological review and call for further research. *Biomedicine & Pharmacotherapy*. 2018;97:67-74.
77. Kahkeshani N, Farzaei F, Fotouhi M, Alavi SS, Bahramsoltani R, Naseri R, et al. Pharmacological effects of gallic acid in health and diseases: A mechanistic review. *Iran J Basic Med Sci*. 2019;22(3):225-37.
78. Priyadarsini KI, Khopde SM, Kumar SS, Mohan H. Free radical studies of ellagic acid, a natural phenolic antioxidant. *Journal of agricultural and food chemistry*. 2002;50(7):2200-6.
79. Liu Z, Ren Z, Zhang J, Chuang C-C, Kandaswamy E, Zhou T, et al. Role of ROS and nutritional antioxidants in human diseases. *Front Physiol*. 2018;9:477-.
80. Repetto M, Semprine J, Boveris A. Lipid peroxidation: Chemical mechanism, biological implications and analytical determination. In: Catala A, editor. *Lipid Peroxidation*.

Rijeka: InTech; 2012. p. Ch. 01.

81. Gentile F, Arcaro A, Pizzimenti S, Daga M, Paolo Cetrangolo G, Dianzani C, et al. DNA damage by lipid peroxidation products: implications in cancer, inflammation and autoimmunity 2017. 103-37 p.
82. Gaschler MM, Stockwell BR. Lipid peroxidation in cell death. *Biochemical and Biophysical Research Communications*. 2017;482(3):419-25.
83. Pizzimenti S, Ciamporcero E, Daga M, Pettazzoni P, Arcaro A, Cetrangolo G, et al. Interaction of aldehydes derived from lipid peroxidation and membrane proteins. *Front Physiol*. 2013;4:242.
84. Davies MJ. Protein oxidation and peroxidation. *Biochemical Journal*. 2016;473(7):805-25.
85. Lund MN, Heinonen M, Baron CP, Estevez M. Protein oxidation in muscle foods: a review. *Mol Nutr Food Res*. 2011;55(1):83-95.
86. Cai Z, Yan LJ. Protein oxidative modifications: Beneficial roles in disease and health. *Journal of biochemical and pharmacological research*. 2013;1(1):15-26.
87. Gill SS, Tuteja N. Reactive oxygen species and antioxidant machinery in abiotic stress tolerance in crop plants. *Plant physiology and biochemistry : PPB*. 2010;48(12):909-30.
88. Aust AE, Eveleigh JF. Mechanisms of DNA oxidation. *Proceedings of the Society for Experimental Biology and Medicine Society for Experimental Biology and Medicine (New York, NY)*. 1999;222(3):246-52.
89. Poetsch AR. The genomics of oxidative DNA damage, repair, and resulting mutagenesis. *Computational and Structural Biotechnology Journal*. 2020;18:207-19.
90. Zhang W, Liu HT. MAPK signal pathways in the regulation of cell proliferation in mammalian cells. *Cell Res*. 2002;12(1):9-18.
91. McCubrey JA, Steelman LS, Chappell WH, Abrams SL, Wong EW, Chang F, et al. Roles of the Raf/MEK/ERK pathway in cell growth, malignant transformation and drug resistance. *Biochimica et biophysica acta*. 2007;1773(8):1263-84.
92. Cagnol S, Chambard JC. ERK and cell death: mechanisms of ERK-induced cell

- death--apoptosis, autophagy and senescence. *The FEBS journal*. 2010;277(1):2-21.
93. Kondoh K, Nishida E. Regulation of MAP kinases by MAP kinase phosphatases. *Biochimica et Biophysica Acta (BBA) - Molecular Cell Research*. 2007;1773(8):1227-37.
94. Lawrence T. The nuclear factor NF- $\kappa$ B pathway in inflammation. *Cold Spring Harbor Perspectives in Biology*. 2009;1(6).
95. Valko M, Leibfritz D, Moncol J, Cronin MT, Mazur M, Telser J. Free radicals and antioxidants in normal physiological functions and human disease. *The international journal of biochemistry & cell biology*. 2007;39(1):44-84.
96. Zhang J, Wang X, Vikash V, Ye Q, Wu D, Liu Y, et al. ROS and ROS-Mediated Cellular Signaling. *Oxidative Medicine and Cellular Longevity*. 2016;2016:4350965.
97. Perillo B, Di Donato M, Pezone A, Di Zazzo E, Giovannelli P, Galasso G, et al. ROS in cancer therapy: the bright side of the moon. *Experimental & Molecular Medicine*. 2020;52(2):192-203.
98. Circu ML, Aw TY. Reactive oxygen species, cellular redox systems, and apoptosis. *Free radical biology & medicine*. 2010;48(6):749-62.
99. Florean C, Song S, Dicato M, Diederich M. Redox biology of regulated cell death in cancer: A focus on necroptosis and ferroptosis. *Free Radical Biology and Medicine*. 2019;134.
100. Fang C, Gu L, Smerin D, Mao S, Xiong X. The interrelation between reactive oxygen species and autophagy in neurological disorders. *Oxidative Medicine and Cellular Longevity*. 2017;2017:8495160.
101. Patel-Hett S, D'Amore PA. Signal transduction in vasculogenesis and developmental angiogenesis. *The International journal of developmental biology*. 2011;55(4-5):353-63.
102. Clapp C, Thebault S, Jeziorski MC, Martinez De La Escalera G. Peptide hormone regulation of angiogenesis. *Physiological reviews*. 2009;89(4):1177-215.
103. Alonso D, Radomski MW. The nitric oxide-endothelin-1 connection. *Heart failure reviews*. 2003;8(1):107-15.
104. Liu J, Pedersen LC. Anticoagulant heparan sulfate: structural specificity and

biosynthesis. *Applied microbiology and biotechnology*. 2007;74(2):263-72.

105. van Hinsbergh VWM. Endothelium—role in regulation of coagulation and inflammation. *Seminars in Immunopathology*. 2012;34(1):93-106.

106. Rajendran P, Rengarajan T, Thangavel J, Nishigaki Y, Sakthisekaran D, Sethi G, et al. The vascular endothelium and human diseases. *International Journal of Biological Sciences*. 2013;9(10):1057-69.

107. Katusic ZS. Vascular endothelial dysfunction: does tetrahydrobiopterin play a role? *American Journal of Physiology - Heart and Circulatory Physiology*. 2001;281(3):H981-H6.

108. Yang Z, Ming XF. Recent advances in understanding endothelial dysfunction in atherosclerosis. *Clinical medicine & research*. 2006;4(1):53-65.

109. Montezano AC, Nguyen Dinh Cat A, Rios FJ, Touyz RM. Angiotensin II and vascular injury. *Current hypertension reports*. 2014;16(6):431.

110. Adam AP, Lowery AM, Martino N, Alsaffar H, Vincent PA. Src family kinases modulate the loss of endothelial barrier function in response to TNF- $\alpha$ : Crosstalk with p38 signaling. *PloS one*. 2016;11(9):e0161975.

111. Di A, Mehta D, Malik AB. ROS-activated calcium signaling mechanisms regulating endothelial barrier function. *Cell calcium*. 2016;60(3):163-71.

112. Mittal M, Siddiqui MR, Tran K, Reddy SP, Malik AB. Reactive oxygen species in inflammation and tissue injury. *Antioxidants & redox signaling*. 2014;20(7):1126-67.

113. Sprague AH, Khalil RA. Inflammatory cytokines in vascular dysfunction and vascular disease. *Biochemical pharmacology*. 2009;78(6):539-52.

114. Ushio-Fukai M. Redox signaling in angiogenesis: role of NADPH oxidase. *Cardiovascular research*. 2006;71(2):226-35.

115. Kim YW, Byzova TV. Oxidative stress in angiogenesis and vascular disease. *Blood*. 2014;123(5):625-31.

116. Kim Y-W, West XZ, Byzova TV. Inflammation and oxidative stress in angiogenesis and vascular disease. *Journal of Molecular Medicine*. 2013;91(3):323-8.

117. Pober JS, Min W, Bradley JR. Mechanisms of endothelial dysfunction, injury, and death. *Annual Review of Pathology: Mechanisms of Disease*. 2009;4(1):71-95.

118. Li Y, Cifuentes-Pagano E, DeVallance ER, de Jesus DS, Sahoo S, Meijles DN, et al. NADPH oxidase 2 inhibitors CPP11G and CPP11H attenuate endothelial cell inflammation & vessel dysfunction and restore mouse hind-limb flow. *Redox Biology*. 2019;22:101143.
119. Kita T, Kume N, Minami M, Hayashida K, Murayama T, Sano H, et al. Role of oxidized LDL in atherosclerosis. *Annals of the New York Academy of Sciences*. 2001;947:199-205; discussion -6.
120. Cervantes Gracia K, Llanas-Cornejo D, Husi H. CVD and oxidative stress. *Journal of Clinical Medicine*. 2017;6(2).
121. Pham-Huy LA, He H, Pham-Huy C. Free radicals, antioxidants in disease and health. *International Journal of Biomedical Science : IJBS*. 2008;4(2):89-96.
122. Small DM, Gobe GC. Oxidative stress and antioxidant therapy in chronic kidney and cardiovascular disease. In: Morales-González JA, editor. *Oxidative Stress and Chronic Degenerative Diseases - A Role for Antioxidants*. Rijeka: InTech; 2013. p. Ch. 10.
123. Carlsen MH, Halvorsen BL, Holte K, Bøhn SK, Dragland S, Sampson L, et al. The total antioxidant content of more than 3100 foods, beverages, spices, herbs and supplements used worldwide. *Nutrition Journal*. 2010;9(1):3.
124. Lee MJ, Lee HS, Park SD, Moon HI, Park WH. *Leonurus sibiricus* herb extract suppresses oxidative stress and ameliorates hypercholesterolemia in C57BL/6 mice and TNF-alpha induced expression of adhesion molecules and lectin-like oxidized LDL receptor-1 in human umbilical vein endothelial cells. *Bioscience, biotechnology, and biochemistry*. 2010;74(2):279-84.
125. Oyama J, Maeda T, Kouzuma K, Ochiai R, Tokimitsu I, Higuchi Y, et al. Green tea catechins improve human forearm endothelial dysfunction and have antiatherosclerotic effects in smokers. *Circulation journal : official journal of the Japanese Circulation Society*. 2010;74(3):578-88.
126. Nagaya N, Yamamoto H, Uematsu M, Itoh T, Nakagawa K, Miyazawa T, et al. Green tea reverses endothelial dysfunction in healthy smokers. *Heart*. 2004;90(12):1485-6.
127. Suzuki-Sugihara N, Kishimoto Y, Saita E, Taguchi C, Kobayashi M, Ichitani M, et al. Green tea catechins prevent low-density lipoprotein oxidation via their accumulation in low-



density lipoprotein particles in humans. *Nutrition research* (New York, NY). 2016;36(1):16-23.

128. Dower JI, Geleijnse JM, Gijsbers L, Schalkwijk C, Kromhout D, Hollman PC. Supplementation of the pure flavonoids epicatechin and quercetin affects some biomarkers of endothelial dysfunction and inflammation in (pre)hypertensive adults: A randomized double-blind, placebo-controlled, crossover trial. *The Journal of nutrition*. 2015;145(7):1459-63.

129. Vijay Y, Goyal PK, Chauhan CS, Anju G, Bhupendra V. *Carica papaya* Linn: an overview. *International Journal of Herbal Medicine*. 2014;2(5 Part A):1-8.

130. Zuhair RA, Aminah, A., Sahilah, A.M. and Eqbal, D. Antioxidant activity and physicochemical properties changes of papaya (*Carica papaya* L. cv. Hong Kong) during different ripening stage. . *International Food Research Journal*. 2013;20(4):1653-9.

131. Srikanth G, Babu SM, Kavitha CHN, Rao MEB, Vijaykumar N, Pradeep CH. Studies on in-vitro antioxidant activities of *Carica papaya* aqueous leaf extract. *Research Journal of Pharmaceutical Biological and Chemical Sciences*. 2010;1(2):59-65.

132. Okoko T, Ere D. Reduction of hydrogen peroxide-induced erythrocyte damage by *Carica papaya* leaf extract. *Asian Pacific journal of tropical biomedicine*. 2012;2(6):449-53.

133. Inam A, Shahzad M, Shabbir A, Shahid H, Shahid K, Javeed A. *Carica papaya* ameliorates allergic asthma via down regulation of IL-4 , IL-5 , eotaxin, TNF-alpha, NF-kB, and iNOS levels. *Phytomedicine : international journal of phytotherapy and phytopharmacology*. 2017;32:1-7.

134. Zhou K, Wang H, Mei W, Li X, Luo Y, Dai H. Antioxidant Activity of Papaya Seed Extracts. *Molecules*. 2011;16(8):6179.

135. Salla S, Sunkara R, Ogutu S, Walker LT, Verghese M. Antioxidant activity of papaya seed extracts against H<sub>2</sub>O<sub>2</sub> induced oxidative stress in HepG2 cells. *LWT - Food Science and Technology*. 2016;66(Supplement C):293-7.

136. Nayak BS, Ramdeen R, Adogwa A, Ramsuhag A, Marshall JR. Wound-healing potential of an ethanol extract of *Carica papaya* (Caricaceae) seeds. *International wound journal*. 2012;9(6):650-5.

137. Yismaw G, Tessema B, Mulu A, Tiruneh M. The invitro assessment of antibacterial effect of papaya seed extract against bacterial pathogens isolated from urine, wound and stool. *Ethiop Med J.* 2008;46(1):71-7.
138. Gurung S, Skalko-Basnet N. Wound healing properties of *Carica papaya* latex: in vivo evaluation in mice burn model. *Journal of ethnopharmacology.* 2009;121(2):338-41.
139. Nayak SB, Pinto Pereira L, Maharaj D. Wound healing activity of *Carica papaya* L. in experimentally induced diabetic rats. *Indian journal of experimental biology.* 2007;45(8):739-43.
140. Dawkins G, Hewitt H, Wint Y, Obiefuna PC, Wint B. Antibacterial effects of *Carica papaya* fruit on common wound organisms. *The West Indian medical journal.* 2003;52(4):290-2.
141. Anuar NS, Zahari SS, Taib IA, Rahman MT. Effect of green and ripe *Carica papaya* epicarp extracts on wound healing and during pregnancy. *Food and chemical toxicology : an international journal published for the British Industrial Biological Research Association.* 2008;46(7):2384-9.
142. Somanah J, Aruoma OI, Gunness TK, Kowelssur S, Dambala V, Murad F, et al. Effects of a short term supplementation of a fermented papaya preparation on biomarkers of diabetes mellitus in a randomized Mauritian population. *Preventive medicine.* 2012;54 Suppl:S90-7.
143. Mandal S, Hazra B, Sarkar R, Biswas S, Mandal N. Assessment of the antioxidant and reactive oxygen species scavenging activity of methanolic extract of *Caesalpinia crista* leaf. *Evidence-based complementary and alternative medicine : eCAM.* 2011;2011:173768.
144. Birasuren B, Kim NY, Jeon HL, Kim MR. Evaluation of the antioxidant capacity and phenolic content of *Agriophyllum pungens* seed extracts from mongolia. *Preventive Nutrition and Food Science.* 2013;18(3):188-95.
145. Valentao P, Fernandes E, Carvalho F, Andrade PB, Seabra RM, Bastos ML. Hydroxyl radical and hypochlorous acid scavenging activity of small centaury (*Centaureum erythraea*) infusion. A comparative study with green tea (*Camellia sinensis*). *Phytomedicine*

: international journal of phytotherapy and phytopharmacology. 2003;10(6-7):517-22.

146. Kumar RS, Sivakumar T, Sunderam RS, Gupta M, Mazumdar UK, Gomathi P, et al. Antioxidant and antimicrobial activities of *Bauhinia racemosa* L. stem bark. Brazilian Journal of Medical and Biological Research. 2005;38:1015-24.

147. Paital B. A modified fluorimetric method for determination of hydrogen peroxide using homovanillic acid oxidation principle. BioMed Research International. 2014;2014:8.

148. Benzie IF, Strain JJ. The ferric reducing ability of plasma (FRAP) as a measure of "antioxidant power": the FRAP assay. Analytical biochemistry. 1996;239(1):70-6.

149. Thaipong K, Boonprakob U, Crosby K, Cisneros-Zevallos L, Byrne D. Comparison of ABTS, DPPH, FRAP, and ORAC assays for estimating antioxidant activity from guava fruit extracts 2006. 669-75 p.

150. Mihaljević B, Katušin-Ražem B, Ražem D. The reevaluation of the ferric thiocyanate assay for lipid hydroperoxides with special considerations of the mechanistic aspects of the response. Free Radical Biology and Medicine. 1996;21(1):53-63.

151. Takao T, Kitatani F, Watanabe N, Yagi A, Sakata K. A simple screening method for antioxidants and isolation of several antioxidants produced by marine bacteria from fish and shellfish. Bioscience, biotechnology, and biochemistry. 1994;58(10):1780-3.

152. Johansson LH, Håkan Borg LA. A spectrophotometric method for determination of catalase activity in small tissue samples. Analytical biochemistry. 1988;174(1):331-6.

153. Weydert CJ, Cullen JJ. Measurement of superoxide dismutase, catalase, and glutathione peroxidase in cultured cells and tissue. Nature protocols. 2010;5(1):51-66.

154. Chularojmontri L, Gerdprasert O, Wattanapitayakul SK. Pummelo protects Doxorubicin-induced cardiac cell death by reducing oxidative stress, modifying glutathione transferase expression, and preventing cellular senescence. Evidence-based complementary and alternative medicine : eCAM. 2013;2013:254835.

155. Ulfig A, Leichert LI. The effects of neutrophil-generated hypochlorous acid and other hypohalous acids on host and pathogens. Cellular and Molecular Life Sciences. 2020.

156. Deng G-F, Shen C, Xu X-R, Kuang R-D, Guo Y-J, Zeng L-S, et al. Potential of fruit

wastes as natural resources of bioactive compounds. *International journal of molecular sciences*. 2012;13:8308-23.

157. Chao P-Y, Lin S-Y, Lin K-H, Liu Y-F, Hsu J-I, Yang C-M, et al. Antioxidant activity in extracts of 27 indigenous Taiwanese vegetables. *Nutrients*. 2014;6(5):2115-30.

158. Esterbauer H, Wäg G, Puhl H. Lipid peroxidation and its role in atherosclerosis. *British Medical Bulletin*. 1993;49(3):566-76.

159. Seto SW, Chang D, Ko W, Zhou X, Kiat H, Bensoussan A, et al. Sailuotong prevents hydrogen peroxide (H<sub>2</sub>O<sub>2</sub>) -induced injury in EA.hy926 cells. *International Journal of Molecular Sciences*. 2017;18:95.

160. Redza-Dutordoir M, Averill-Bates DA. Activation of apoptosis signalling pathways by reactive oxygen species. *Biochimica et Biophysica Acta (BBA) - Molecular Cell Research*. 2016;1863(12):2977-92.

161. Cai H. Hydrogen peroxide regulation of endothelial function: Origins, mechanisms, and consequences. *Cardiovascular research*. 2005;68(1):26-36.

162. Fiordelisi A, Iaccarino G, Morisco C, Coscioni E, Sorriento D. NFκB is a key player in the crosstalk between inflammation and cardiovascular diseases. *International journal of molecular sciences*. 2019;20(7):1599.

163. Transcriptional Regulation by Nrf2 . *Antioxidants & redox signaling*. 2018;29(17):1727-45.

164. Makino N, Mochizuki Y, Bannai S, Sugita Y. Kinetic studies on the removal of extracellular hydrogen peroxide by cultured fibroblasts. *The Journal of biological chemistry*. 1994;269(2):1020-5.



## VITA

NAME Wattanased Jarisarapurin  
DATE OF BIRTH 17 June 1992  
PLACE OF BIRTH Sunpasit Hospital Ubon Ratchathani province  
INSTITUTIONS ATTENDED Srinakharinwirot university  
HOME ADDRESS 125 Chawaranok road Ubon Ratchathani province

